Harpur Hill, Buxton
Derbyshire, SK17 9JN
T: +44 (0)1298 218000
F: +44 (0)1298 218986
W: www.hsl.gov.uk

HEALTH & SAFETY LABORATORY

Technical Assessment of Petroleum Road Fuel Tankers
Work Package 1 - Full scale testing and associated modelling
MODELLING TO PROVIDE LOAD CASE DATA FOR ROLLOVER - VALIDATION AND APPLICATION
ES/14/39/06rev06

Report Approved for Issue By:	**Nigel Corlett, BEng(Hons), MSc, PhD, ACSM**
Date of Issue:	**27 November 2014**
Lead Author:	**James Hobbs, MEng, PhD**
Contributing Author(s):	**Duncan Webb, BSc(Hons)**
Technical Reviewer(s):	**Michael Stewart, MSc, PhD, FIMechE**
Editorial Reviewer:	**Rob Richardson, BEng(Hons), CEng, MIMechE**
HSL Project Number:	**PE05832**

DISTRIBUTION

Steve Gillingham	Principal Engineer, Department for Transport
Nigel Corlett	HSL, Head of Engineering and Personal Safety
Authors	
Duncan Webb	HSL Project manager
HSL Reports and papers Library	pdf only

Technical Assessment of Petroleum Road Fuel Tankers

Disclaimer

Certain aspects of this report, and any results and conclusions set out within it, may be disputed by the tank manufacturer.

Report Approved for Issue by:	**Nigel Corlett, BEng(Hons), MSc, PhD, ACSM**
Date of issue:	**27 November 2014**
Lead Author:	**James Hobbs, MEng, PhD**
Contributing Author(s):	**Duncan Webb, BSc(Hons)**
HSL Project Manager:	**Duncan Webb, BSc(Hons)**
Technical Reviewer(s):	**Michael Stewart, MSc, PhD, FIMechE**
Editorial Reviewer:	**Rob Richardson, BEng(Hons), CEng, MIMechE**
HSL Project Number:	**PE05832**

CONTENTS

List of Figures

List of Tables

EXECUTIVE SUMMARY

Background

Following examination, certain petroleum road fuel tankers have been found to not be fully compliant with the provisions of Chapter 6.8 of the European Agreement on the Carriage of Dangerous Goods by Road (ADR). Amongst other things, these tankers are seen to exhibit extensive lack-of-fusion defects in the circumferential weld seams which, based on a leak-before-break assessment[1], could rupture under rollover and ADR load conditions.

The Department for Transport (DfT) commissioned research consisting of three work packages (WPs):

- WP1 – Full scale testing and associated modelling; Health and Safety Laboratory (HSL).
- WP2 – Detailed Fracture and Fatigue Engineering Critical Assessment (ECA); TWI Ltd.
- WP3 – Accident data and regulatory implications, and production of an overall summary report of the research; TRL Ltd.

HSL has taken forward the tasks set out in WP1 to:

1. Develop an independent non-proprietary structural hydrodynamic model of GRW tankers, validate this model against the results of tanker tests, and report modelling findings.
2. Design, construct and commission a test rig for tests of tankers, including selecting and procuring suitable instrumentation for data gathering.
3. Undertake tests on tankers, including preparing the tankers, assessing the tanker test method and results, and reporting the findings.
4. Determine suitability of tankers for large scale tests and acquire tankers, as appropriate, in accordance with project objectives as specified by DfT.
5. Capture collision and/or deformation data from relevant impacts, for example by laser scanning, to corroborate the modelling and tanker tests, and reconcile any inconsistencies.
6. Engage in peer review activities on the overall DfT research programme.

This report describes work undertaken to refine, validate and apply the model in task 1. Choice of modelling approaches and creation of the first iteration of the GRW tanker rollover model is described in HSL report ES/14/39/05.

Objectives

The work described in this report contributes towards the overall objective for task 1, namely:

- Create and validate a structural hydrodynamic model of GRW tankers under rollover conditions.

The specific objectives of the work being:

- Refine the structural hydrodynamic model of the GRW tanker to describe GRW tankers J2580 and J3910 which were topple tested by HSL.
- Validate a suitably refined GRW tanker finite element model against topple test data.
- Apply the validated GRW tanker finite element model to a real-world fuel load representative of real-world conditions and consider the model outputs.

[1] *'Short-term Fitness for Service Assessment of [non-compliant] Road Tankers, TWI (Draft) Report 23437/1/13, September 2013 and 'Project 23437 Contract Amendment: Additional FEA for assessment of [non-compliant] road tankers, TWI (Draft) Report 23437/2/13, October 2013.*

Main Findings

Model refinement

Finite element models of GRW tankers J2580 and J3910 were created, and the effect of differences between the tankers on model outputs considered. The key differences were the extrusion profile and the position of fillet welds between the extrusion band and the shell. There were only small differences between the J2580 and J3910 finite element model results. This was a similar outcome to the topple test results, which were very consistent between the tests of GRW tankers J2580 and J3910.

Impact velocity did not have a major influence on the results from the finite element analysis for the conditions modelled, which were water with impact velocities of 1.89 rad/s and 2.0 rad/s, and fuel oil with impact velocities of 2.0 rad/s and 2.6 rad/s.

The orientation of the bulkheads was shown to have a large effect on the bending moments in the tanker shell near to the extrusion bands. The bending moments were higher in the positive direction (putting the inner surface of the tanker shell in tension) on the convex side of the bulkheads. This was probably due to the buckling of the bulkheads during impact resulting in a slight twisting of the extrusion band.

Results from the models suggest that internal fillet welds between the extrusion band and the shell reduce the bending moment in the shell next to the extrusion bands. It would appear that the bending moments at the shell/extrusion band interface are reduced, and not just moved to the fillet weld location. More detailed examination, with more detailed modelling of the fillet weld, would be needed to confirm the extent of the benefits of the fillet weld and the effect of intermittent, rather than continuous, fillet welds.

Model validation

As there was little difference between the J2580 and J3910 finite element models, for validation the outputs from the J3910 model were compared to topple test data for GRW tanker J3910. Good agreement was obtained between the modified finite element model results for deformation and the topple test results based on laser scan data. All the flat lengths measured were within 15%, with the majority of locations showing less than a 5% difference.

The bending moments near to the extrusion bands generally showed good agreement between the test values and the finite element values. The largest difference between test and model results was 22%, with most other results within a few percent. The membrane stress results showed a larger variation between test and model results. Membrane stresses were generally much lower than the bending stresses at these locations, and therefore greater differences are not as important.

The finite element models did not predict the bending stresses in the central regions of the compartments well. In particular, bending moments in the longitudinal direction were significantly overestimated by the finite element models, although at this location, the bending moments were very small.

Good agreement was found between the pressures recorded during the test and those generated in the finite element analyses for the overall trends during the impact event. The magnitude of the initial pressure spikes was found, in the finite element model, to reduce rapidly as the measurement distance from the tanker wall increased. Differences in the magnitude of the initial pressure spikes between the finite element model and test values can be attributed to difficulties in correlating the location of the finite element gauge points to the physical locations of the pressure transducers during tests.

The highest levels of plastic strain were observed in the bulkheads, at the top and bottom of the flat generated by the impact, and were of a magnitude that could cause failure. It was at the top of this flat where obvious leaks occurred during the topple tests on GRW tankers J2580 and J3910.

Overall, HSL's finite element model for J3910 correlates strongly with the topple test data for GRW tanker J3910, thus providing good validation of the model.

Modelling a real-world fuel load

Modelling a tanker with representative loads of fuel oil and petrol, as opposed to water, led to significantly higher deformations in the tanker. In the fuel oil scenario, the tanker was filled to the stated capacity for each compartment except the third compartment of six from the front (the first compartment after the tanker's expanding conical section) which was left empty, in line with industry practice. The empty compartment was to prevent the tanker being overloaded due to the higher density of fuel oil than petrol.

This empty compartment resulted in differences in the stresses in the tanker shell close to the bulkheads separating the filled and empty compartments. The lower half at the front of the bulkhead at the front of the empty compartment, where pressure was applied by fuel oil to the *convex* side of the bulkhead, was partially inverted, being deformed into the empty compartment. This deformation was significantly different to that for water on both sides of the bulkhead. In contrast, deformation of the bulkhead at the rear of the empty compartment, where pressure was applied by fuel oil to the *concave* side of the bulkhead, rather than to both sides of the bulkhead by water, was not significantly different in this model to that for water.

By comparing the results for fuel models with the model for an equivalent mass of water, the water model showed lower levels of deformation and plastic strain. Therefore, the topple tests with water may not be as severe on the tanker as topple tests using fuel oil or petrol.

Outputs for WP2 Engineering Critical Assessment (ECA)

Using the 2.6 rad/s fuel oil model, single values for bending moment (1460 N·mm/mm) and membrane stress (21.5 MPa) at the front side of the rear extrusion band in compartment 4 were extrapolated from model elements close to the circumferential weld and supplied to WP2 for the detailed ECA. The limiting effect of the plastic strains in the shell means that other loading scenarios would be unlikely to give significantly different results. In addition, to support WP2 assessment of the through-wall crack along the rearmost circumferential weld at the top of the impact zone for GRW tanker J2580, values for a 1.89 rad/s water model were supplied to WP2. At the location corresponding to the crack, bending moments up to 1500 N·mm/mm were extrapolated in the same way.

1 INTRODUCTION

This work has been conducted as part of the Department for Transport's (DfT) technical assessment of petroleum road fuel tankers.

Following examination, certain petroleum road fuel tankers have been found to not be fully compliant with the provisions of Chapter 6.8 of the European Agreement on the Carriage of Dangerous Goods by Road (ADR). Amongst other things, these tankers are seen to exhibit extensive lack-of-fusion defects in the circumferential weld seams which, based on a leak-before-break assessment[2], could rupture under rollover and ADR load conditions.

The Department for Transport (DfT) commissioned research consisting of three work packages (WPs):

- WP1 – Full scale testing and associated modelling; Health and Safety Laboratory (HSL).
- WP2 – Detailed Fracture and Fatigue Engineering Critical Assessment (ECA); TWI Ltd.
- WP3 – Accident data and regulatory implications, and production of an overall summary report of the research; TRL Ltd.

HSL has taken forward the tasks set out in WP1 to:

1. Develop an independent non-proprietary structural hydrodynamic model of GRW tankers, validate this model against the results of tanker tests, and report modelling findings.
2. Design, construct and commission a test rig for tests of tankers, including selecting and procuring suitable instrumentation for data gathering.
3. Undertake tests on tankers, including preparing the tankers, assessing the tanker test method and results, and reporting the findings.
4. Determine suitability of tankers for large scale tests and acquire tankers, as appropriate, in accordance with project objectives as specified by DfT.
5. Capture collision and/or deformation data from relevant impacts, for example by laser scanning, to corroborate the modelling and tanker tests, and reconcile any inconsistencies.
6. Engage in peer review activities on the overall DfT research programme.

This report describes work undertaken to refine, validate and apply the model in task 1. Choice of modelling approaches and creation of the first iteration of the GRW tanker rollover model is described in HSL report ES/14/39/05.

The work described in this report contributes towards the overall objective for task 1:

- Create and validate a structural hydrodynamic model of GRW tankers under rollover conditions.

The specific objectives of the work being:

- Refine the structural hydrodynamic model of the GRW tanker to describe GRW tankers J2580 and J3910 which were topple tested by HSL.
- Validate a suitably refined GRW tanker finite element model against topple test data.
- Apply the validated GRW tanker finite element model to a real-world fuel load representative of real-world conditions and consider the model outputs.

[2] *'Short-term Fitness for Service Assessment of [non-compliant] Road Tankers, TWI (Draft) Report 23437/1/13, September 2013 and 'Project 23437 Contract Amendment: Additional FEA for assessment of [non-compliant] road tankers, TWI (Draft) Report 23437/2/13, October 2013.*

Previous assessments of fuel tanker integrity during a rollover event have simply applied internal pressures to a structural finite element model. The pressures used for these analyses were based on work undertaken on behalf of the Health and Safety Executive by Frazer Nash in 1996 [1]. This work used finite element modelling to assess the pressures developed in the fluid due to impact with a flat surface, but the assessment did not consider any stresses in the structure due to the impact itself.

The main aim of this work package was to develop a new finite element model to predict more accurately the behaviour of a tanker in a rollover event; in particular, modelling the action of the fluid more accurately, and taking into account the structural impact. The model has been validated by comparing it with measurements from full scale tests on a tanker filled with water. Once validated, the model can then be used to assess a variety of different loading cases, the first of which would be for a similar impact but using fuel instead of water.

This report briefly describes the model and refinements, and then compares the model results with the results from the experimental tests. A detailed description of the model and modelling approaches is given in HSL report ES/14/39/05. This report is part of a package describing HSL's work on WP1 up to 29 August 2014. The reports in this package are given in Table 1.

Table 1 List of HSL reports in this report package for Work Package 1

ES/14/39/00	Technical Assessment of Petroleum Road Fuel Tankers; Work Package 1 - Full scale testing and associated modelling; Overall Summary
ES/14/39/07	Technical Assessment of Petroleum Road Fuel Tankers; Work Package 1 - Full scale testing and associated modelling; Assessment and Supply of Tankers
ES/14/39/04	Technical Assessment of Petroleum Road Fuel Tankers; Work Package 1 - Full scale testing and associated modelling; Tanker Topple Test Methods and Results
ES/14/39/05	Technical Assessment of Petroleum Road Fuel Tankers; Work Package 1 - Full scale testing and associated modelling; Modelling to Provide Load Case Data for Rollover – Approach and Initial Development
ES/14/39/06	Technical Assessment of Petroleum Road Fuel Tankers; Work Package 1 - Full scale testing and associated modelling; Modelling to Provide Load Case Data for Rollover - Validation and Application **THIS REPORT**

The modelling results presented apply to the specific impact conditions modelled, based on the topple tests. Other impact conditions may not give the same results. Where bending moments are expressed per unit length, the usual N·mm/mm units have been expressed more simply as N.

The modelling software used was ANSYS Autodyn version 15. A list of models used is included in Table 2.

Table 2 List of models created

Model	Impact Velocity rad/s	Extrusion profile used	Fillet weld locations	Liquid	Notes
J2580 2.0	2.0	J2580	As GRW drawing	Water	
J2580 1.89	1.89	J2580	As GRW drawing	Water	
J3910 Original	2.0	J3910	Based on J3910 tanker	Water	
J3910 Modified	1.89	J3910	Based on J3910 tanker	Water	Some non-structural members thickened to increase mass. Mesh refined.
Fuel Oil 2.0	2.0	J3910	Based on J3910 tanker	Fuel Oil	Based on J3910 Original model. Compartment 3 empty.
Fuel Oil 2.6	2.6	J3910	Based on J3910 tanker	Fuel Oil	Based on J3910 Original model. Compartment 3 empty.
Petrol	2.0	J3910	Based on J3910 tanker	Petrol	All compartments full

2 GENERAL MODELLING APPROACH

2.1 GEOMETRY

The geometry of the tanker was based on an eight-banded tanker, like the GRW tankers J2580 and J3910 used in the experimental topple tests. The main dimensions were taken from Drawing No 085-45-500-03 supplied by GRW. Where dimensions were not found on the drawing, or where the drawing did not match the physical tanker, measurements were taken from the relevant tanker. An example of such a variation was the front support, where on the GRW J2580 tanker, the main longitudinal member consisted of a simple L section, whereas the drawing showed a V profile.

The ground was represented by a concrete block 150 mm thick, with a steel plate, 20 mm in thickness on top of the concrete. The ground was angled slightly (about 0.5 degrees) away from the topple pivot point to replicate the test pad. It was also angled very slightly along the length of the tanker to achieve the impact profile observed in the test, i.e. with the rear of the tanker impacting very slightly earlier than the front (~1 ms). The tanker and ground models are shown in Figure 1.

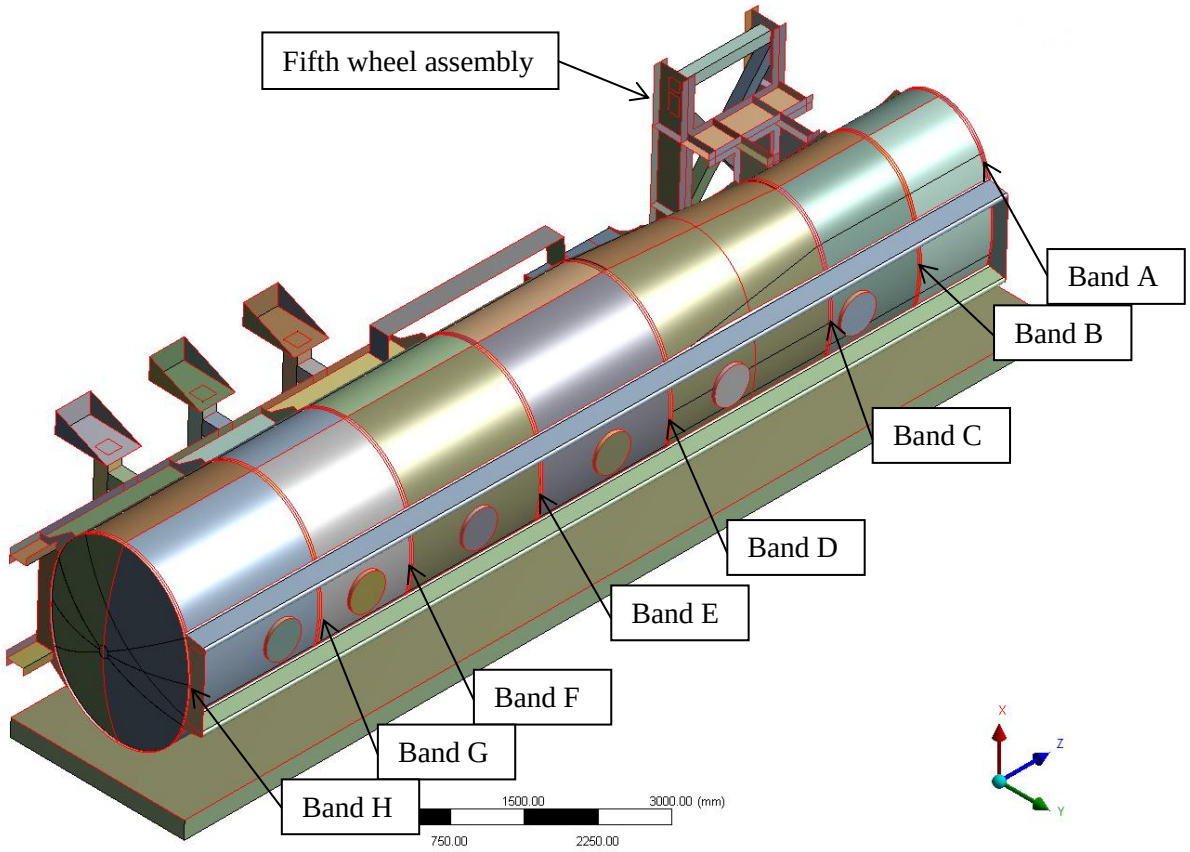

Figure 1 Overview of tanker model, showing band naming convention (see **Figure 5** for more details)

The details that were included in the geometry of the model were the main shell, the extruded bands (the modelling of which is described in more detail in Section 2.1.1), the bulkheads and

baffle, the comb along the top, and basic representations of the support structures at the front (fifth wheel location), the landing gear support and the rear. Simplified representations of the suspension, axles, steel wheels and manway covers were used. For simplicity, the model used steel wheels on both sides of the tanker.

Details omitted included smaller holes in the baffle, the sumps and pump, the guttering and vapour recovery tubes through the compartments, and any other small, non-structural attachments.

2.1.1 Connections

As all the structural elements of the tanker were modelled using shell elements, special consideration had to be given to the method of modelling the connection between the tanker shell, the extruded bands and the bulkheads (or baffle in the case of band B). The extruded bands were significantly thicker than the shell, had non-uniform thickness and were connected to the shell part way along the extrusion, as illustrated in Figure 2. To model the behaviour of the tanker during impact accurately, these three characteristics should be captured. The requirement for a continuous coupling surface for the fluid-structure interaction also needed to be considered.

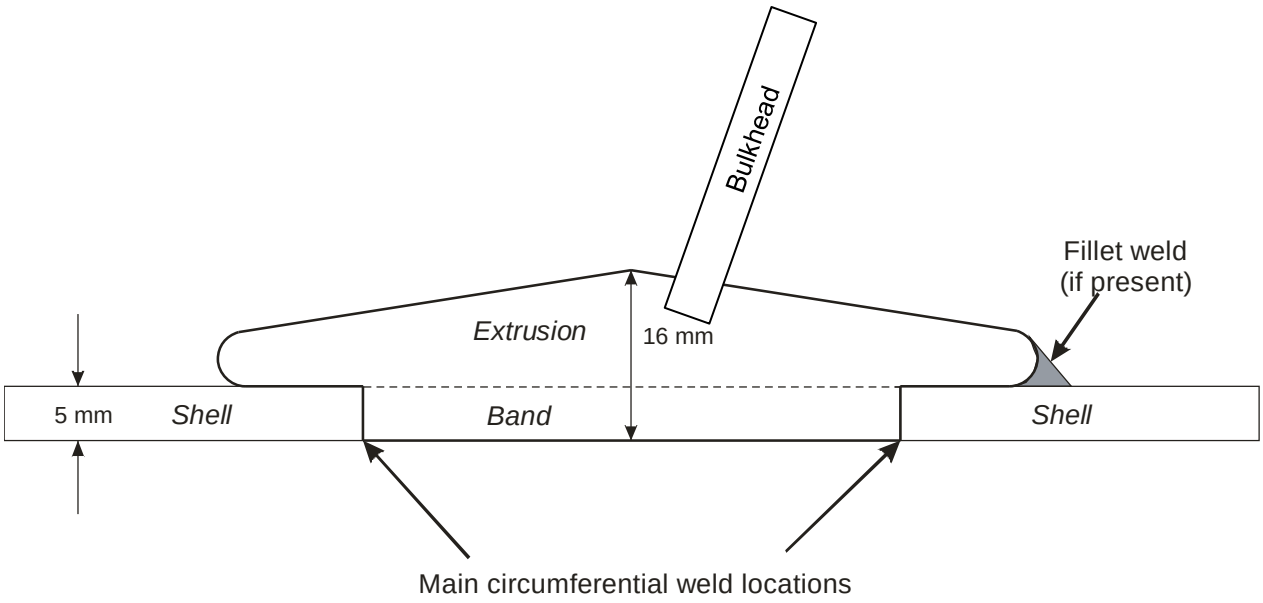

Figure 2 Diagram of the extruded band and shell connections, with nomenclature used for description of modelling arrangement (approximate location of bulkhead shown)

The approach adopted is illustrated in Figure 3. The extruded band was assumed to be split into two sections, as shown in Figure 2; the lower 5 mm thick section (the *band*), which was directly connected to the tanker *shell*, and the main part of the extrusion (the *extrusion*). The *extrusion* part had a varying thickness, from 5.5 mm at the ends to 11 mm at the centre. The bulkhead was connected to the centre of the *extrusion* by merging the end nodes bulkhead to the central extrusion nodes.

In the model, bonded contact was used to connect the *band* to the *extrusion*. With bonded contact, the nodes on one face are kept in the same relative position on the face to which they

are bonded. Standard contact boundary conditions were assumed between the *shell* and *extrusion* where no fillet weld was present. This arrangement enabled sections of the bands to be easily modified to represent areas where the internal fillet weld was present. In these areas, the *extrusion* part was bonded to the *shell*, in addition to the *band*, as shown in Figure 4. This arrangement provided a continuous coupling surface using the *shell* and *band* parts.

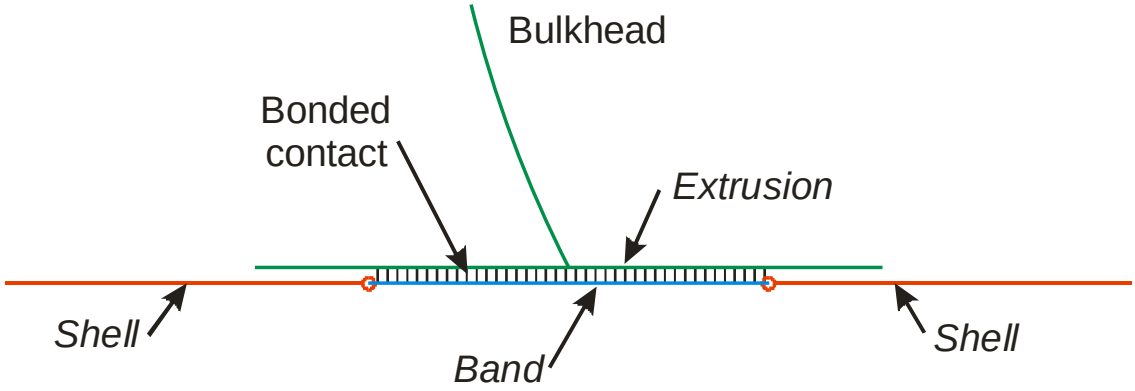

Figure 3 Schematic of arrangement for modelling the extruded bands (not to scale) where no fillet welds were assumed

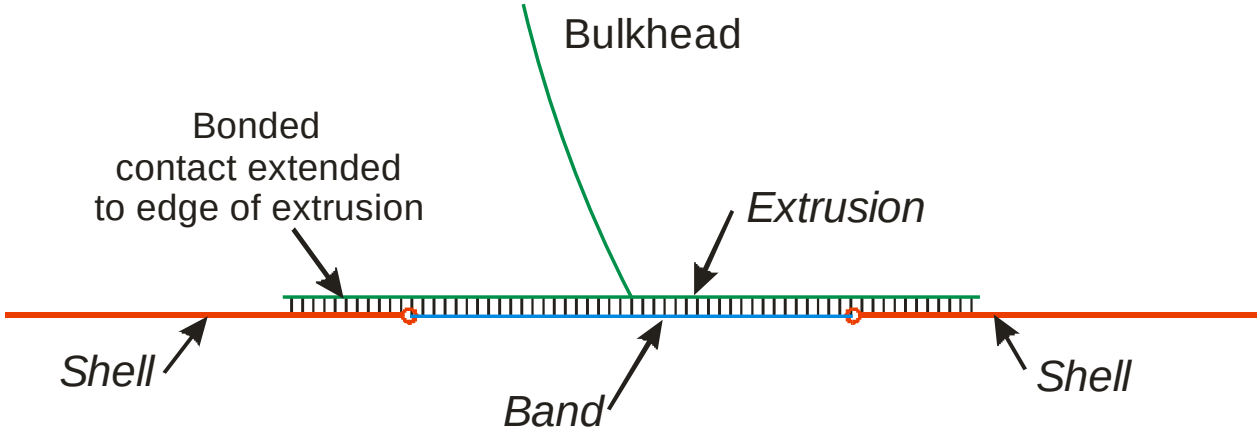

Figure 4 Schematic of arrangement for modelling the extruded bands (not to scale) where fillet welds were assumed

2.2 MATERIAL PROPERTIES

2.2.1 Aluminium

The relationship between stress and strain beyond the point of yield was described using a multi-linear isotropic hardening relationship, with the values shown in Table 3. This was based on test data for GRW tanker J3025 supplied by TWI.

Table 3 Stress – plastic strain relationship used for the aluminium of the tanker

True Stress (MPa)	*Model Plastic True Strain (%)*
100	**0**
130	**0.07**
150	**0.5**
175	**1.4**
200	**2.5**
250	**5.3**
300	**9.3**
350	**15.5**
370	**20.0**

Other material properties set for the tanker material were density of 2770 kg/m^3, Young's modulus of 71 GPa and Poisson's ratio of 0.33. These were the standard values of the non-linear aluminium alloy material in the software's material library.

2.2.2 Concrete

The material properties used for the concrete of the test pad were taken from the software's material library for 35 MPa concrete. This had a value of density of 2314 kg/m^3 and shear modulus of 16.7 GPa. The model also had a polynomial equation of state and a porosity equation of state. As the concrete was solely acting as a hard surface for the impact and would be unlikely to be subject to high levels of stress, the exact material model used for the concrete was unlikely to be important to the model of the tanker.

2.2.3 Steel

As the steel components of the model (i.e. the fifth wheel, axles, suspension, steel wheels and the plate covering the landing pad) were not expected to experience significant stresses or deformations, the standard structural steel elastic material properties were used. These were a density value of 7850 kg/m^3, Young's modulus of 200 GPa and Poisson's ratio of 0.3. The material was assumed to be under elastic conditions only, so no yield properties were necessary.

2.2.4 Water

The water material properties were taken from the software's material library. These were a density value of 1000 kg/m^3 and a shear modulus of zero. The library water properties also contain a shock equation of state. A failure mode was also defined, which was a minimum hydro pressure of 0 MPa. This prevented negative pressures occurring in the model.

2.3 BOUNDARY CONDITIONS

2.3.1 General

The lower surface of the concrete was fixed in all directions. The steel plate was bonded to the top face of the concrete.

Contact was defined between the tanker shell, bands and baffle and the ground steel plate. No contact was defined between the supporting structure of the tanker and any of the other components.

The tanker shell, bands, front and rear supports, ancillary items, and rear suspension and wheels were all defined as one part. The suspension was modelled as a solid block as the suspension was blocked in the experimental tests. These items shared topology, so that the mesh was consistent and nodes were shared. Therefore, all the items were fully bonded to each other.

The fifth wheel assembly was defined as a separate component, with bonded contact defined between the top of the fifth wheel and the bottom of the front support at the king pin location.

Each bulkhead (and the baffle) was defined as a separate part, with its extrusion. The extrusions were then bonded to the bands using bonded contact, as described in Section 2.1.1.

2.3.2 Initial Velocity

As the time to solve explicit models is proportional to the length of the event being modelled, it is far more efficient to model a short duration event. In order to make more efficient use of computer resources, the model of the tanker topple will begin at the moment just before impact. Therefore, the impact velocity must be an input to the model.

As the primary purpose of the model in this stage of the project was to be validated against experimental results, the impact velocity obtained from the high speed video of the test was used. The linear velocity on impact was translated to an angular velocity about the pivot point (the outer edge of the steel wheels). Initial estimates were for an angular velocity of 2 rad/s, which was used in most models reported. Further analysis refined the estimate of angular velocity to 1.89 rad/s, which was used in the validation models.

The models were run over 120 ms of event time.

2.3.3 Initial Water Conditions

At the point of instability, the water will have a horizontal top surface (with respect to the ground). If the topple event were very slow, the water would be able to maintain the top surface horizontal to the ground until impact. This would require the water to move relative to the tanker and have a different angular velocity. However, at the other extreme, if the topple event were very rapid, the water would not have time to settle and would maintain its shape relative to the tanker, as it was at the point of instability.

For a tanker angular velocity of 2 rad/s, the angular velocity of the water was estimated to be 0.84 rad/s, with the centre of rotation approximately 3 m beyond the pivot point for the tanker (the edge of the steel wheels).

Where the impact velocity of the tanker was changed (i.e. to 1.89 rad/s for the validation models and 2.6 rad/s for the higher velocity fuel oil model) the fluid was given the same velocity and centre of rotation as the tanker.

2.4 ASSESSMENT OF RESULTS

The assessment of membrane stresses and bending moments was at the locations of the strain gauges on GRW tanker J3910. The overall arrangement of the tanker is shown in Figure 5, with compartment numbers (C1 at the front to C6 at the rear) and band naming (band A/8 at the front to band H/8 at the rear). The /8 identifies the band as being from an 8-banded tanker, to distinguish it from a 10-banded tanker. In the remainder of this report, the /8 will be omitted, as only 8-banded tankers have been covered. Where a specific side of a band is referred to, the suffix + has been used to denote the side closer to the front, and – for the side closer to the rear of the tanker. For example, from inside compartment 4, the welds at E- and F+ can be seen.

The M-*n* numbers refer to the naming convention used by a radiography company. The BH and B letters under the band names indicate whether the associated internal elements are full bulkheads separating compartments or baffles within a compartment. Only compartment 1 contained a baffle.

A more detailed illustration of the strain gauge locations is presented in Figure 6.

All the finite element results were filtered using a moving point average method, over a time period of 0.4 ms (which equated to approximately 200 points). This was the same time period over which the experimental test data was averaged.

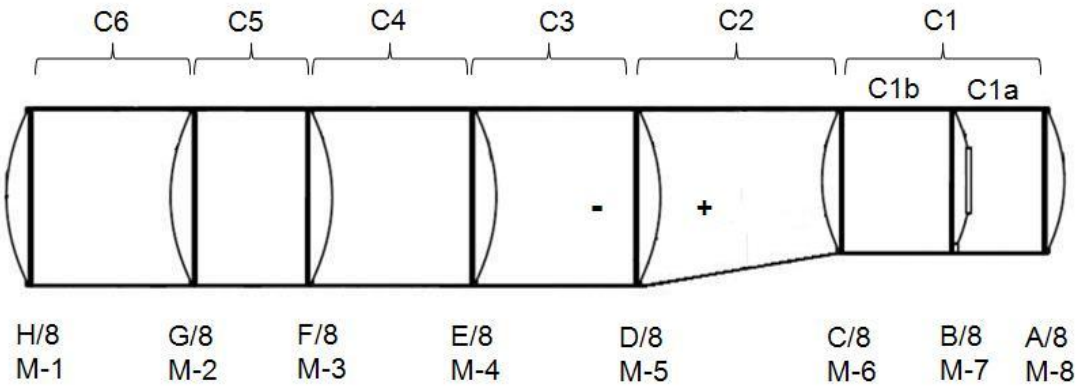

Figure 5 Eight-banded tanker schematic, showing numbering of bands, compartments and orientations of bulkheads and baffle

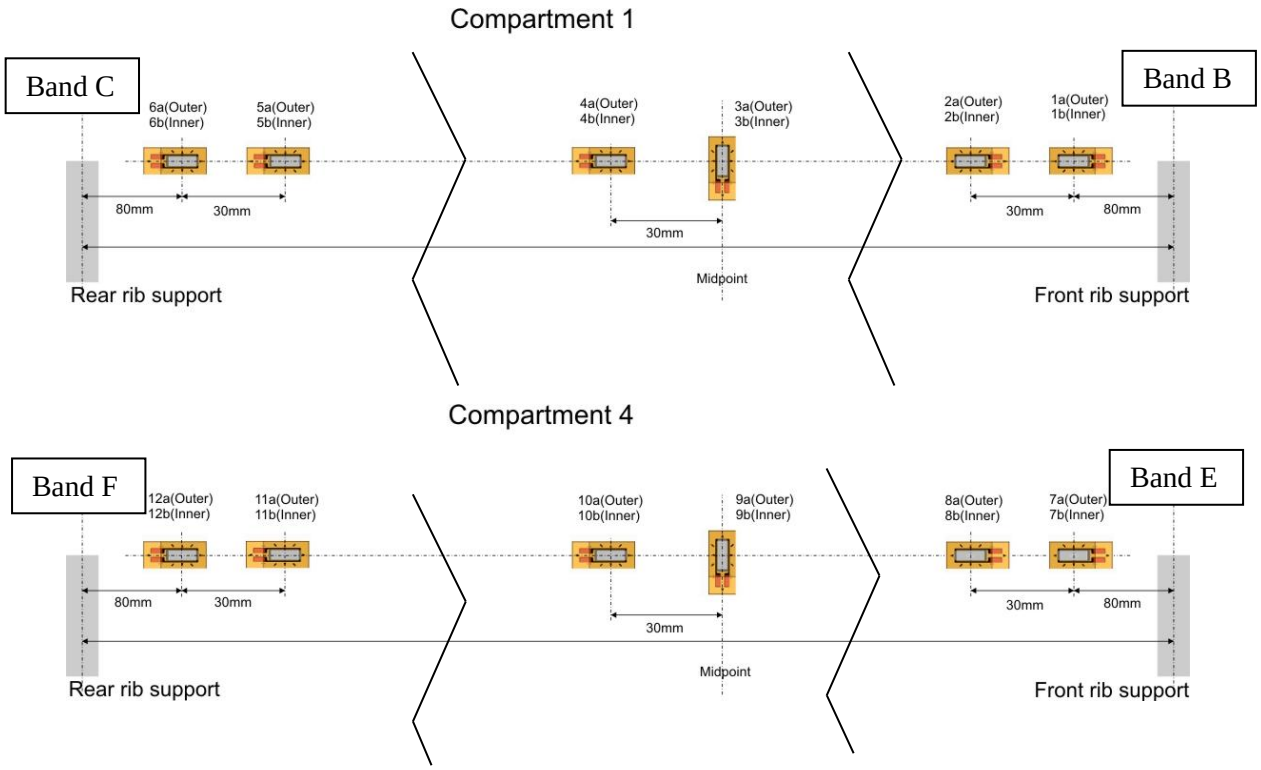

Figure 6 Locations of strain gauges used on GRW tanker J3910, and for assessment of membrane stresses and bending moments in the finite element models (not to scale)

3 COMPARISON OF J2580 AND J3910 MODELS

3.1 DIFFERENCES BETWEEN GRW TANKERS J2580 AND J3910

There were a number of small differences between the GRW tankers J2580 and J3910. It was noticed that the front longitudinal support was different, and there were three members between the combs on top of GRW tanker J3910 that were not present on J2580. These features were assumed to be insignificant to the behaviour of the tanker so were not reflected in the models.

The profile of the extruded bands and the welds connecting the bulkheads to the extrusions was different. For the extrusions in GRW tanker J3910, the profile was as shown in Figure 7, with a slot cut into the top for the bulkhead. The bulkhead was welded to the extrusion on both sides. For the extrusions in GRW tanker J2580, the profile was generally similar but incorporated a block, as illustrated in Figure 8. However, the pattern of welding was different, with only one weld, placed on the convex side of the bulkhead. The difference in profile was incorporated into the model for J2580 by increasing the thickness of the shell elements in the central region of the extrusion.

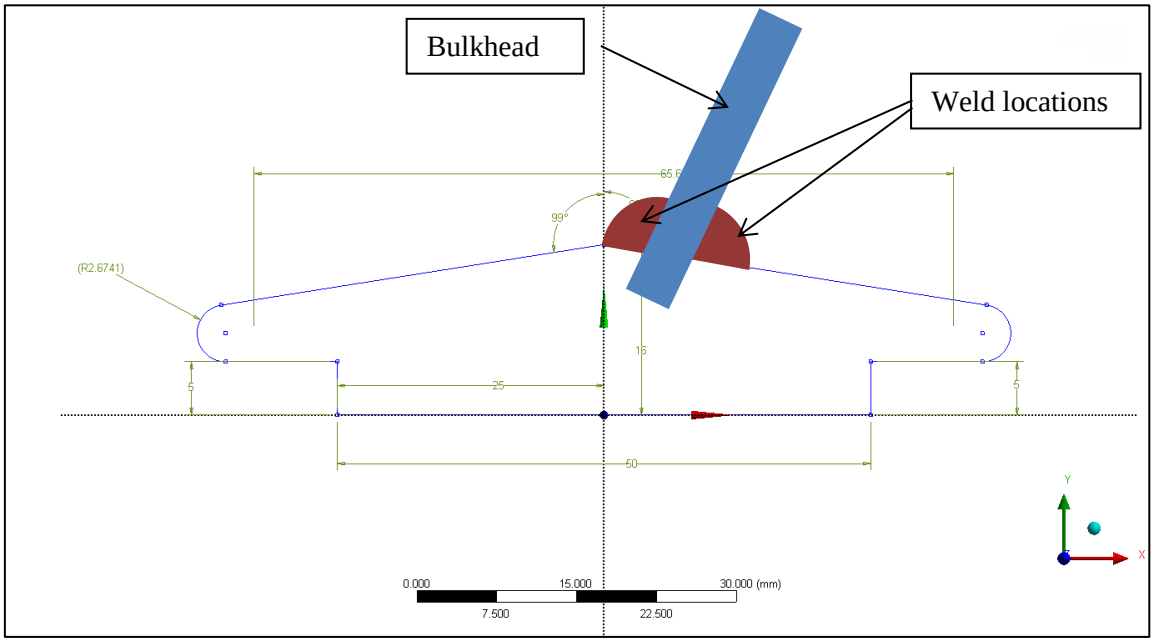

Figure 7 Band extrusion profiles for GRW tanker J3910 (dimensions approximate) with bulkead and weld locations shown

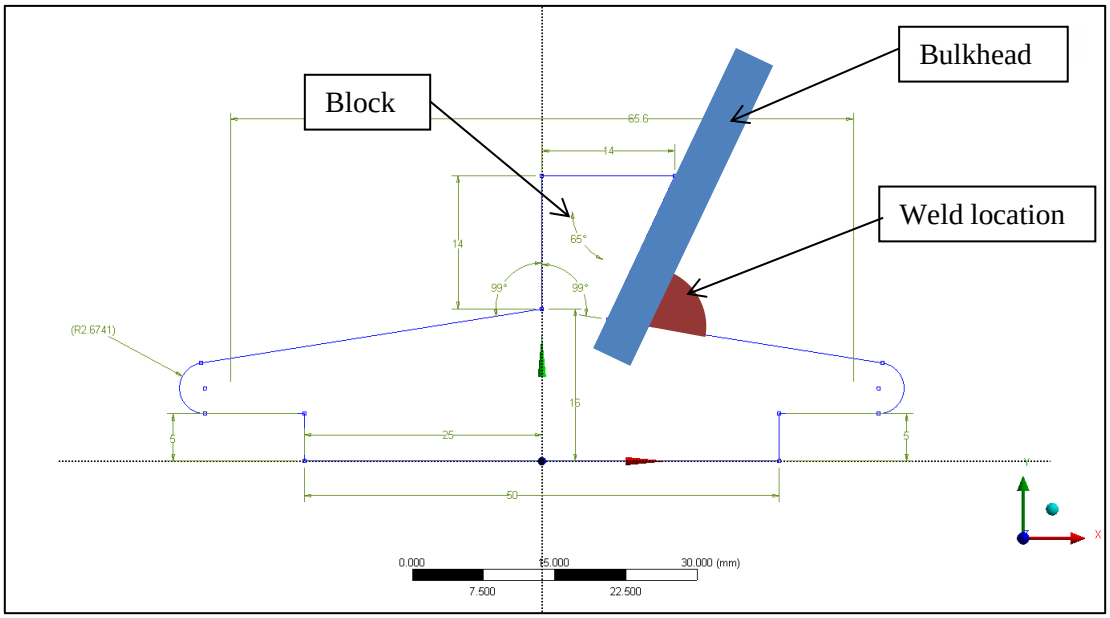

Figure 8 Band extrusion profiles for GRW tanker J2580 (dimensions approximate) with bulkead and weld location shown

The final difference between the two tankers was in the location of the fillet welds. In the supplied drawings, fillet welds were only specified on the lower half (90º to 270º from top dead centre) for bands C, D and E. The locations of fillet welds in the actual tankers is covered in Report ES/14/39/04. It was found that GRW tanker J3910 had more fillet welds than J2580, and where long stretches of weld were not present, short sections (approximately 70 mm in length) were spaced at approximately 200 mm intervals. Therefore, most of the circumference of the bulkheads was within approximately 70 mm of a section of fillet weld on GRW tanker J3910.

Modelling the fillet welds was achieved by extending the bonded contact to the full extent of the extrusion, as shown in Figure 4. Representing the precise locations of the fillet welds in full detail would be very time consuming, therefore a simplified approach was adopted. For J2580, the fillet weld was only modelled in the areas specified in the drawing, i.e. the bottom half of bands C, D and E. These were the only areas where the fillet welds were designed to be; assuming the presence of a fillet weld in other areas may be non-conservative when performing an assessment.

For the model of J3910, the fillet welds were added according to where the main sections of fillet weld were located. The geometry of the tankers is based on two radii of curvature; one for the sides and a larger curvature for the top and bottom. This naturally provides four sections in each band in the model. The sections were further reduced by taking vertical and horizontal longitudinal slices through the model, resulting in eight sections for each band. The definition of the fillet welds was based on these sections; where the majority of a given section contained a fillet weld, that section was defined as a fillet weld in the model. The small sections of fillet weld were ignored.

3.2 RESULTS - J2580 vs J3910

3.2.1 Deformation

The deformation of the tankers was quantified by assessing the deflection at each band location. This was achieved by placing two gauge points on each of the bands, diametrically opposed at the 3 and 9 o'clock positions (with respect to the tanker in the upright position). The change in distance between the gauges in each pair was calculated and taken as the level of compression.

The results for the two models are shown in Figure 9. For clarity, only bands A, D, and H are shown. As can be seen, there was very little difference between the two sets of results, with less than 1% difference between the maxima for each band.

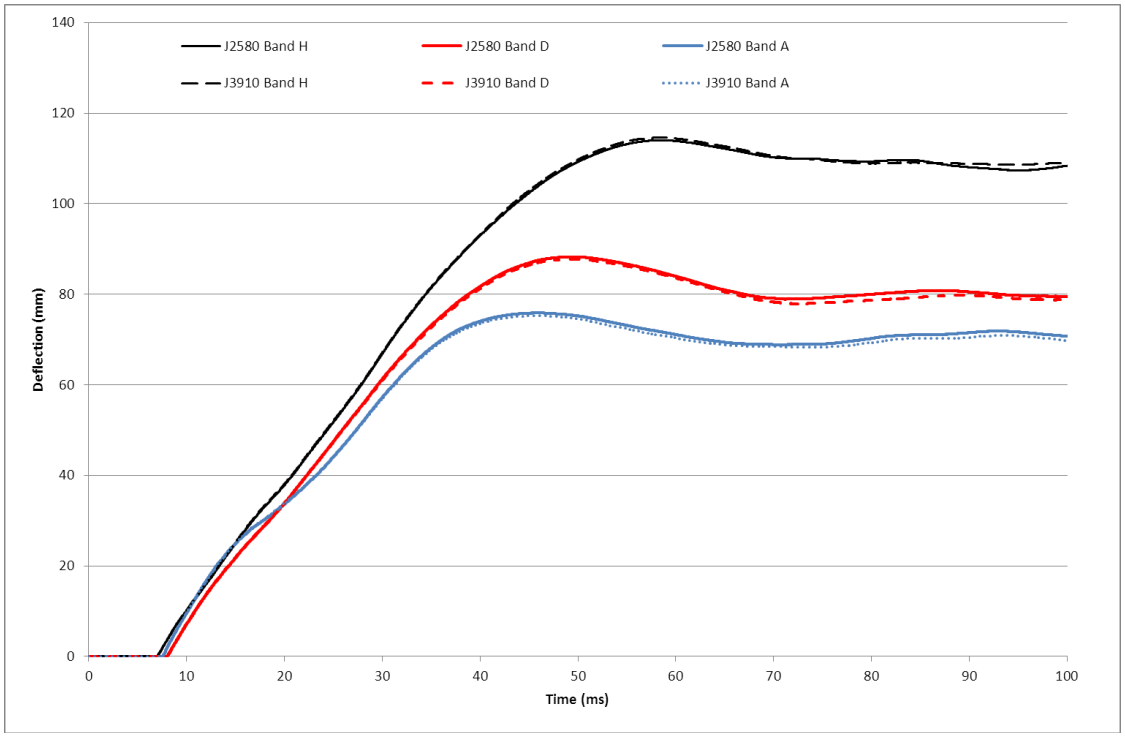

Figure 9 Variation in deformations of bands with time (J2580 vs J3910 for impact velocity of 2 rad/s)

3.3 STRESSES AND BENDING MOMENTS

The results from the models for membrane stresses and bending moments, at the gauge locations in Figure 6, are all in Appendix A. At the majority of locations, there was very good agreement between the results obtained from the J2580 and J3910 models, as illustrated in Figure 10. Where there were differences it was not always the same model that gave the higher values.

A more significant difference can be seen between the results for bending moment at gauge location 6, near to band C, as shown in Figure 11. At this location, a fillet weld had been added to the J3910 model, which may account for the lower bending stresses.

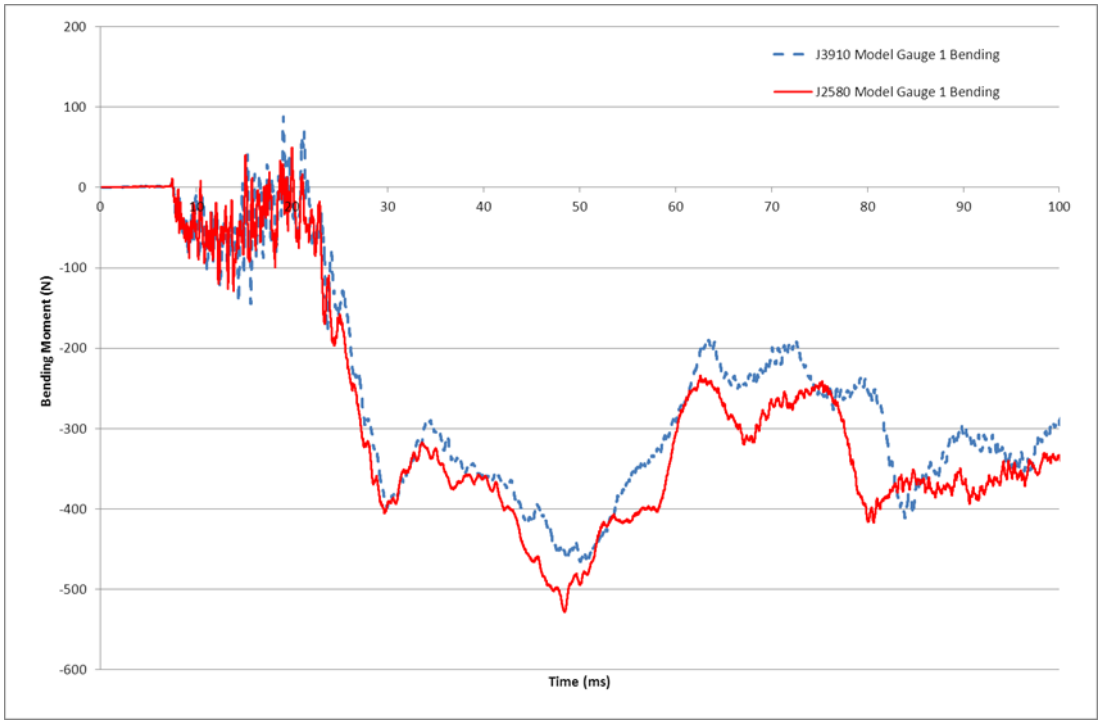

Figure 10 Bending moment results for gauge 1 location (near to band B)

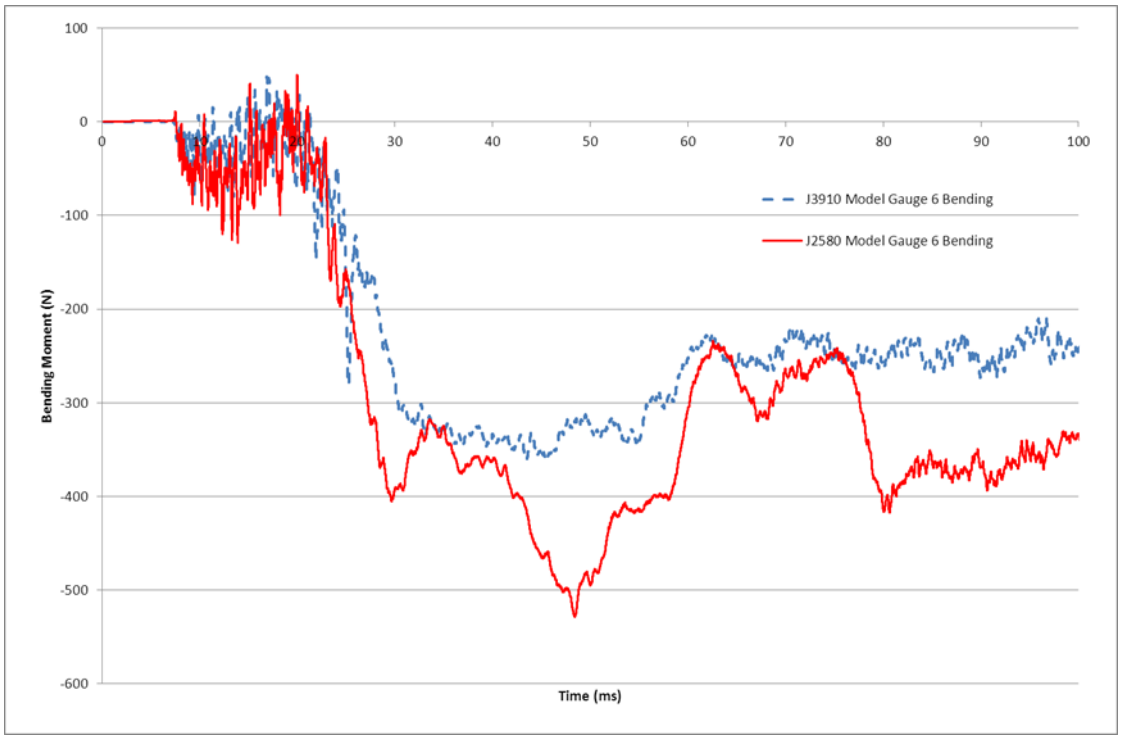

Figure 11 Bending moment results for gauge 1 location (near to band C)

3.3.1 Effect of bulkhead orientation

In both models, the bending moments near to the bands were affected by the orientation of the bulkheads. Figure 12 shows significantly higher internal stresses due to bending to the left of this band, which corresponded to the convex side of the bulkhead at that location. The same pattern was observed for the other bands on both models. Figure 13 shows the deformation of the bulkhead at the same location.

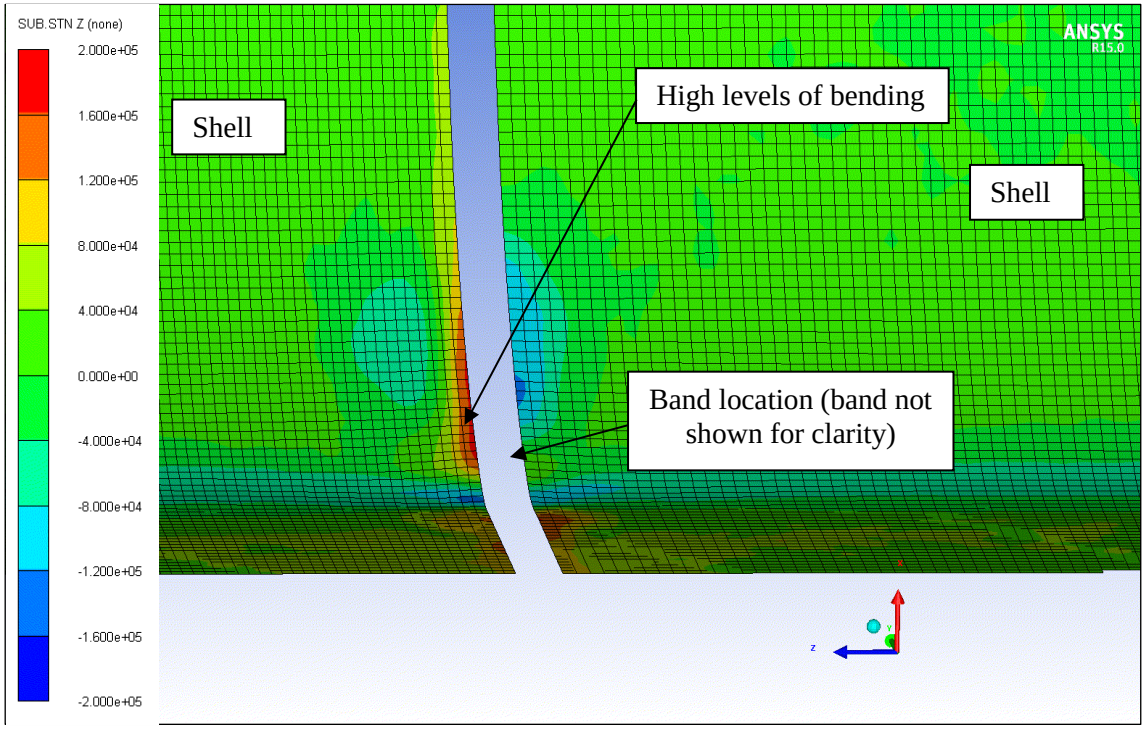

Figure 12 Internal stresses in the tanker shell (J2580 model) near to bands

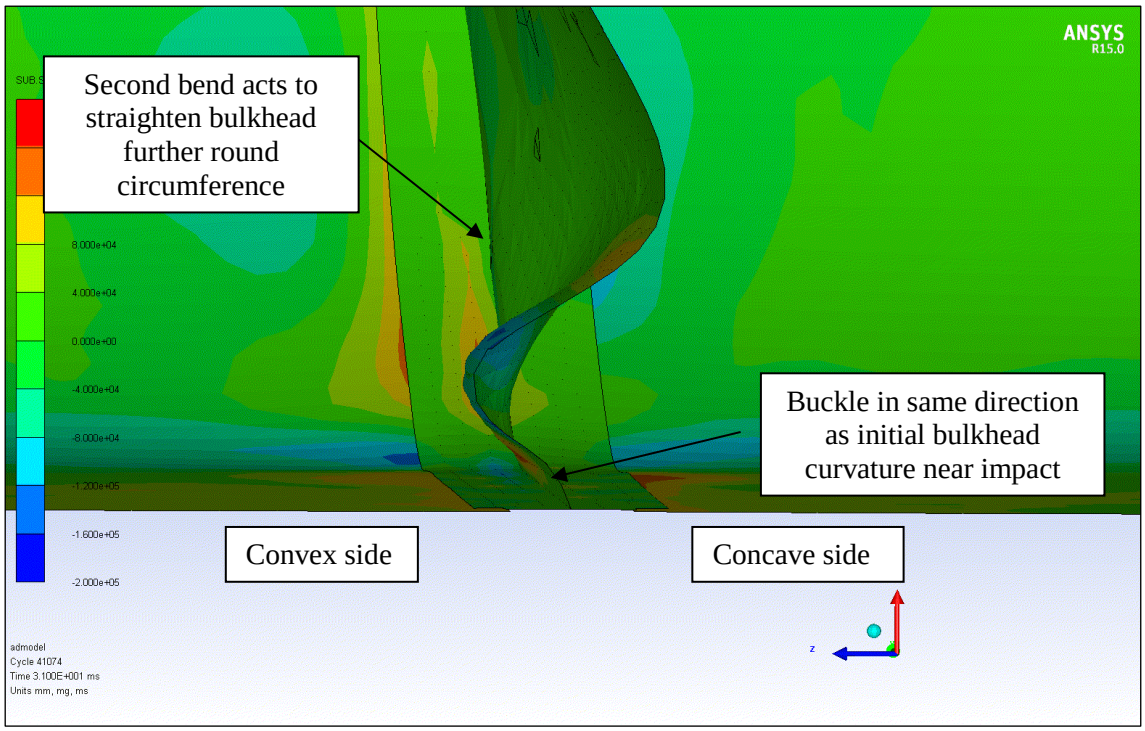

Figure 13 Deformation of bulkhead showing same location as Figure 12

In the impact area, as the tanker impacts the ground, the bulkheads buckle, with the first bend going in the direction of the original curvature of the bulkhead, as indicated in Figure 13. This would act to impart a moment on to the band that would cause the band to twist. Here the moment would act to place the inside of the shell on the concave side in tension, as illustrated in Figure 14. However, as the band may be in contact with the ground at this point, some of the twisting of the band may be resisted by the ground.

Further round the circumference, beyond the flattened section of the shell, the second bend of the buckled bulkhead is acting to twist the band in the opposite direction. At this location the inner surface of the shell on the convex side of the bulkhead is placed in tension. At the boundary between the impact zone the stresses may be highly complex.

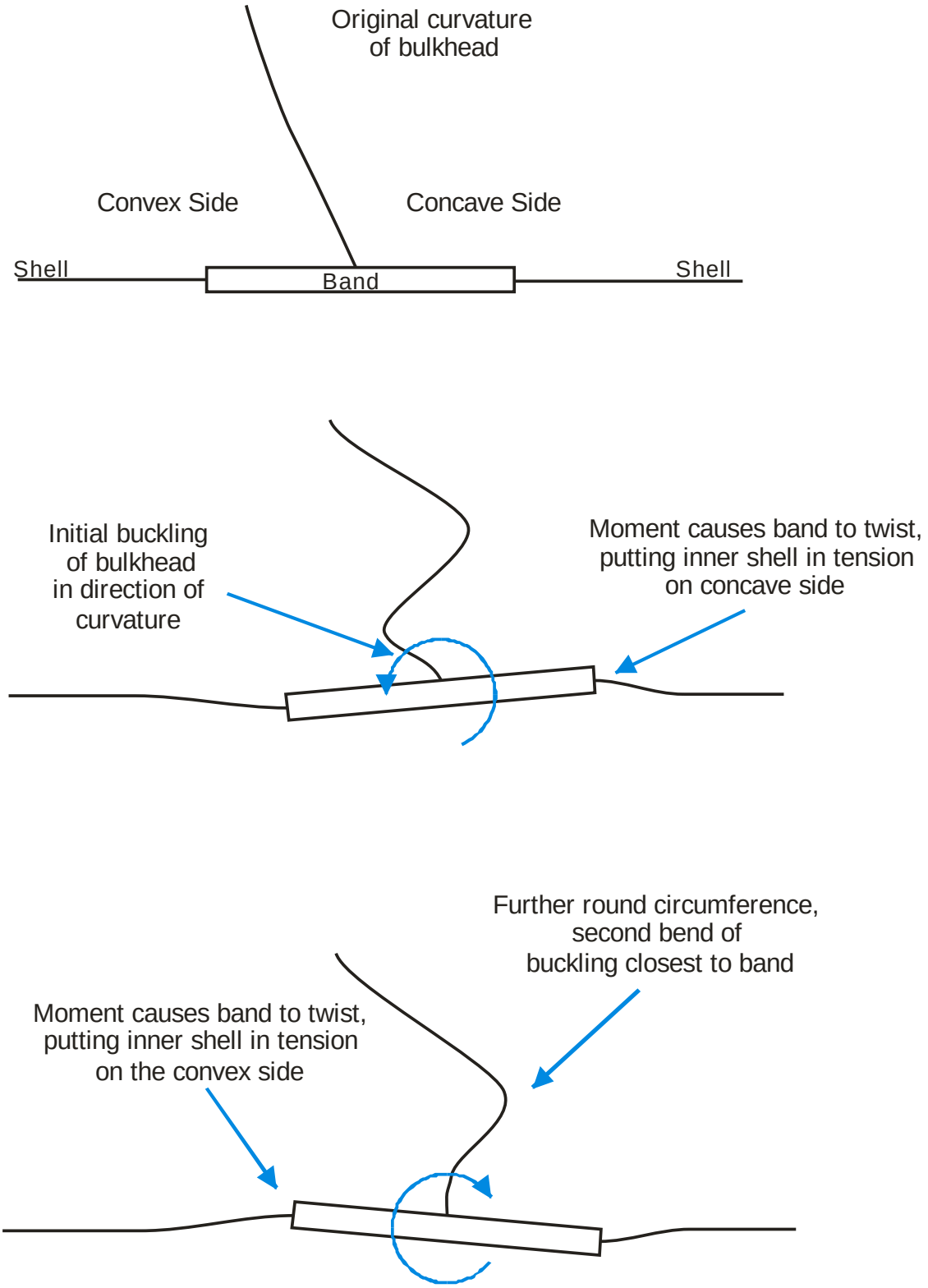

Figure 14 Schematic showing how buckling of bulkheads may affect the bending moments in the tanker shell

The effect on the bending moment can be seen if the bending moment in the shell is plotted against distance from the band, as shown in Figure 15 and Figure 16, for locations near to the convex and concave sides of the bulkhead. The only location in these two compartments on the convex side of a bulkhead was at the rear of compartment 4 (band F+ in Figure 16). The positive bending moment (which would act to open any defects in the main circumferential weld) was approximately 8 times higher in the element next to this band than at the locations near to the concave side, although some of the difference may be due to different locations being analysed.

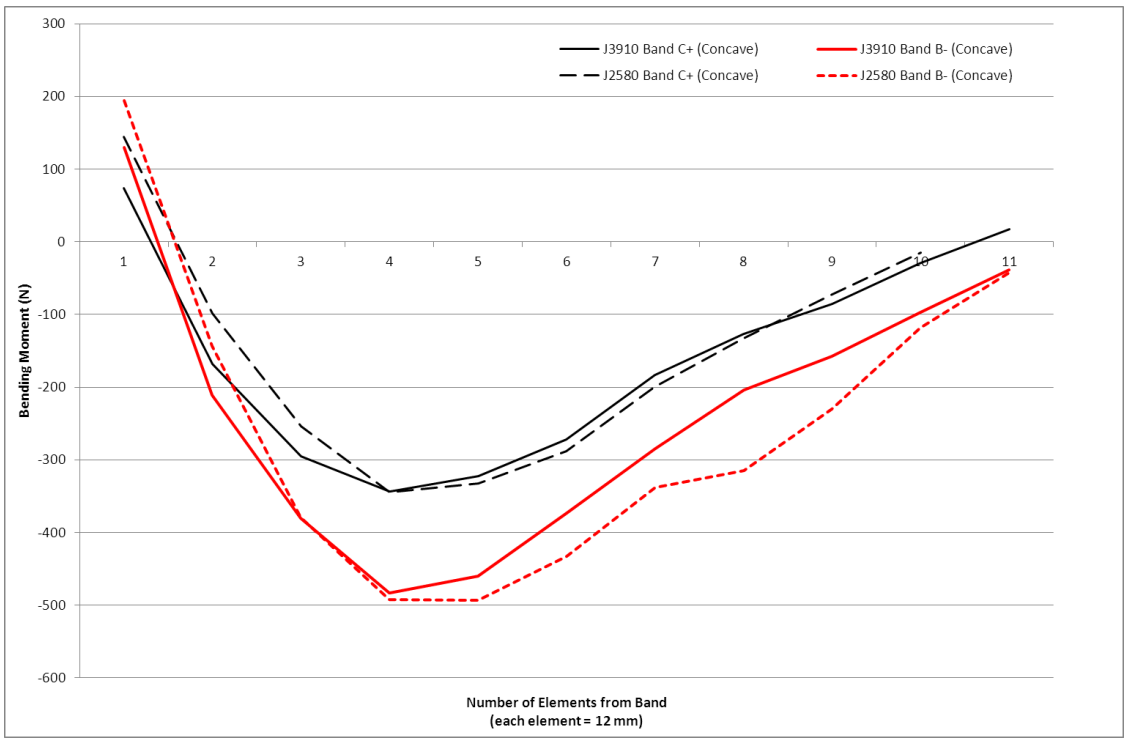

Figure 15 Bending moments at 50 ms as a function of distance from the band for locations for compartment 1b (bands B and C)

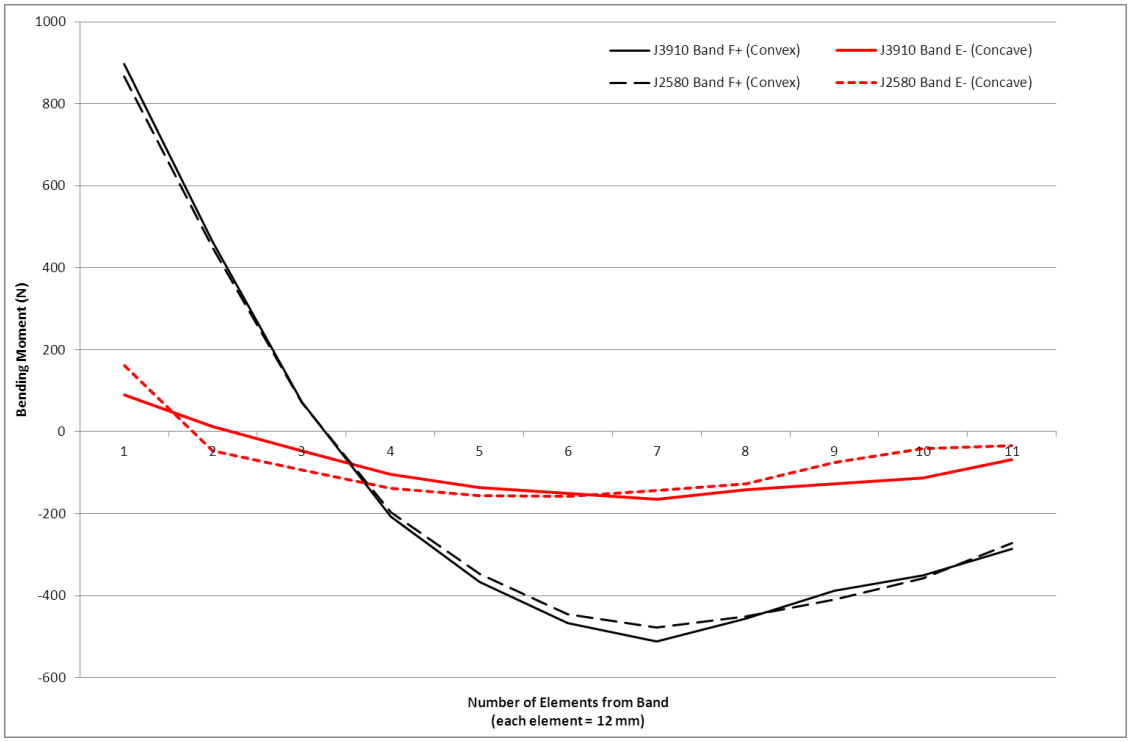

Figure 16 Bending moments at 50 ms as a function of distance from the band for locations for compartment 4 (bands E and F) illustrating effect of bulkhead orientation

4 EFFECT OF IMPACT VELOCITY

4.1 IMPACT CONDITIONS

Re-evaluation of the impact velocity of the tankers during the topple tests showed that the actual velocity was slightly slower than the 2.0 rad/s assumed in the original models. The J3910 model was rerun with the impact velocity reduced to 1.89 rad/s. This value was the average of the angular velocities calculated from the high speed video footage from the front and the rear of the GRW tanker J3910 topple test.

The behaviour of the water was estimated to have a slightly different behaviour to that of the tanker, with a lower angular velocity but a larger radius of rotation, giving a similar linear velocity. This was used in the first models. It would be difficult to calculate accurately the behaviour of the water for different tanker impact velocities, especially when assuming higher impact velocities which may occur in real life impacts where the behaviour of the fluid prior to impact may not be known. Therefore, the water was given the same angular velocity and centre of rotation as the tanker, i.e. 1.89 rad/s about the outside edge of the offside steel wheels.

4.2 RESULTS

The effect of impact velocity on deformation of the bands is shown in Figure 17 for bands A, D and H. As can be seen, changing the impact velocity (including the change to the centre of rotation of the water) has not had a significant effect on the deformation of the bands.

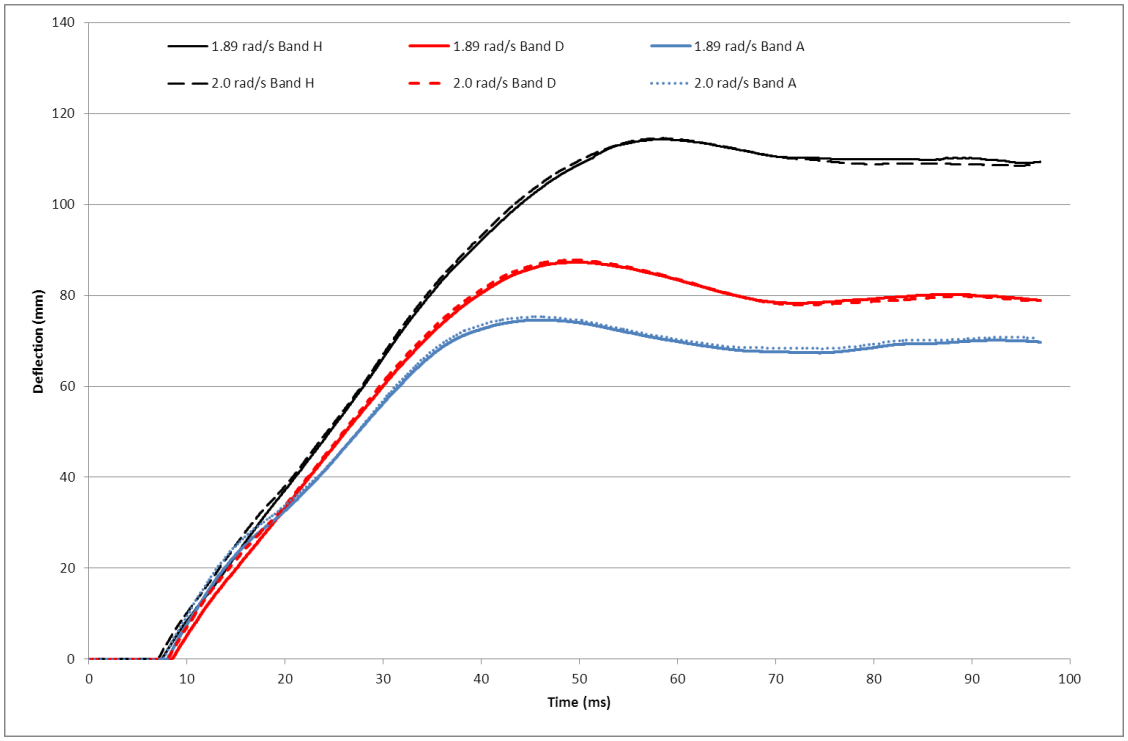

Figure 17 Comparison of band deformations for J3910 models with 2.0 rad/s impact velocity and 1.89 rad/s impact velocity

The results for all gauge locations are shown in Appendix B. Some results are included in this section for illustration.

The bending moment results from both the models with impact velocities of 2.0 rad/s and 1.89 rad/s show very little difference, as shown in Figure 18. The difference at this location is approximately 4 %, with the slightly lower velocity impact having the higher magnitude bending moment.

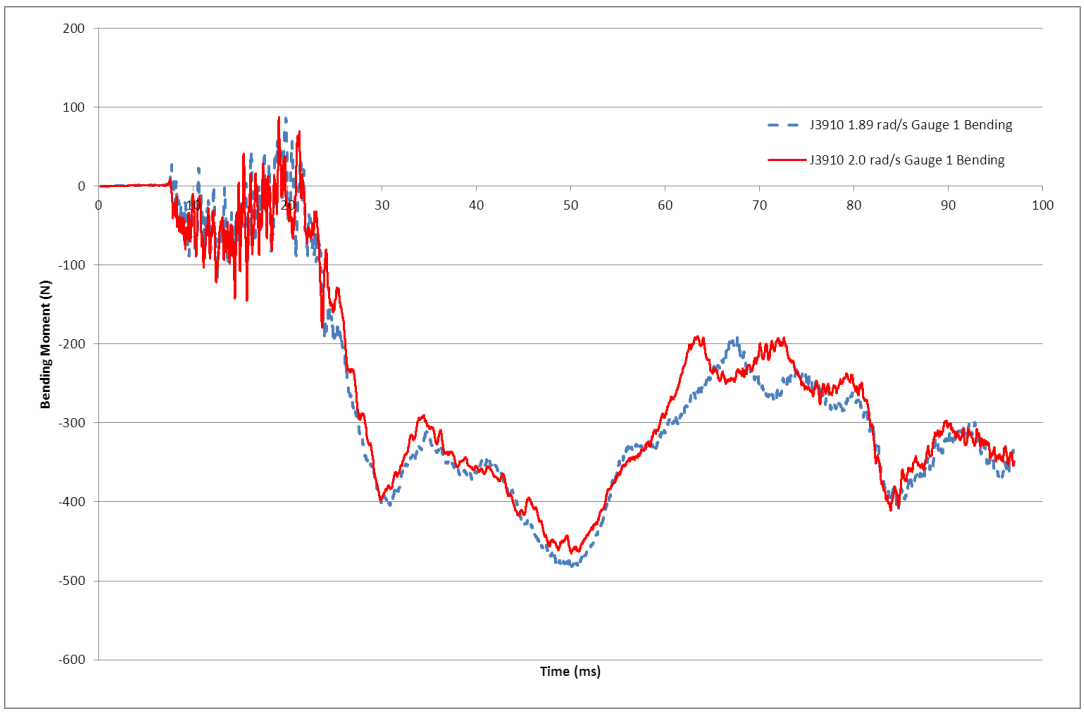

Figure 18 Effect of impact velocity on bending moment (gauge position 1)

The effect of impact velocity variation is not uniform at different locations. Larger differences were seen at gauge point 6 (closest gauge to band C) as shown in Figure 19. At this location, the higher velocity impact results in the larger magnitude bending moment. There would appear to be no obvious pattern to the differences caused by the changes in impact velocity.

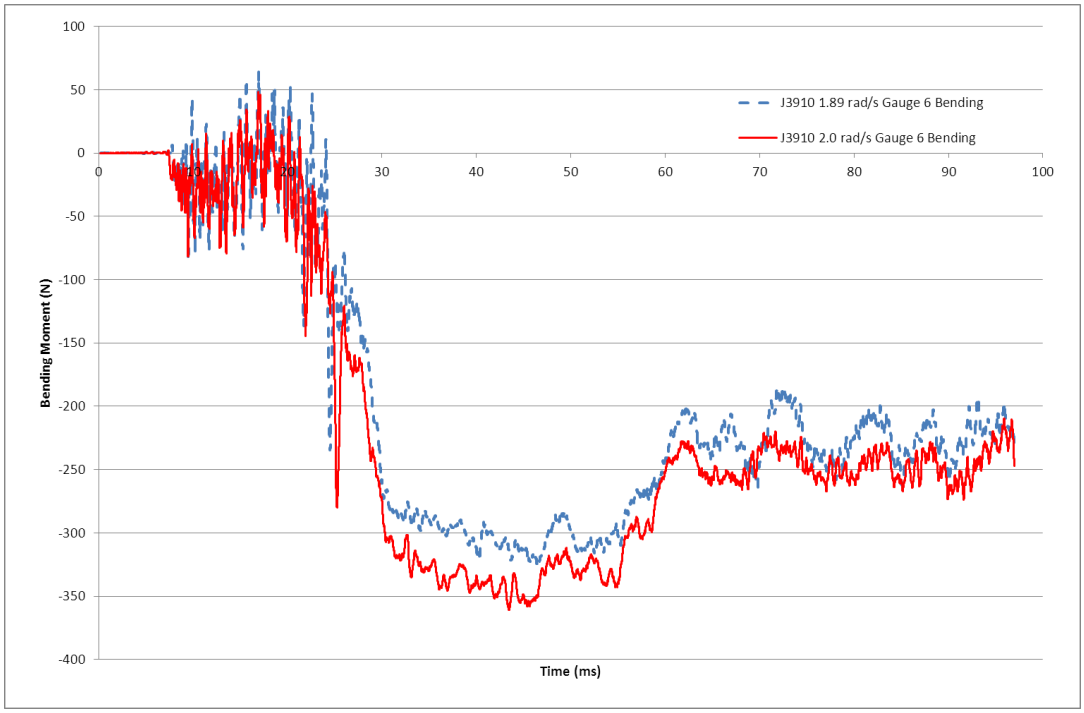

Figure 19 Effect of impact velocity on bending moment (gauge position 6)

5 VALIDATION – COMPARISON OF GRW TANKER J3910 TEST AND MODEL DATA

For any numerical model it is important to validate the model in some way to ensure confidence in the results. There are various methods for validation, but the ideal method is to validate the model with full scale, repeatable experimental data. The case used for validation should also be as close as possible to the case for which final data is sought. Where the final data sought is for either a highly dangerous situation, or a highly complex loading condition that would be difficult to replicate accurately, a compromise would have to be reached for the validation case; too realistic, and the number of different, possibly uncontrollable, variables would make the validation exercise unreliable, but too simplistic a validation case may be too far from the real event to maintain confidence as the model moves to incorporate the added variables.

A simple topple test was chosen as the validation case, using water as the liquid in the tanker. This arrangement achieved the requirements of a repeatable, safe test, with highly controlled parameters, while still creating similar types of damage as would be generated in a real life incident.

A number of different parameters were available for the validation of the finite element model as follows:

- the deformed shape of the tanker,
- the pressures measured using pressure transducers in compartments 1b and 4,
- strain data from internal and external strain gauges in the same compartments.

While ideally all variables would be matched, the main variable will be deformation. The deformed shape of the tanker is effectively the sum of all the plastic strains throughout the tanker. Strains taken at points may be highly variable in both time and space domains and may not be reliable for validation.

For the topple tests, the pressure transducers were fixed to the inner surface of the tanker, and therefore moved with the tanker. In the finite element models, it was not possible to output pressure results relative to the moving structural elements of the tanker. The fluid (Euler) domain in the model was fixed in space and therefore, the model pressure transducers were also at fixed locations. It would have been possible to use moving gauge points in the model, but in this case, the gauge would move to keep track with the fluid, rather than the structure.

Therefore, accurate correlation between the test and model pressures would be difficult for precise locations.

5.1 MODIFIED MODEL OF J3910 USED FOR VALIDATION

As the differences between the GRW tankers J2580 and J3910 were so small in both the test results and the model results, it was decided to concentrate on the GRW tanker J3910 test and models for the purpose of validation.

The original model described in previous sections was modified slightly in order to be more representative of the actual tanker. The main changes to the model were:

- The mass of the tanker was increased by thickening some non-structural items. When the GRW tanker J3910 was lifted into position, the mass was calculated to be

approximately 6.5 tonnes, including the fifth wheel support structure. The original model was approximately 5.5 tonnes, so mass was added by increasing the thickness of the manway lids, some of the support structure and the combs, adding a bar to represent the landing gear and adding the cross members between the combs. The final mass was approximately 6 tonnes. While this was still below actual mass, adding further mass may have produced point loads if point masses were added, or increased structural stiffness if the thickness of components was increased. The method used was a compromise between achieving the correct mass and retaining the structural representation of the tanker. Compared to the 31 tonnes of water contained in the tanker, the discrepancy in structural mass was small.

- The mesh was refined in two areas. The mesh on the bulkheads was refined around the contact area in both models, but the size of the fine mesh area was increased in the modified model. Also, the size of the elements close to the welds at the gauge locations was reduced slightly from 12 mm to 10 mm.

The results for both the original model and the modified model are shown in the following sections for comparison. Both models used the more accurate impact velocity of 1.89 rad/s.

5.2 DEFORMATION

5.2.1 Measurement methodology

The experimental deformation was based on laser scan data. In the absence of a quick and reliable full-field method for deformation analysis, comparison between test and model was achieved by measuring certain features at specific locations. The main feature was the length of the flat formed on the side of the tanker at the impact location. This was measured at each band, and also at evenly-spaced locations on the shell, 1.5 m apart, as indicated in Figure 20.

Slices through the finite element model results were also taken at the same locations at the end of the run (120 ms). The length of the flat produced by the impact was then measured for each location by estimating a continuous curve from either side of the flat, and then measuring the length of the flat where it intersects the curve. This methodology is illustrated in Figure 21 and Figure 22 for the laser scan and finite element data respectively.

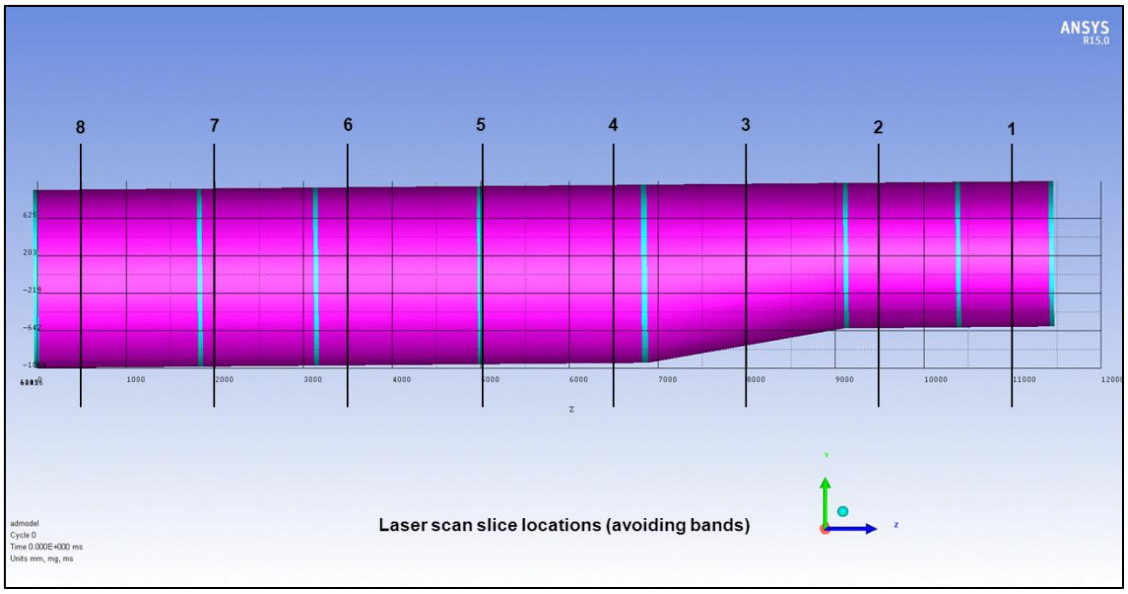

Figure 20 Locations of slices taken from the laser scan data for analysis

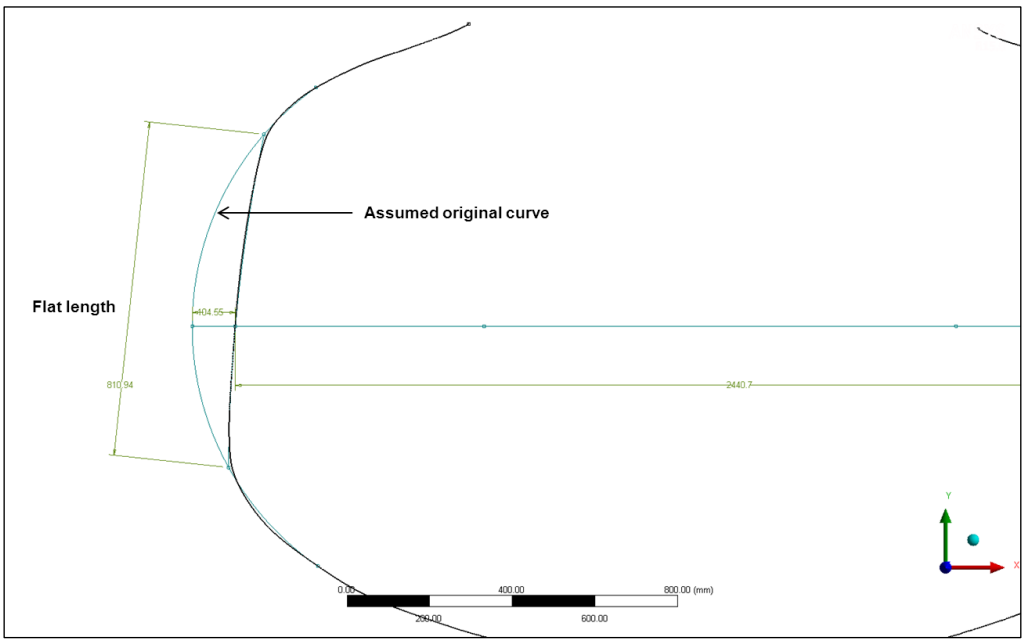

Figure 21 Measurement of the flat length on a laser scan slice

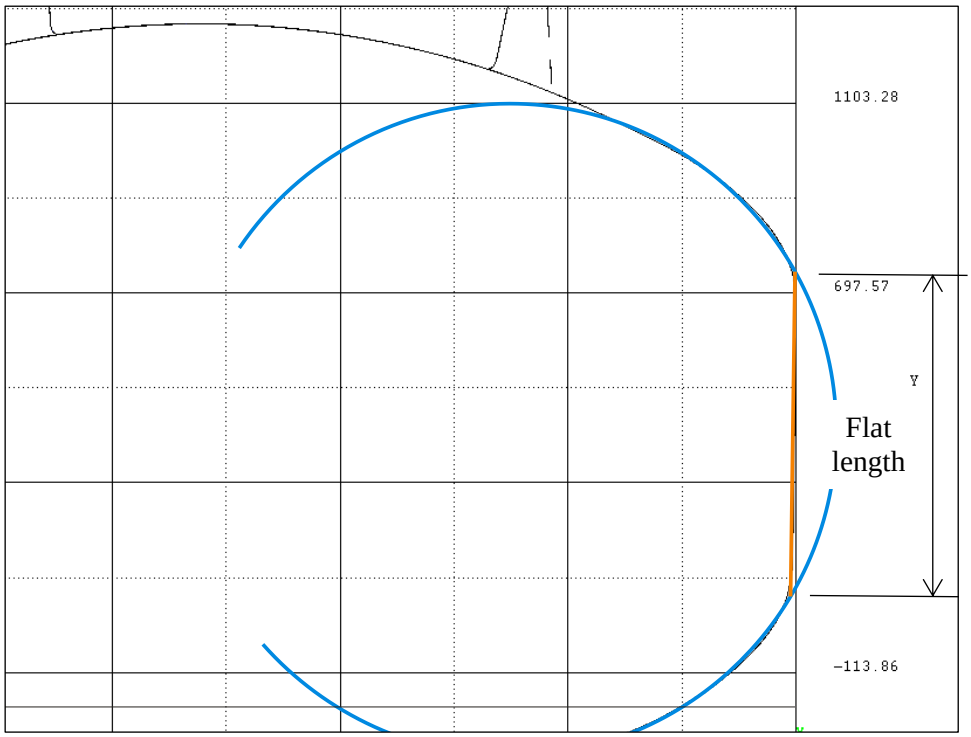

Figure 22 Measurement of the flat length from the finite element analysis data

5.2.2 Results

The results for both models are shown compared to the test results in Figure 23 and Figure 24 for the band locations and the slice locations respectively. Band A is at the front of the tanker, with band H at the back. The slices are numbered from the front to the back as shown in Figure 20.

The difference between the flat lengths measured from the test laser scans and the finite element models are listed in Table 4 in percentage terms. These were calculated by dividing the differences by the laser scan length. Differences of less than 10% are highlighted in green, with values over 10% highlighted in yellow.

Although the number of positions where the differences were less than 10% was the same between both finite element models, at the majority of locations the modified model gave closer results. For the modified model, all the flat lengths obtained from the model were within 15% of the test lengths, and at more than half the locations, the difference was less than 5%.

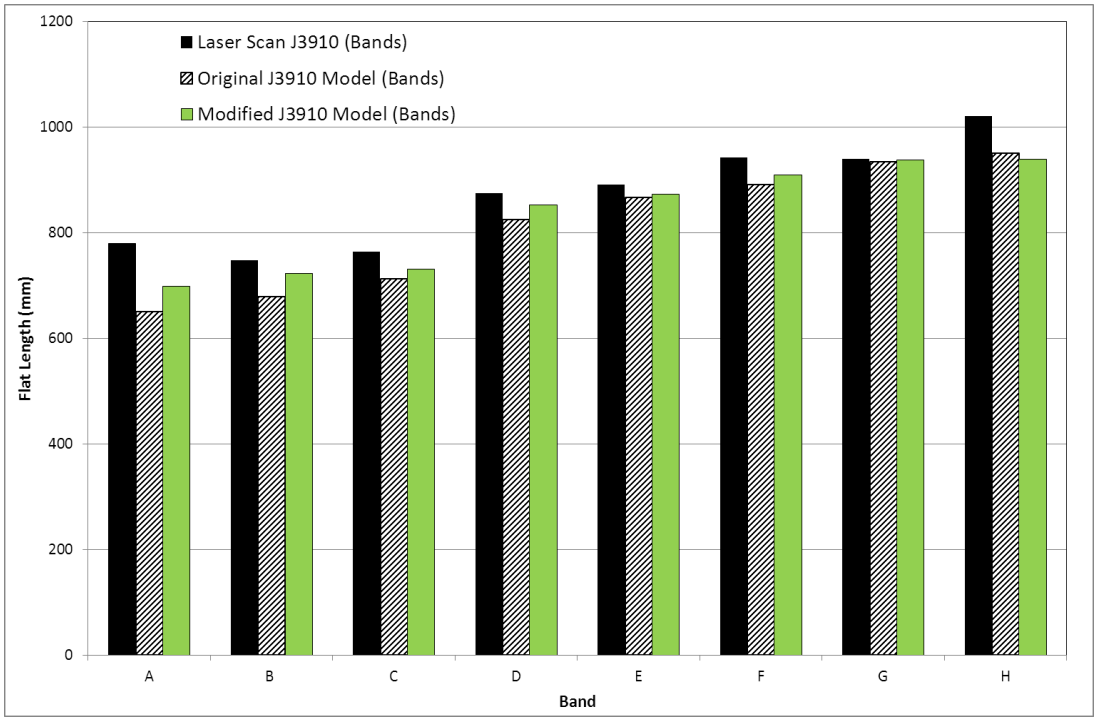

Figure 23 Comparison of flat lengths between GRW tanker J3910 test data (from laser scans) and J3910 finite element model at band locations

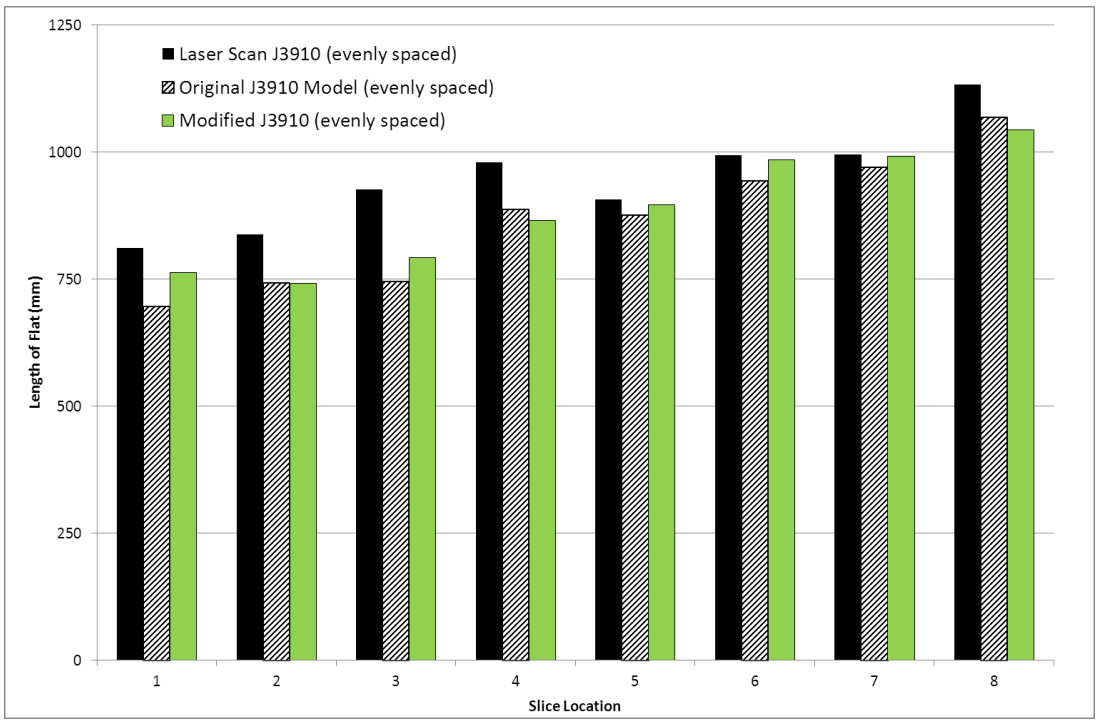

Figure 24 Comparison of flat lengths between GRW tanker J3910 test data (from laser scans) and J3910 finite element model at evenly spaced slice locations

Table 4 Differences between flat lengths calculated from laser scan data from GRW tanker J3910 and flat lengths obtained from the original and modified models of J3910

Location	*Difference between Test and Original Model*	*Difference between Test and Modified Model*
Band A	-16.4%	-10.3%
Band B	-9.2%	-3.2%
Band C	-6.7%	-4.2%
Band D	-5.8%	-2.6%
Band E	-2.8%	-2.0%
Band F	-5.5%	-3.5%
Band G	-0.7%	-0.3%
Band H	-6.9%	-8.1%
Slice 1	-14.2%	-5.9%
Slice 2	-11.3%	-11.4%
Slice 3	-19.5%	-14.5%
Slice 4	-9.4%	-11.7%
Slice 5	-3.4%	-1.1%
Slice 6	-5.0%	-0.8%
Slice 7	-2.5%	-0.3%
Slice 8	-5.6%	-7.8%
MEAN	-7.9%	-5.5%

5.3 PRESSURE

The pressure results from the GRW tanker J3910 test and finite elements models are shown in Figure 25 and Figure 26 for compartment 1b and compartment 4, respectively. The results are from the pressure transducer nearest to the impact point. There is generally good agreement between the three sets of results 20 ms after impact. There are larger differences for the first 20 ms, where differences in the magnitude of the initial peaks can be seen. These peaks were of very short duration (approximately 0.5 ms) and very localised.

The pressure transducers were attached to the internal shell of the tanker using clips which held the centre of the transducer 33 mm from the wall. The size of the Euler domain cells was 30 mm, therefore the pressure transducers may sample an area approximating half way between the first two Euler cells. However, the Euler grid does not necessarily line up with the shell of the tanker or the ground.

The large variation in pressures close to the impact point are shown in Figure 27. The graph shows the pressure spike in the element at the impact location, with the two elements adjacent. There is a very large difference in the magnitude of the pressure spike between the cell at the impact location, and the adjacent element, but a much smaller different between the second and third elements. After approximately 10 ms, the difference significantly reduces. In this instance, the average of the pressure spikes for the first two elements would be approximately 7 bar, close to the spike recorded for the first compartment in the topple test.

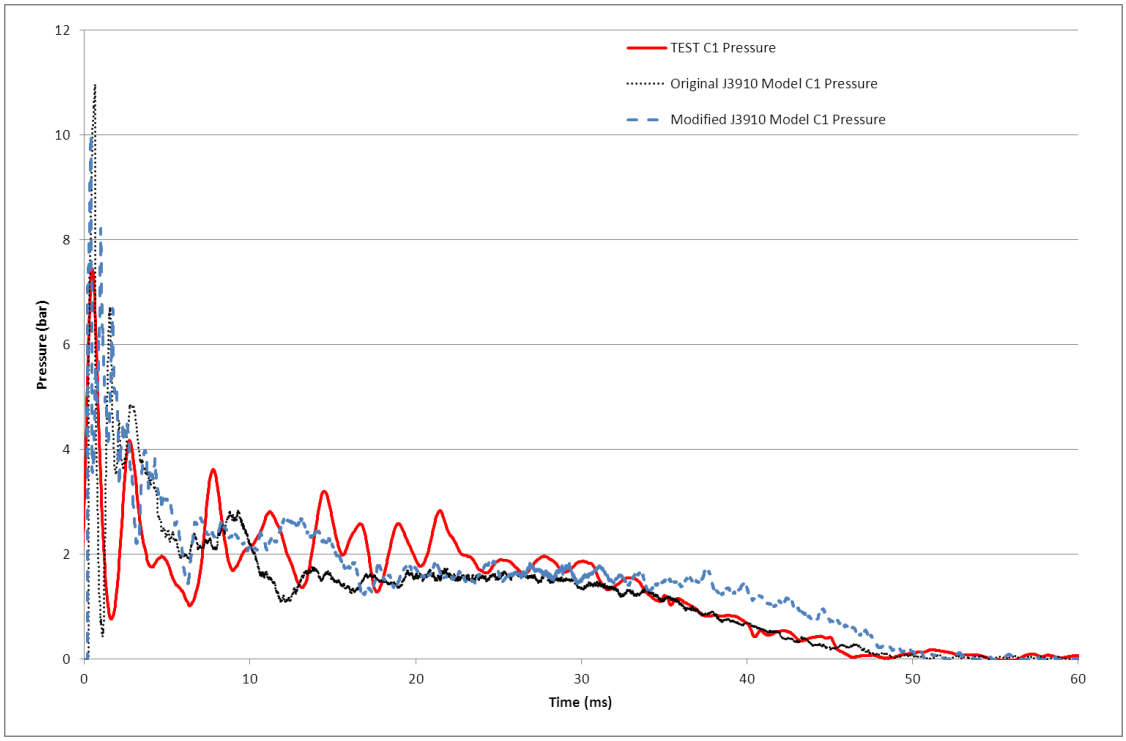

Figure 25 Comparison of pressures near to the impact location in compartment 1b

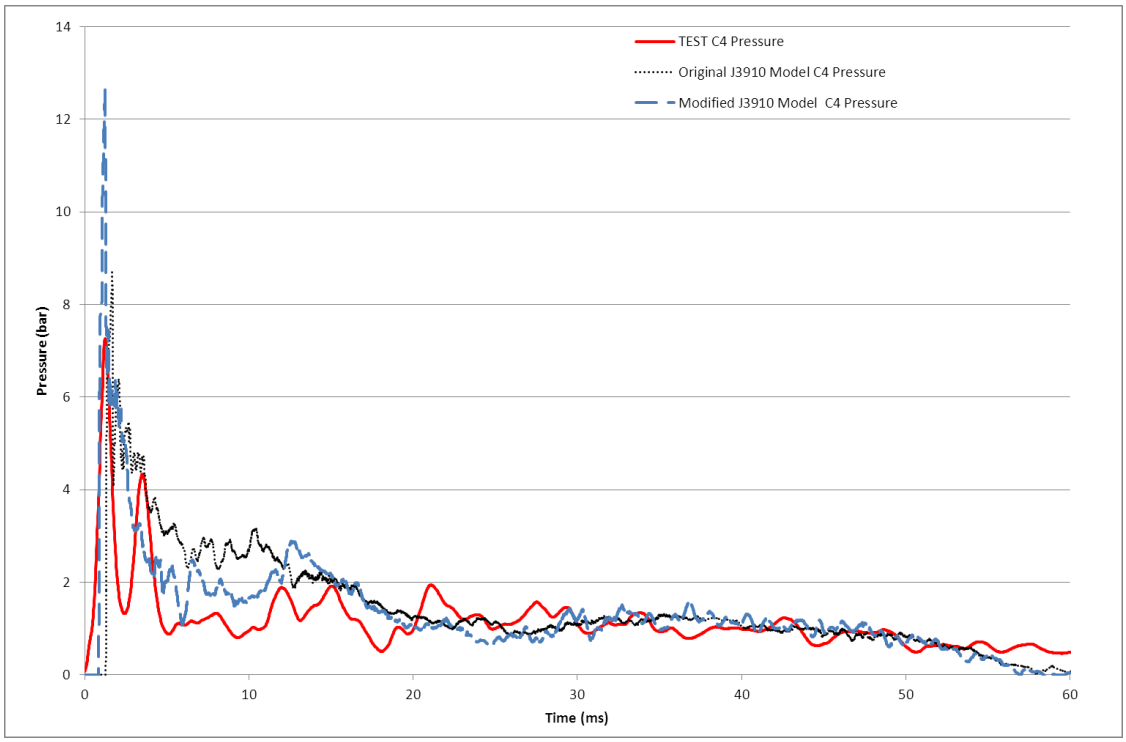

Figure 26 Comparison of pressures near to the impact location in compartment 4

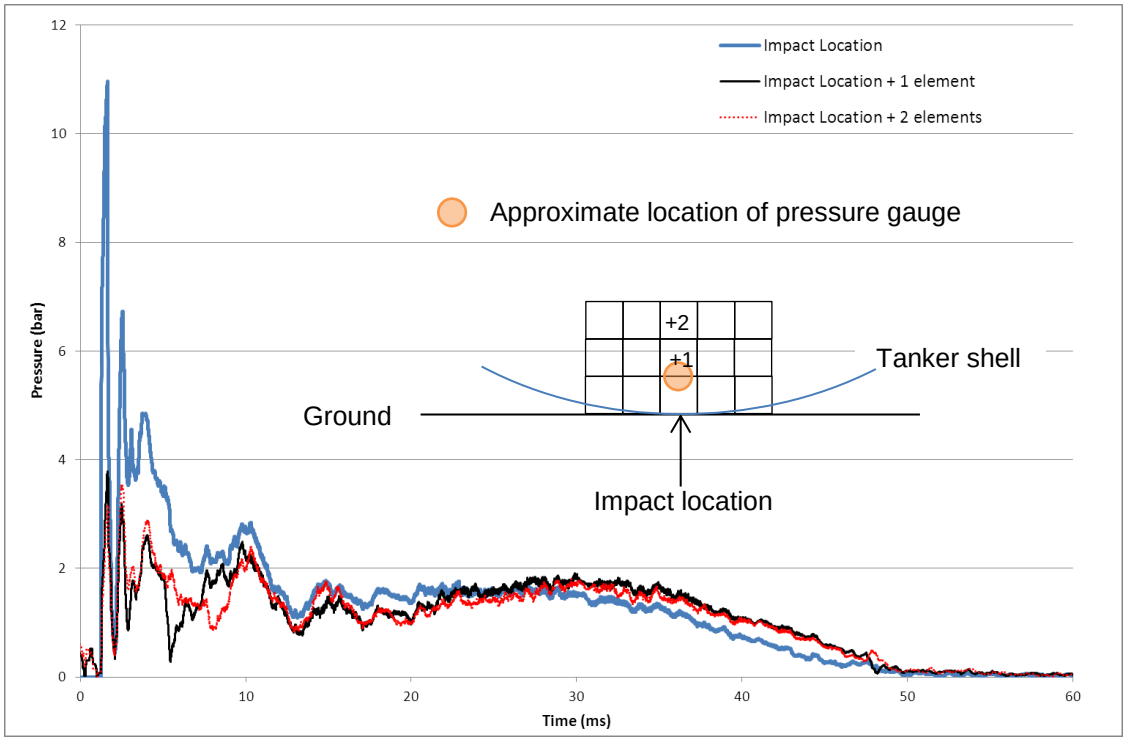

Figure 27 Variation in pressure with vertical distance from impact position (original J3910 model, compartment 1b) showing schematic of possible fluid element and pressure gauge locations

5.4 STRAINS

5.4.1 Methodology

In the software used, there are two main options for outputting the results. These are:

- the results file, which records variables for all points of the model, and from which the analysis can be restarted,
- the history file, which can record data more frequently, but with a limit of 500 gauge points. The high frequency output from the history file can be useful as the output is sometimes noisy and filtering or smoothing can then be applied.

When using shell elements in finite element analysis, a number of integration points through the shell thickness are assumed, effectively dividing the thickness into a number of sublayers. In terms of sublayer variables available, only the first sublayer results are available for output into the history files. The first sublayer output point does not lie on the surface of the shell, so obtaining surface stresses or strains is difficult.

Therefore, it was decided to compare the experimental strain results to the finite element results using the average (membrane) stress and bending moments. The conversion from surface strains to membrane and bending moments involved the following steps:

1. The membrane strain, $(\frac{\varepsilon_1+\varepsilon_2}{2})$, and bending strain, $(\frac{\varepsilon_1-\varepsilon_2}{2})$, were calculated;

2. Strains were then calculated at the Gauss integration points, assuming 5 points through the thickness as was used in the finite element analysis. This is illustrated in Figure 28;

3. The strains at each of the points were then converted to a stress using the stress-strain relationship (see material properties, section 2.2.1);

4. The membrane stress was then calculated by summing the stress at each point, multiplied by the Gauss weight for that point, as shown in Figure 29 and;

5. The bending moment was calculated by summing the stress at each point, multiplied by the weight factor and the distance of the point from the centre of the shell.

A limitation of this method is that any residual plastic strains recorded by the strain gauges would be interpreted as current membrane stress and/or bending moments. Therefore, any bending moment of membrane stress occurring after a peak strain that would be beyond yield may not be accurate.

A second limitation is that the strain gauges are uniaxial, whereas the yield criteria were based on von Mises equivalent stresses, which are triaxial. Therefore, the conversion from strain to stress may not be accurate beyond yield if the stress state was highly biaxial. However, this would not be likely in this case.

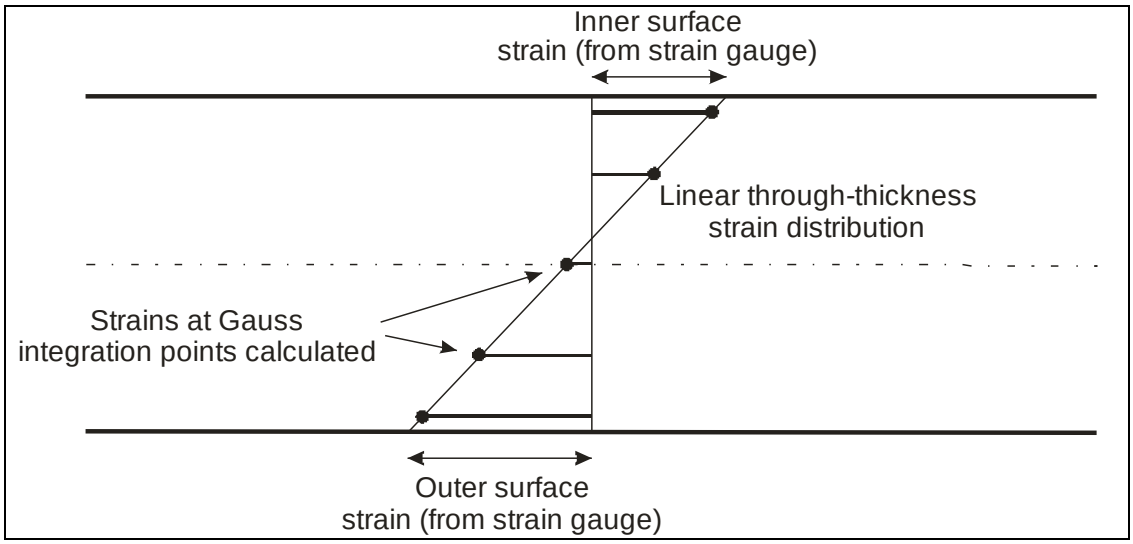

Figure 28 Schematic of through-thickness stress distribution with Gauss integration points

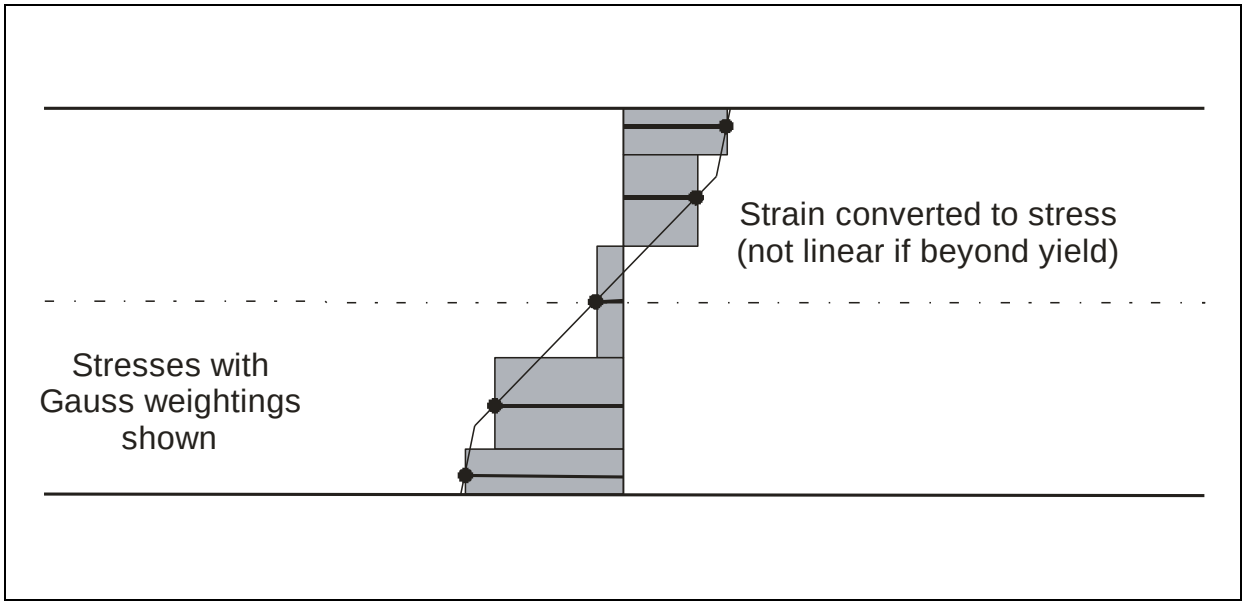

Figure 29 Schematic of possible stress distribution through thickness with Gauss integration points and weights indicated

The strain gauges in GRW tanker J3910 were numbered from front to back, with the first 6 pairs in compartment 1b, and gauge pairs 7 to 12 in compartment 4, as shown in Figure 6. In each compartment, the first 2 gauges were orientated longitudinally close to the front-most band, two central gauges (one longitudinal and one hoop) and the final two gauges orientated longitudinally near the rear bands. For the two gauges near to the bands, the closer gauge was 80 mm from the centre of the band, with the second gauge an additional 30 mm from the band.

5.4.2 Results

The full set of membrane stress and bending moment results are in Appendix C.

An example of good correlation is shown in Figure 30, which shows bending moments near to band B. In this case, the difference between the peak values from the experimental data and from the modified finite element model was approximately 2%. There was also reasonable correlation between the shapes of the graphs up to the peak value; the experimental values beyond the peak may be higher than the true values due to plastic strain being interpreted as a bending moment

Poor correlation was seen for some bending moment results for the gauges at the centre of the compartment, as illustrated in Figure 31. Here, the bending moment has been overestimated by both of the finite element models. The bending moment shown in this longitudinal direction shows a similar pattern with time to the bending in the hoop direction (see Figure C- 3) but with a lower magnitude. This suggests that the bending in the longitudinal direction was a result of bending mainly, but not completely, in the hoop direction. Also, the magnitudes of the bending predicted by the model, while much higher than the experimental data in percentage terms, were still small, with the 150 N moment equivalent to a bending stress of approximately 35 MPa. The bending moments are expressed per unit length, so the (N·mm)/mm units have been expressed throughout this report more simply as N.

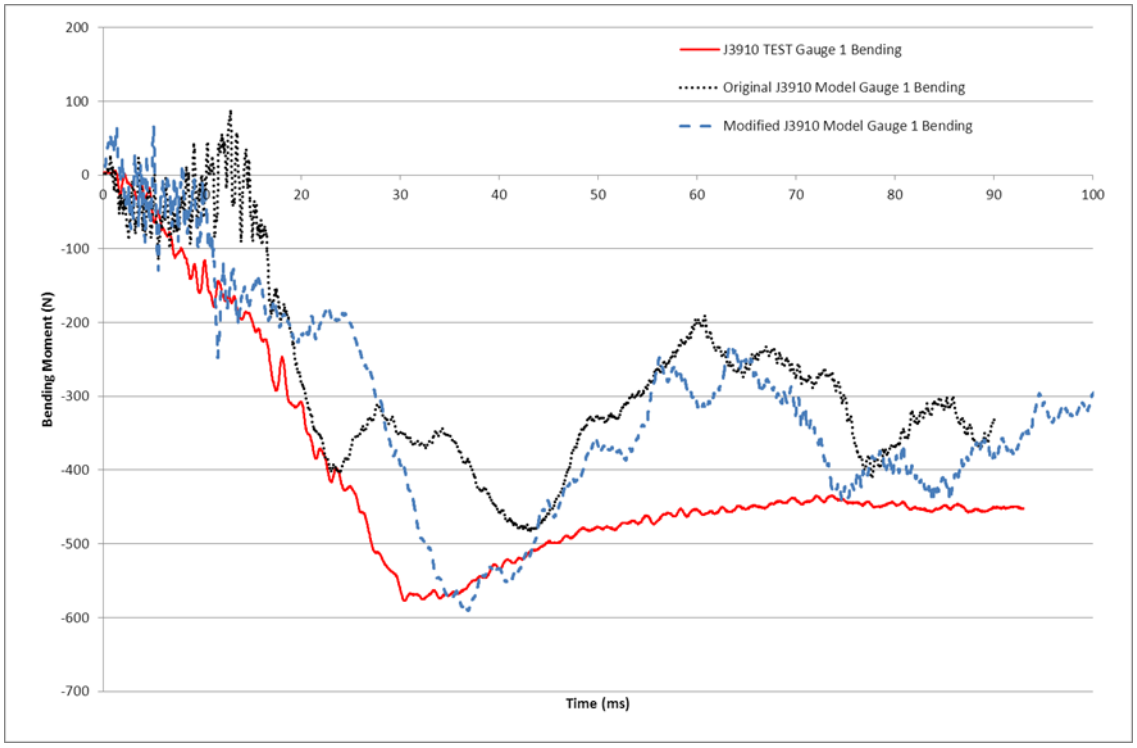

Figure 30 Bending moment results for the GRW tanker J3910 topple test compared to those from the original and modified finite element models for gauge location 1 (near to band B)

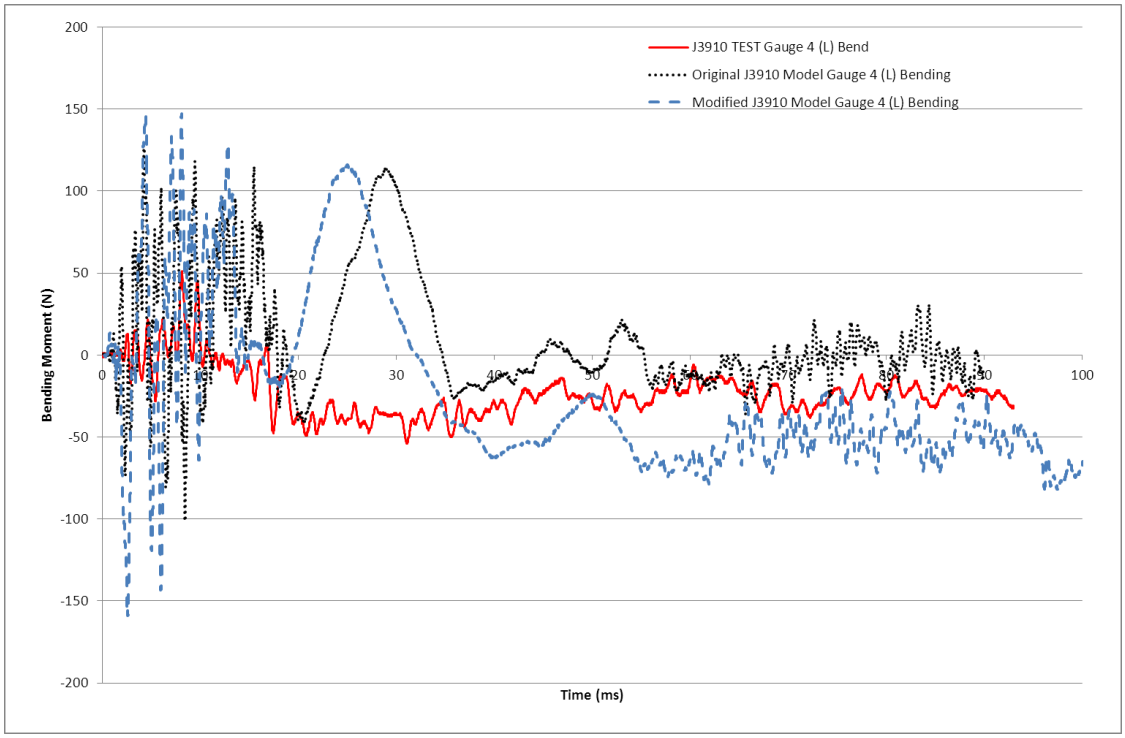

Figure 31 Bending moment results for the GRW tanker J3910 topple test compared to those from the original and modified finite element models for gauge location 4 (longitudinal direction gauge in the centre of compartment 1b)

5.5 VALIDATION DISCUSSION

The correlation between test and model results has been graded as follows; good correlation defined as being within 10%, moderate between 10% and 50% and poor for more than 50% difference between test and model results. Similar approaches have been used in other validation exercises described in literature.

5.5.1 Deformation

The deformations of the modified model show good agreement with the experimental topple test. At all locations, the flat lengths obtained from the finite element model were within 15% of the test values, with the majority within 5%. The mean difference was 5.5%.

5.5.2 Stresses and Bending Moments

The dominant stresses in the tanker near to the important band locations were bending stresses. Therefore, the most important variables to validate the model against are the bending moments near to the bands. It was not possible to calculate bending moments or membrane stresses where the internal strain gauges failed (gauges 5, 7 and 8).

A comparison of the peak bending moments and membrane stresses between the test results and those from the modified finite element model near to the bands are shown in Table 5. The results are expressed in terms of percentage difference between the model and test results. The differences were divided by the test results (test result normalisation) or by the yield stress of 133 MPa (yield stress normalisation). The yield stress normalised results give an indication of the relative importance of the differences when values are small. Where the traces indicate a strong bias to negative or positive values, only the differences in values in that direction have been quoted. The shading represents good correlation in green (within 10%) and moderate correlation (between 10% and 50%) in yellow. Generally good agreement has been demonstrated for the important bending moments near to the bands, with moderate agreement shown for the lower magnitude membrane stresses.

Table 5 Difference in bending moments and membrane stresses calculated from test data and modified finite element model for gauges near to the bands.

(Where two values are reported, they are for minima and maxima)

	Test Result Normalisation		***Yield Stress Normalisation***	
Location	***Bending moment (% difference)***	***Membrane stress (% difference)***	***Bending moment (% difference)***	***Membrane stress (% difference)***
G1 (band B)	+2	+21 / -22	+2	+4 / -7
G2 (band B)	-22	-3 / -7	-16	-0.7 / -2
G5 (band C)			-	-
G6 (band C)	-11	-20	-8	-14
G7 (band E)			-	-
G8 (band E)			-	-
G11 (band F)	-2.3	+36 / -44	-2.6	+6 / -12
G12 (band F)	-0.3	-47	-0.3	-14

The results for the gauges located in the central areas of the compartments are listed in Table 6. Finite element results within 10% of the experimental values are highlighted in green, between 10% and 50% highlighted in yellow, and over 50% highlighted in red. Where two values have been quoted (where positive and negative values are both relevant) the highlighting has been based on the higher difference result. As can be seen, agreement was not as good for the gauges near to the bands. Much of the difference would appear to be due to higher longitudinal bending being predicted by the finite element models.

Table 6 Difference in bending moments and membrane stresses calculated from test data and modified finite element model for gauges at the centre of the compartments.

(Where two values are reported, they are for minima and maxima)

	Test Result Normalisation		*Yield Stress Normalisation*	
Location	***Bending moment (% difference)***	***Membrane stress (% difference)***	***Bending moment (% difference)***	***Membrane stress (% difference)***
G3 (Comp 1b - Hoop)	+35 / 1	+24	+20 / +0.4	+6
G4 (Comp 1b - Longitudinal)	+194 / +188	-27	+19 / +17	-16
G9 (Comp 4 - Hoop)	-27 / -72	-30 / +10	-20 / -87	-3 / +2
G10 (Comp 4 - Longitudinal)	+61 / +88	-8	+7 / +8	-7

5.5.3 Pressure

The pressure results agreed well, in the general trend of the pressures, between the experimental data and the finite element results. Differences in the magnitude of the initial high pressure spikes were observed, but these differences are likely to be due to discrepancies in the precise location of the gauge points.

5.6 OTHER OBSERVATIONS FROM MODELS

5.6.1 Effect of Fillet Welds

The only location where strain gauges were located near to the convex side of a bulkhead was band F, at the rear of compartment 4 (gauges 11 and 12). Gauge locations for the finite element model were based on the test gauge locations. No fillet weld was present at this location, so the effect of fillet welds on the highly tensile internal stresses has not been fully analysed.

However, contour plots of the bending moments show the effect of fillet welds. Each location where a fillet weld has been modelled on a convex side of a bulkhead has been identified in Figure 32 and Figure 33 (taken from modified model).

At locations where no fillet weld had been modelled, the bending moments approaching the band were typically in the order of 1 000 N. Where fillet welds had been modelled, the bending moments were significantly lower, with values in the order of 600 N. Interestingly, the addition

of the fillet weld would appear to reduce the peak bending moment, rather than simply moving the peak to outside the fillet weld location.

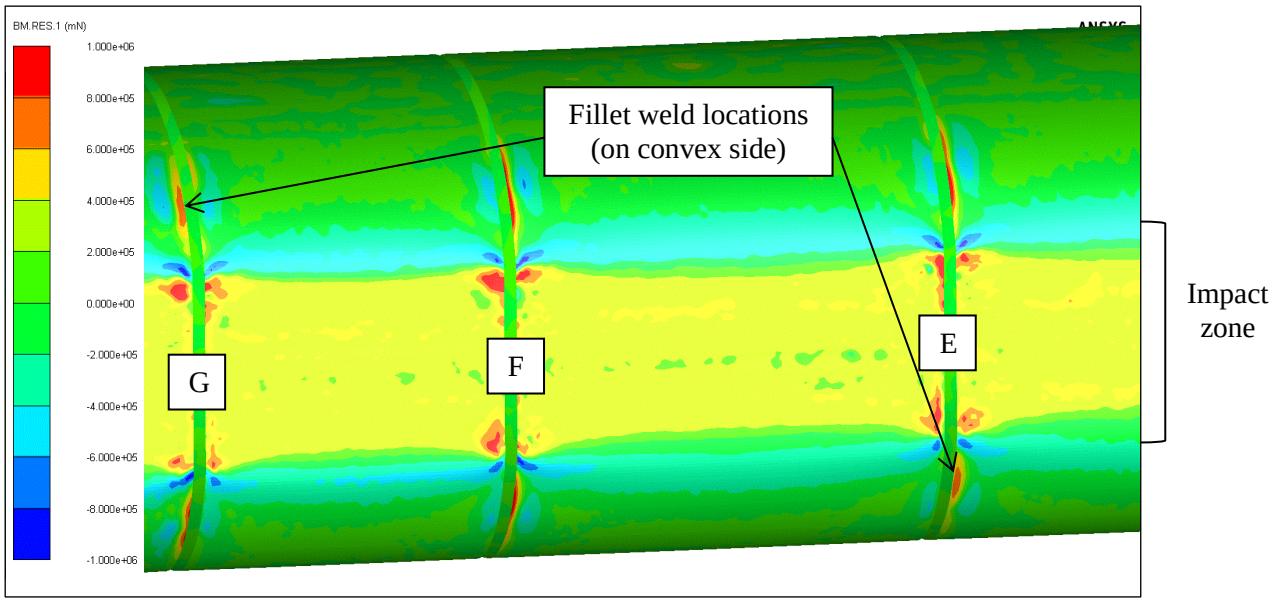

Figure 32 Bending moments in the tanker shell near bands G, F and E with the convex side to the left of band G and to the right of bands F and E

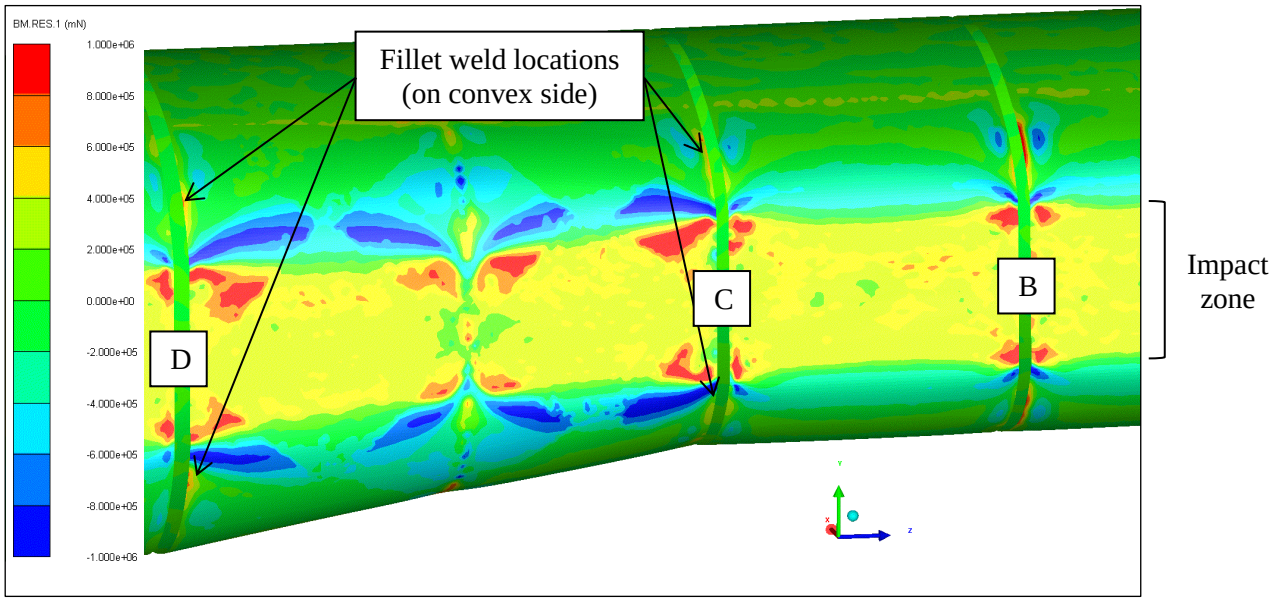

Figure 33 Bending moments in the tanker shell near bands D, C and B with the convex side to the right of bands D and B and to the left of band C

5.6.2 Plastic Strain

The plastic strain in the rear bulkheads is shown in Figure 34. The location of the highest plastic strains was in the buckled sections near to the impact locations, as would be expected.

The peak plastic strains occur to the top and bottom of the flattened section, which corresponds well to the locations of the leaks in the test tankers. The magnitude of the peak plastic strains was in the order of 0.2 (i.e. 20%), a level at which failure may be expected. These values represent the average plastic strain through the thickness of the shell; as the deformation is predominantly bending, higher plastic strains would be likely on the shell surfaces, increasing the likelihood of failure occurring.

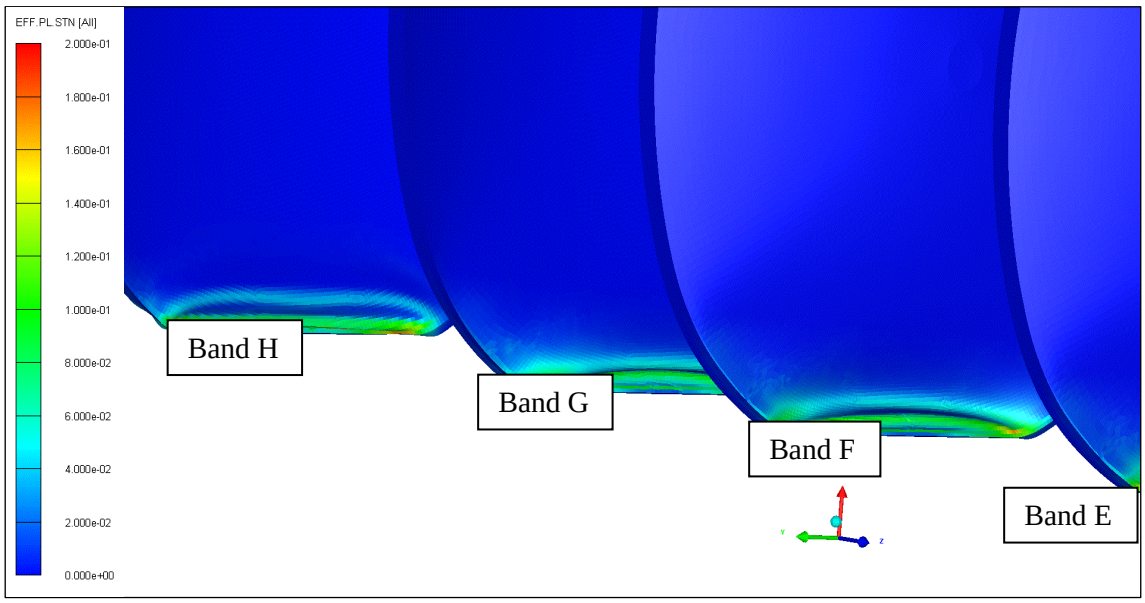

Figure 34 Plastic strain in the bulkheads in the J3910 modified model

6 FUEL LOADS

6.1 FUEL INPUT CONDITIONS

A spreadsheet was supplied by Wincanton detailing the numerous different configurations that could be carried by their fuel tankers for a range of different fuels. In the information provided, the fuel with the highest density was fuel oil, with a density of 0.855 kg/L. Due to the higher density than petrol, filling each compartment to the stated capacity with fuel oil would result in the maximum load for the tanker being exceeded. Therefore, in the Wincanton configuration, compartment 3 is left empty when carrying only fuel oil, with compartment 5 slightly below capacity. Due to a slightly different split in compartment capacities between the GRW tankers being tested and those assumed in the Wincanton configurations, it was not necessary to reduce the level in compartment 5 to remain below the maximum tanker weight. This configuration is illustrated in Figure 35.

With the previous models, only the end bulkheads were modelled as coupling surfaces; all other bulkheads and the baffle would have similar pressures on both sides. However, with compartment 3 left empty, the bulkheads on each side of this compartment, at band D and band E, were defined as coupling surfaces. In both cases, the artificial thickness was applied to the coupling surface so that it lay in compartment 3, therefore not resulting in any unwanted fluid loss.

The total volume of fuel oil modelled was 35 750 L, with a total mass of 30 566 kg, compared to a maximum of 31 380 kg (based on the maximum gross mass of 37 000 kg and a stated tare mass of 5 620 kg).

Two impact velocities were modelled; 2.0 rad/s to provide a direct comparison with the water model, and 2.6 rad/s to assess a possible worst case scenario. Impact velocities for rollover in real accidents of between 100 degrees/s to 150 degrees/s were reported [2] which correspond to 1.75 rad/s to 2.62 rad/s.

The petrol model was filled to the same level as for the fuel oil model, with the exception being that the third compartment was filled to the same level as the other rear compartments, as shown in Figure 36. This resulted in a fluid volume of 42 335 L, equivalent to a mass of 30 693 kg assuming a density of 0.725 kg/L.

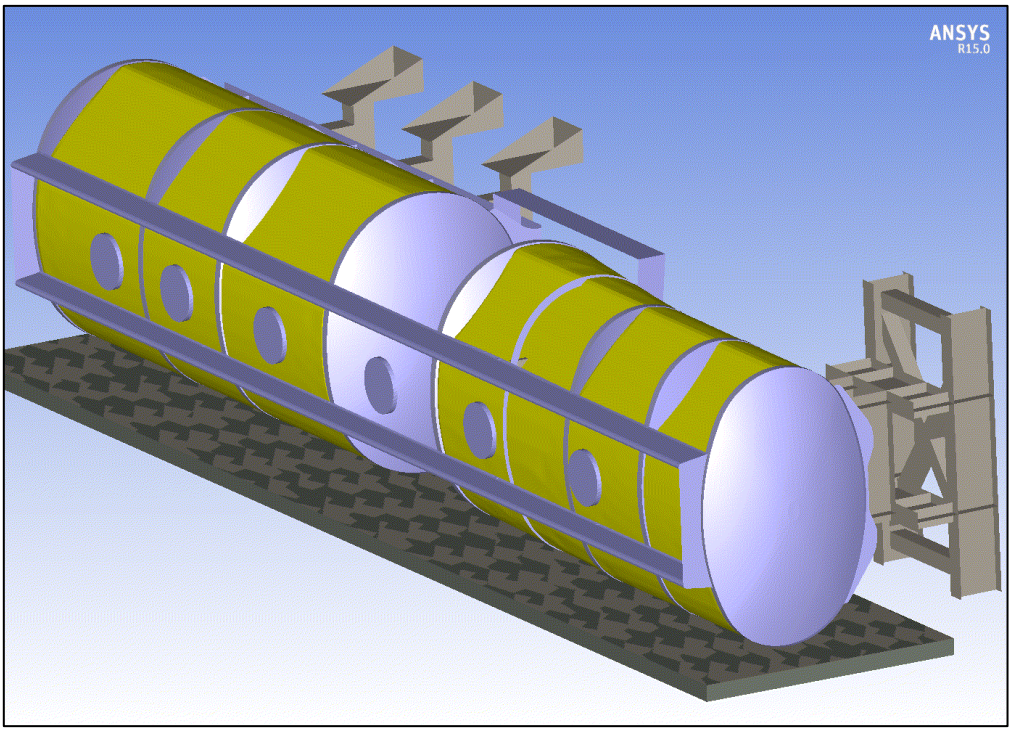

Figure 35 Fuel oil model showing initial location of the fuel

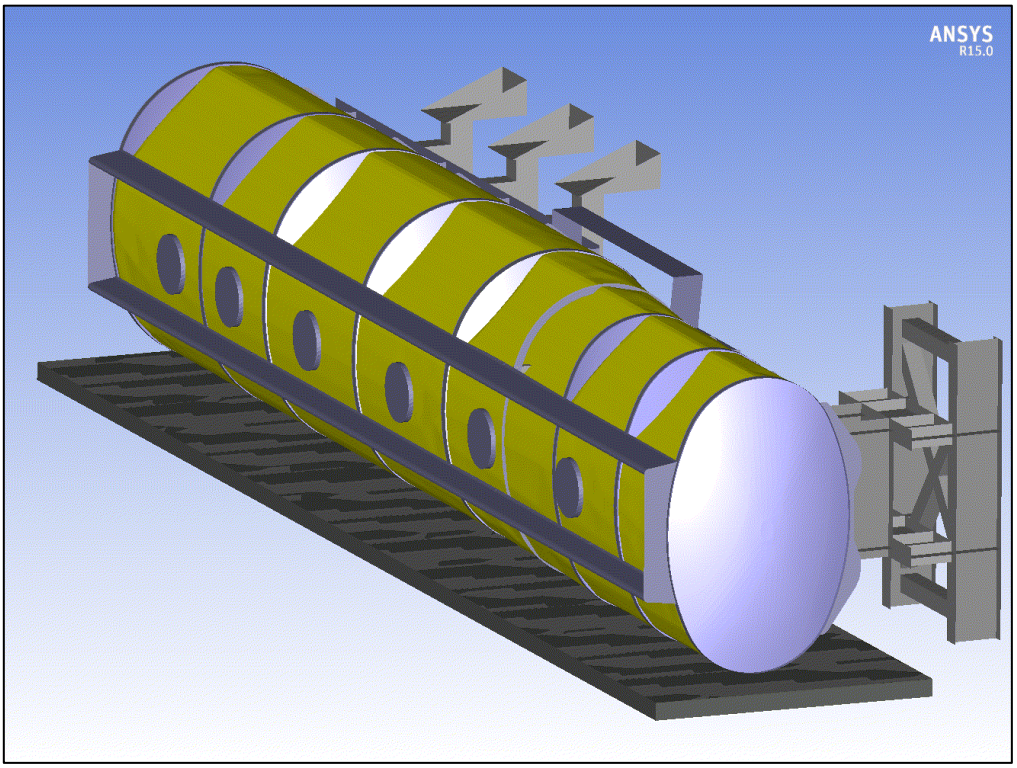

Figure 36 Petrol model showing initial location of the fuel

6.2 DEFLECTION RESULTS

The compression of the front band (A), rear band (H) and the band at the rear of the conical section (D) are shown in Figure 37 for water with an impact velocity of 2.0 rad/s and fuel oil with impact velocities of 2.0 rad/s and 2.6 rad/s. The deflection of the front band shows little variation between water and fuel oil. However, the deflection of the rear band was approximately 17 % higher for the tanker filled with fuel oil. The impact velocity was shown to have little influence on the deflections recorded for fuel oil. The higher impact velocity model solution failed at approximately 70 ms due to excessive deflection near to the bands. The data up to this point remains valid.

The effect of filling the tanker with different liquids is shown in Figure 38, all for an impact velocity of 2.0 rad/s. In contrast to the fuel oil model, where compartment 3 was empty, the petrol model shows an increase in deflections at all band locations compared to water. Increases of 12 % and 22 % were obtained at the front and rear respectively for petrol compared to water.

It is not clear why deflections of the tanker vary so much with different liquids when the overall mass, and therefore inertia and energy, are the same. For an equivalent mass, a lower density liquid, such as petrol, would have a larger volume, and therefore a higher fill level. The different fill levels and densities should give the same pressure head at the lowest point using the equation; pressure head = density × acceleration due to gravity × height of liquid. However, at any position above the lowest point, the pressure due to the petrol fill would be higher, as illustrated in Figure 39. This example assumed a circular tanker with a 1 m radius, with the water fill at 70 % of total volume, and petrol fill at 95 % of total volume, giving the same total mass of liquid. The hatched area on the chart shows the difference in pressure between water and petrol fills. This factor may be a mechanism that leads to higher levels of deflection for the fuel cases.

An alternative explanation may be related to the amount of free space in the different scenarios. For a water fill, 30 % of the volume of the tanker would be free space, allowing movement of the liquid during the impact. Reducing the free space to just 5 %, as for the petrol model, significantly reduces the opportunity for sloshing movement. Without further research it is not possible to determine which of these effects is most significant.

The levels of plastic strain in the bulkheads are listed in Table 7, and increase with increasing levels of deflection. Both the through-thickness average and values near the inner surface are listed, with the strains near the surface significantly higher due to the predominantly bending nature of the strain.

Table 7 Maximum plastic strains occurring in the bulkheads

Liquid	***Maximum equivalent plastic strain (through- thickness average)***	***Maximum equivalent plastic strain (near inner surface)***
Water	20 %	32 %
Fuel Oil	25 %	37 %
Petrol	34 %	41 %

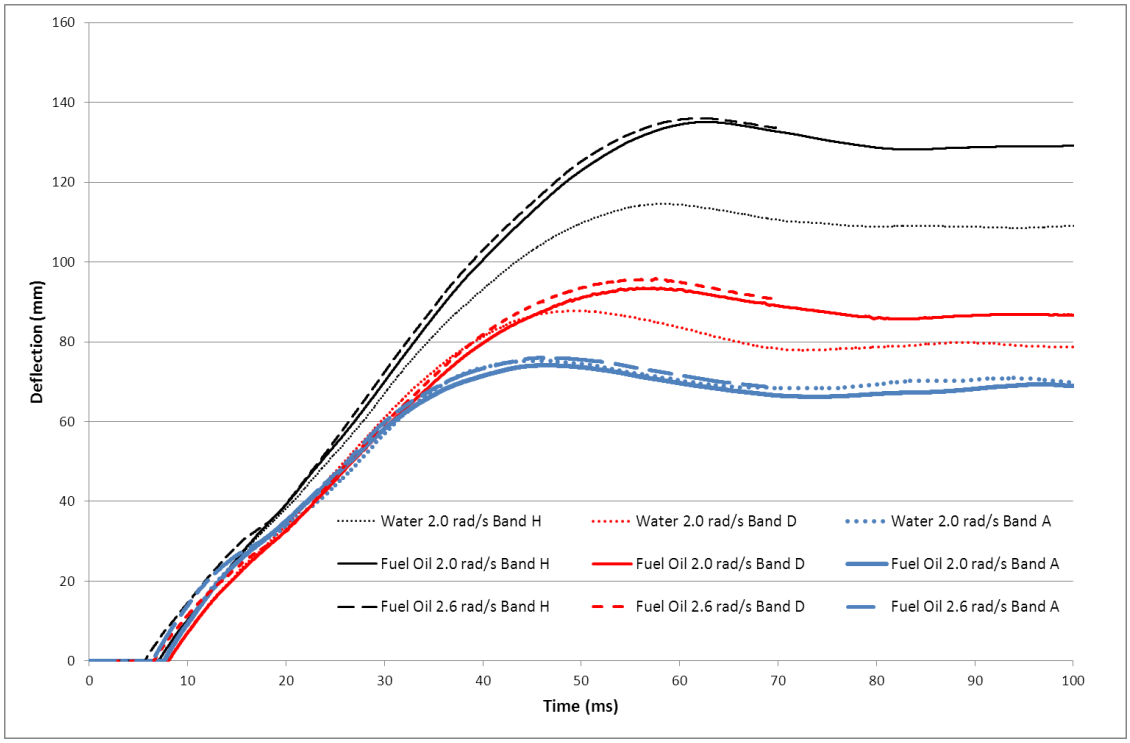

Figure 37 Effect of tanker load (fuel oil/water) and impact velocity on deflections of the bands

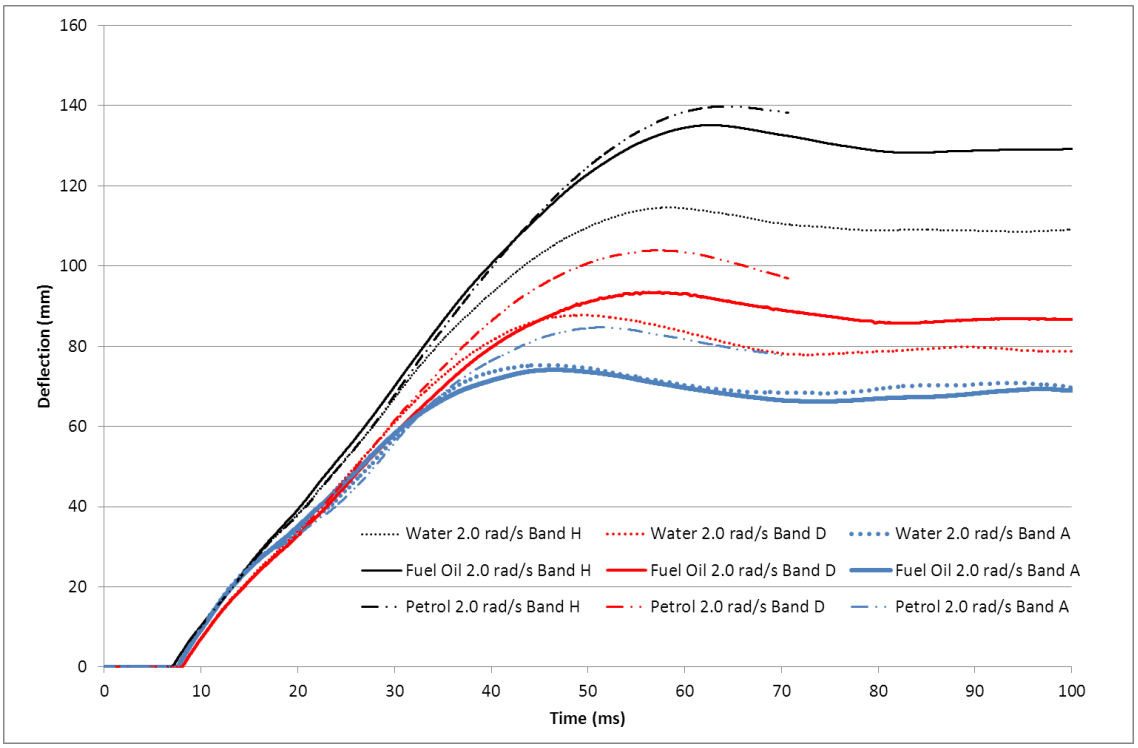

Figure 38 Effect of tanker load (fuel oil/water/petrol) on deflections of the bands

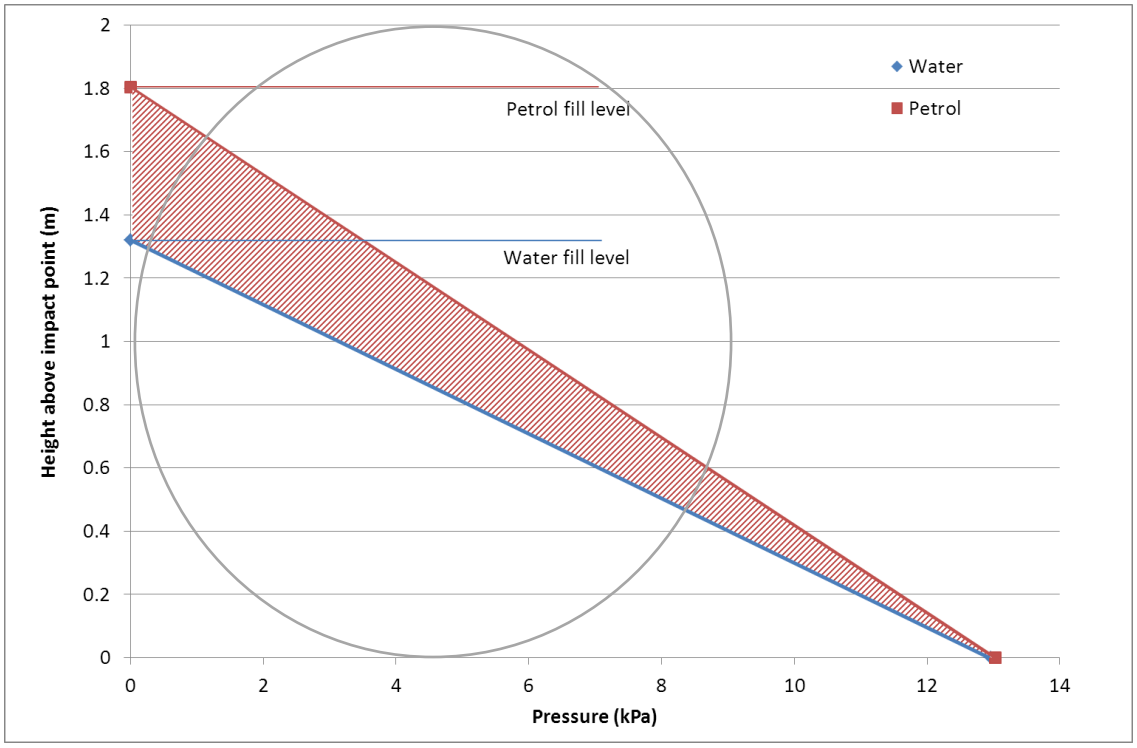

Figure 39 Illustration of the effect of different liquid densities and fill levels on pressure

6.3 PRESSURE RESULTS

The pressure results for the impact location are shown in Figure 40 and Figure 41 for compartments 1b and 4 respectively. The charts show higher pressures for the fuel oil models than the water models after the initial impact event has occurred (i.e. from 30 ms to 60 ms). At this time, the liquid is still decelerating (the pressure is much higher than the static head). Although the fuel oil is of lower density than water, the increased volume of fuel oil in the filled compartments compared to water would mean a greater mass of liquid, and therefore a higher pressure. Pressure traces for the petrol model were not recorded.

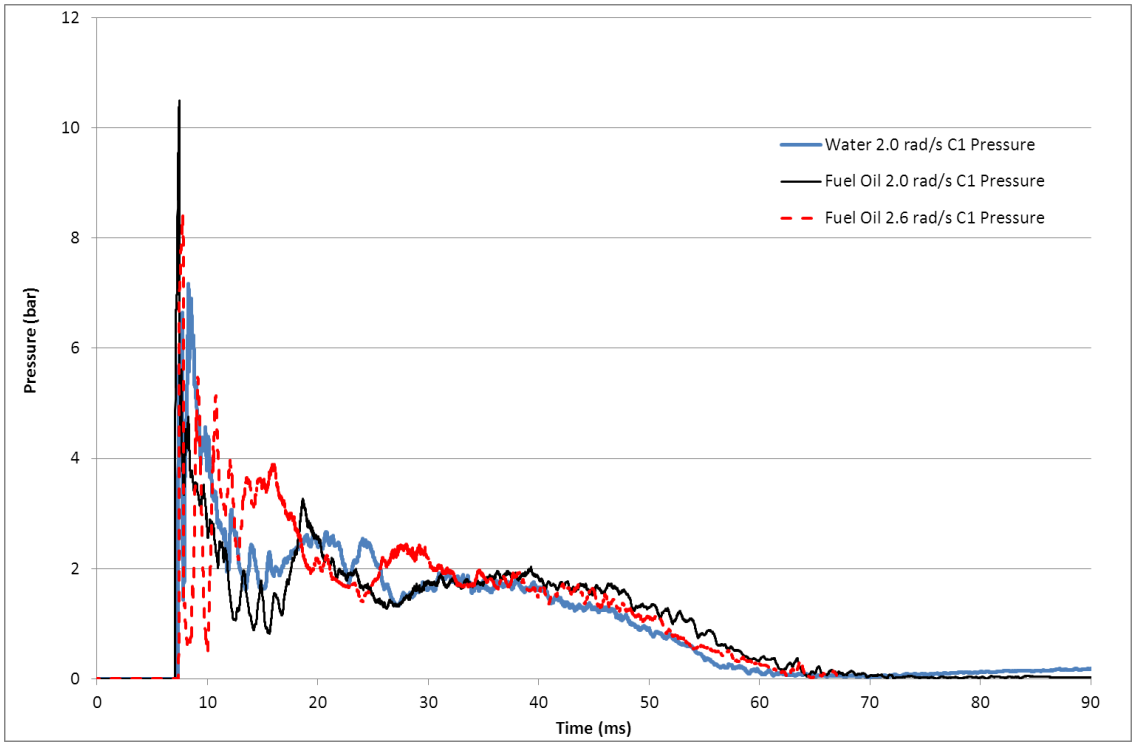

Figure 40 Comparison of compartment 1b pressures for water and fuel oil (2.0 rad/s and 2.6 rad/s impact velocities) loads

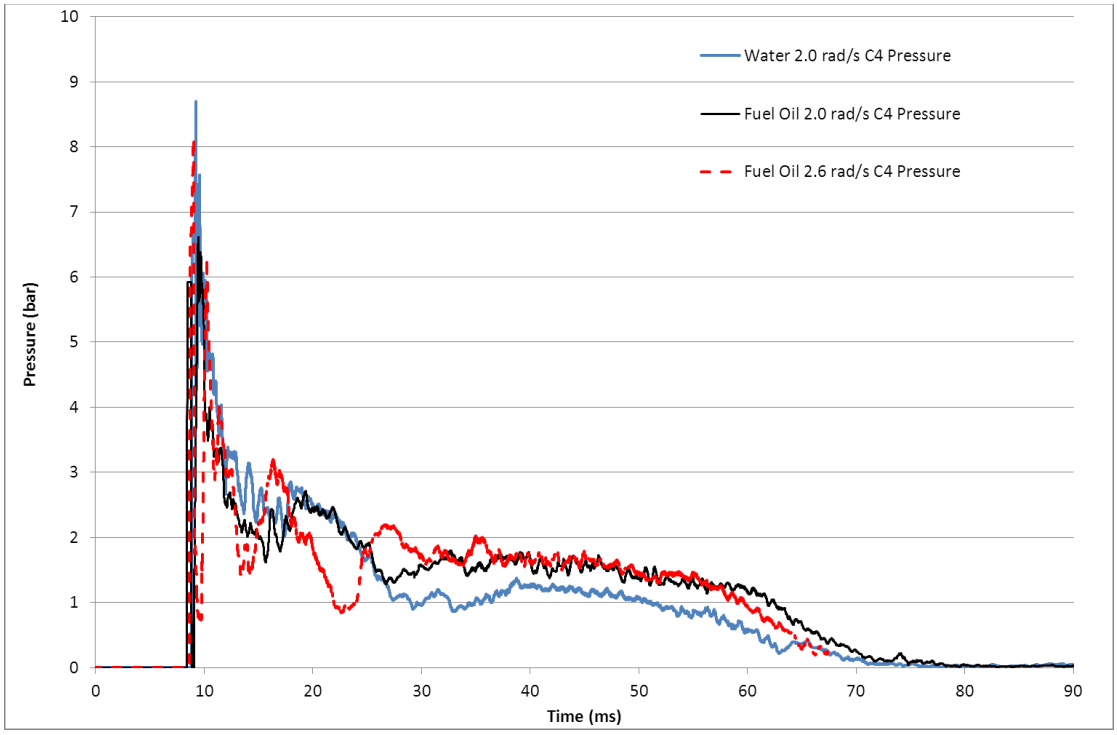

Figure 41 Comparison of compartment 4 pressures for water and fuel oil (2.0 rad/s and 2.6 rad/s impact velocities) loads

6.4 STRESS AND BENDING MOMENT RESULTS

The full membrane stress and bending moment results for water and fuel oil models are provided in Appendix D.

The effect of the different load being carried would appear to be highly dependent on locations. At the front of the tanker, little difference can be seen in the bending moment, as shown in Figure 42. The petrol model resulted in slightly higher levels of bending, which corresponds to the higher levels of deflection at this location.

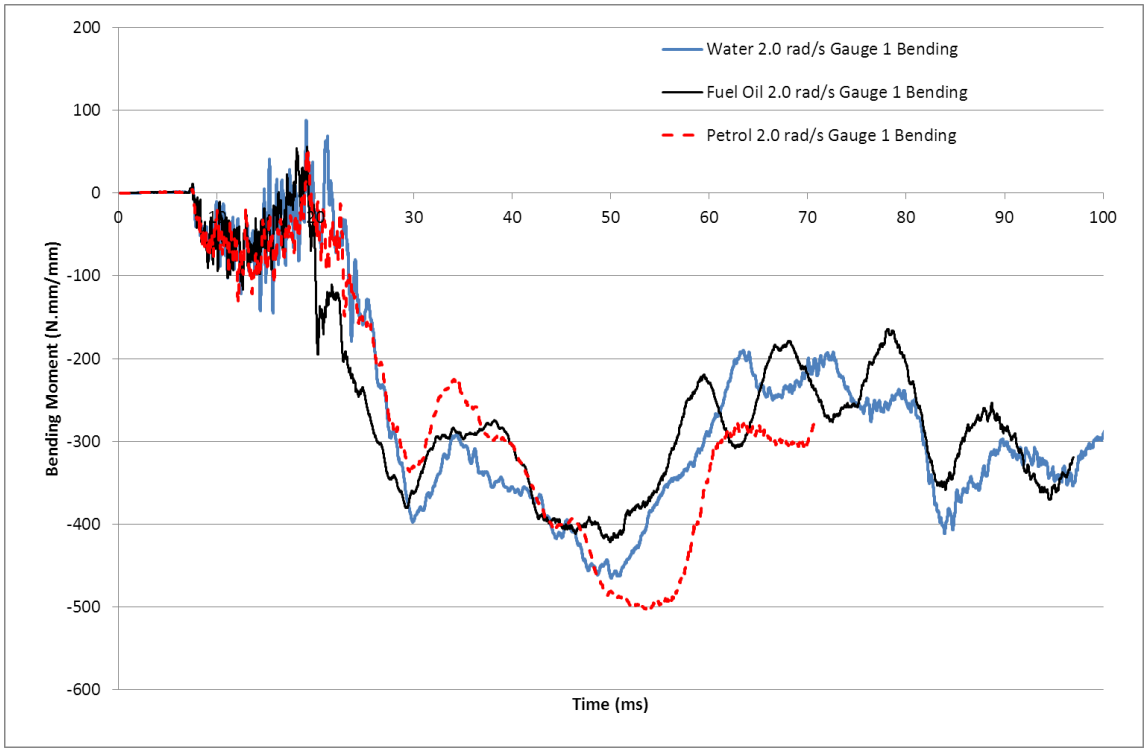

Figure 42 Bending moments near to band B showing little difference

The bending moments near to band E show large differences between the models with water and petrol and the model with fuel oil, as shown in Figure 43. In the fuel oil model, compartment 3 was left empty, and band E was the bulkhead separating compartments 3 and 4. Therefore, significant differences would be expected as the pressure due to the fuel oil was just acting on one side.

At the rear of the compartment 4, near the rear of the tanker, the bending moments due to the fuel oil and petrol were higher than for the water, although the pattern was similar, as shown in Figure 44. This corresponds to the higher deflections observed at the rear of the tanker.

The bulkhead between compartments 2 and 3 (band D) was convex towards compartment 2. With compartment 3 empty for the fuel oil model, the pressure only on the convex side led to unusual deformation on this bulkhead, as shown in Figure 45. This type of deformation was not observed for the water or petrol cases (shown in Figure 46) where no compartment was left empty. No gauges were located at either side of this band so a full assessment of the effect of this deformation on the stresses in the shell was not possible from this model.

It would appear that the impact velocity has less effect on the bending moment and stress results than the change in load configuration.

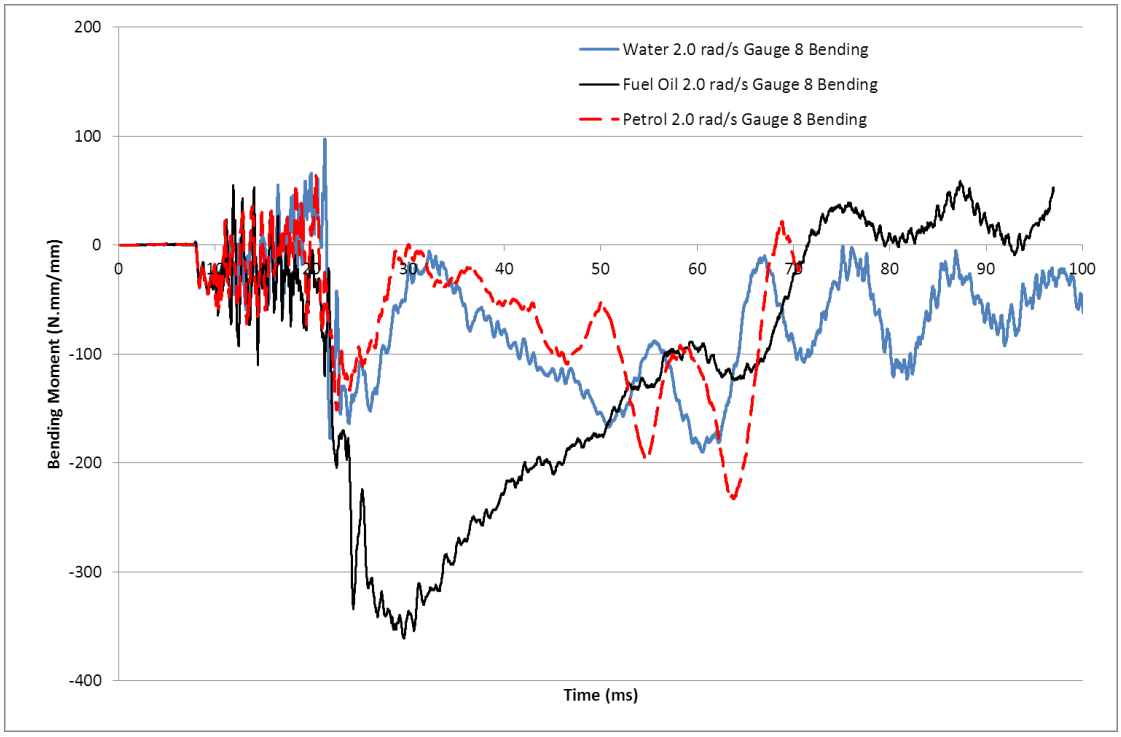

Figure 43 Bending moments near to band E showing large differences

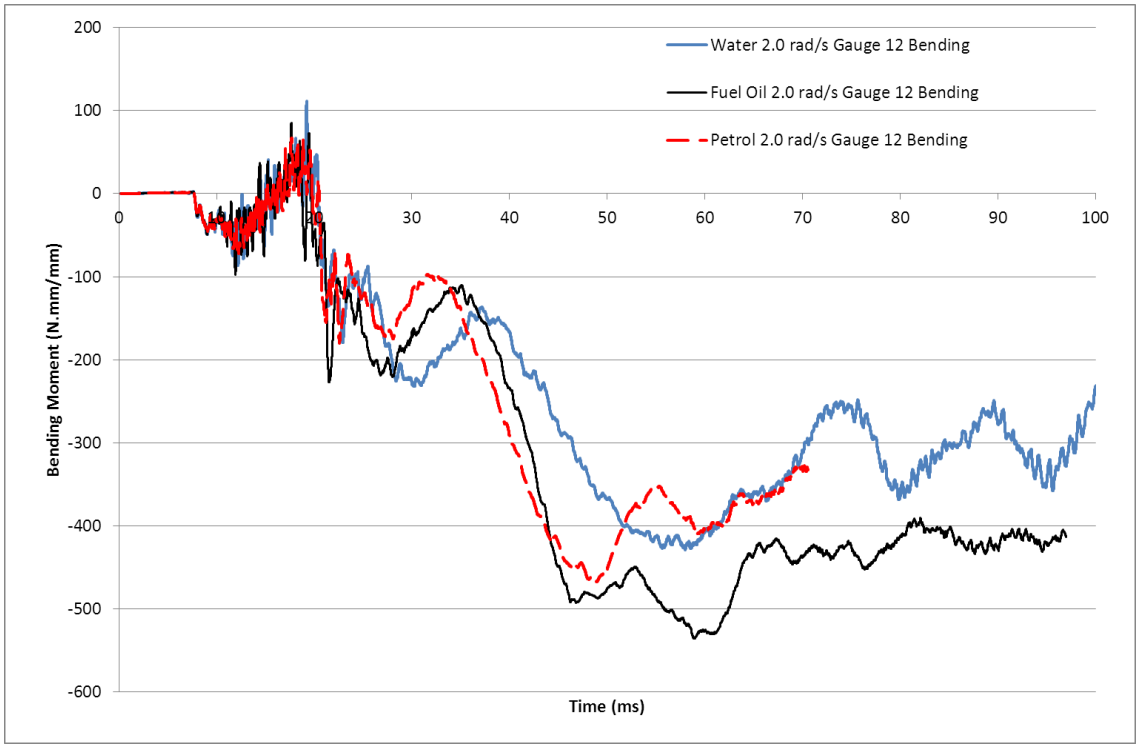

Figure 44 Bending moments near to band F

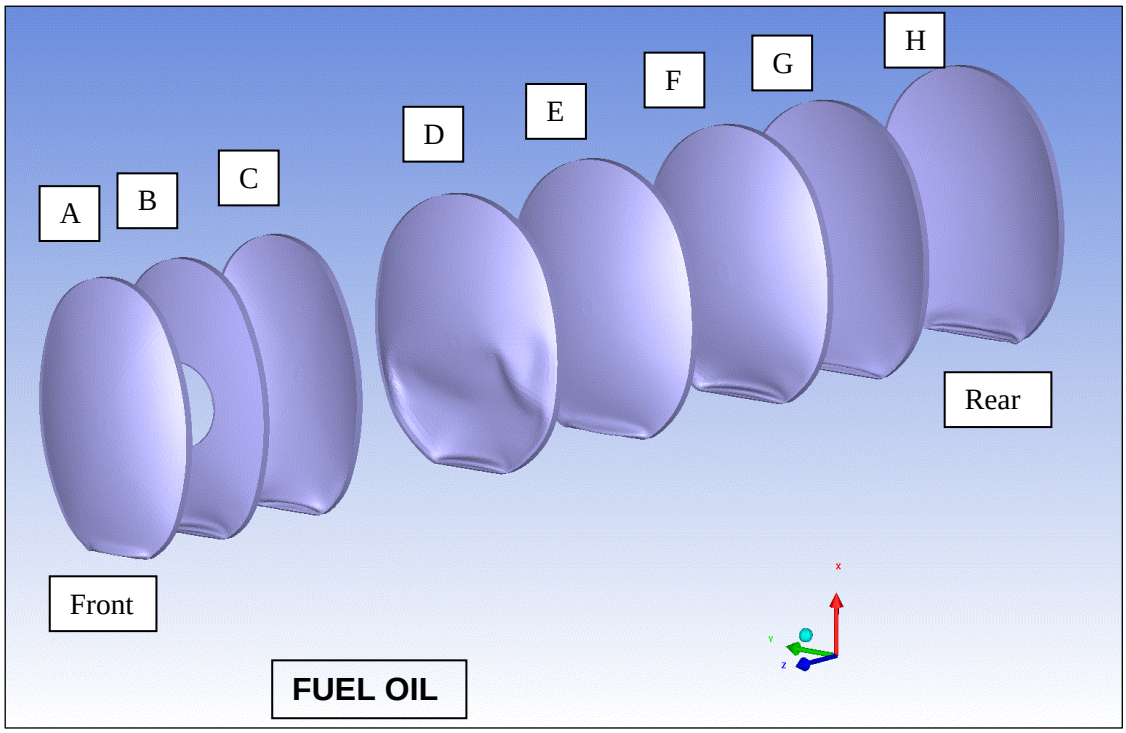

Figure 45 Deformed bulkheads due to fuel oil impact at 2.6 rad/s clearly showing effect of pressure only on the convex side of bulkhead D

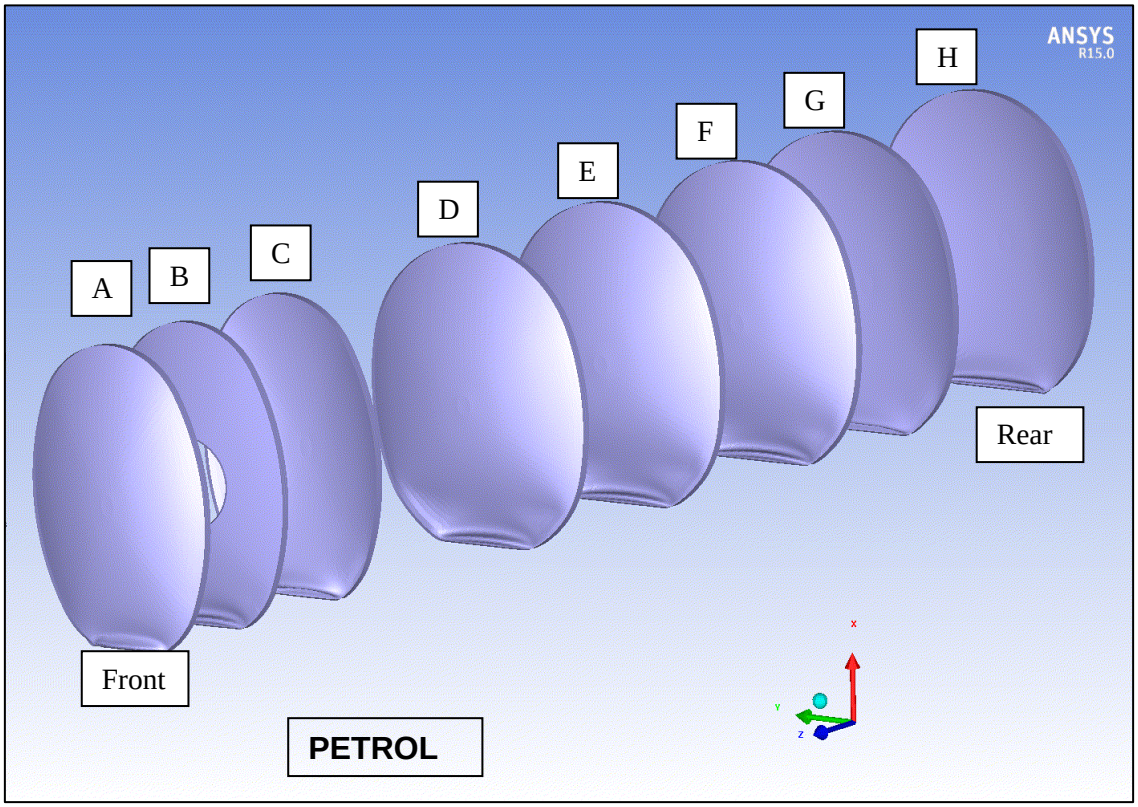

Figure 46 Deformed bulkheads due to petrol impact at 2.0 rad/s

6.5 FUEL FILL CONCLUSIONS

It is clear that the behaviour of a tanker is dependent on the load that it carries. From the modelling of a tanker with full loads of fuel oil and petrol it has been shown that there is the potential for higher levels of damage to occur than if an equivalent mass of water were used. It has also been shown that loading configuration (for example, running with a compartment empty) can change the pattern of the deformation. This has been shown by the increased deflection at the rear of the tanker, the higher levels of bending moment, and the different behaviour of some bulkheads due to the empty compartment.

7 OUTPUT FOR WP2 ENGINEERING CRITICAL ASSESSMENT

7.1 FUEL MODELS

For the WP2 Engineering Critical Assessment (ECA) of the circumferential welds, the membrane and bending stresses acting on the joint were required. TWI created axisymmetric finite element models of the weld geometries to obtain stress intensity factor and reference stress solutions for different crack depths and weld cap geometries. The inputs for these models were bending moment and membrane stress. As these variables were more readily obtained from the tanker models than through-wall bending stresses, it was bending moments that were supplied. Also, the relationship between bending moment and through-wall bending stress was dependent on the thickness of the section at the point of interest, which was a variable in the ECA work, and the stress-strain relationship assumed.

The bending moments were highest at the rear of the tanker, which is shown in Figure 47 for the fuel oil model and Figure 48 for the petrol model. The patterns and values of bending moments were very similar for the two models, with the exception of the area adjacent to band E, when the compartment was empty for the fuel oil model. There were areas of high bending moment within the impact zone, and also outside the impact zone close to the bands. The high bending moments here lie between the end of the impact zone and the comb, with the highest moments moving up as the size of the impact zone flat increases. This is shown in graphical form in Figure 49. As can be seen, the high bending moment areas cover a relatively large section, with bending moments in excess of 1000 N·mm/mm for over 200 mm. As this bending moment is due to the deformation of the bulkheads, rather than a pressure pulse, the duration is longer. The bending moments near to band F were very similar between the fuel oil and petrol models, as shown in Figure 50.

In these areas, which occur on the convex side of the bulkheads, the bending moment increased rapidly as proximity to the weld increased, as shown in Figure 51. The membrane stresses were comparatively low and constant with weld proximity so are not shown. Despite the large difference in the levels of deflection observed for the different liquids modelled, the maximum levels of bending moment near to the bands varied only slightly. This is likely to be due to the plastic strains in the shell limiting the level of bending moments possible. Values of bending moment and membrane stress were obtained for the weld location by extrapolating the values from the fuel oil model with an impact velocity of 2.6 rad/s. These values of 1460 N·mm/mm for bending moment and 21.5 MPa for membrane stress were given to TWI for the ECA. Due to the limiting effect of the plastic strains in the shell, other loading scenarios would be unlikely to give significantly different results.

7.2 WATER MODEL

During post-mortem examination of the rear of GRW tanker J2580 by TWI, a through-wall crack along the circumferential weld at the top of the impact zone in Band H+ was examined. This crack was located at the upper end of the flat created by the impact. The values of the bending moments in this area have been obtained from the modified finite element model (with a water load) using the same 1.89 rad/s impact velocity as in the J2580 topple test. The results are shown in Figure 52. Where the bending moment was increasing towards the weld plane extrapolation was performed using the two closest values to give the value at the weld plane. Bending moments at the band H+ weld plane for the locations assessed ranged from 1350 N·mm/mm to 1500 N·mm/mm. These values were given to TWI for the ECA, and were similar to those obtained for the fuel cases at Band F+.

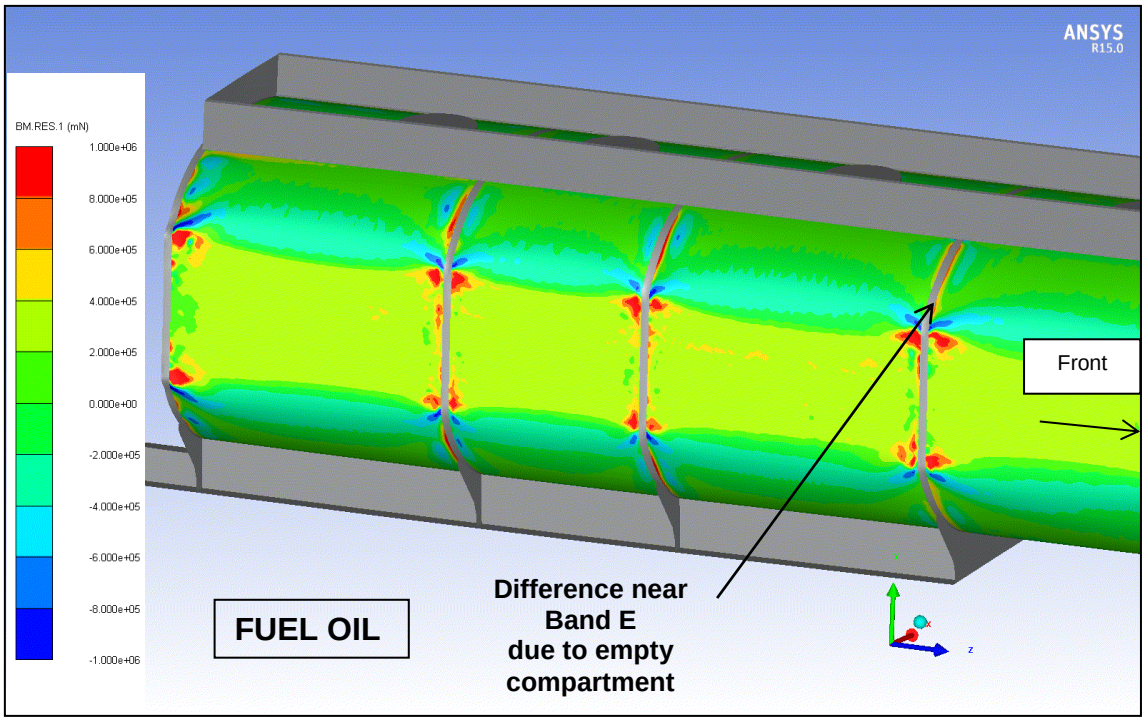

Figure 47 Bending moments per unit length at the rear of the tanker shell under fuel oil (2.6 rad/s) loading conditions

(for clarity, moments in other components not shown)

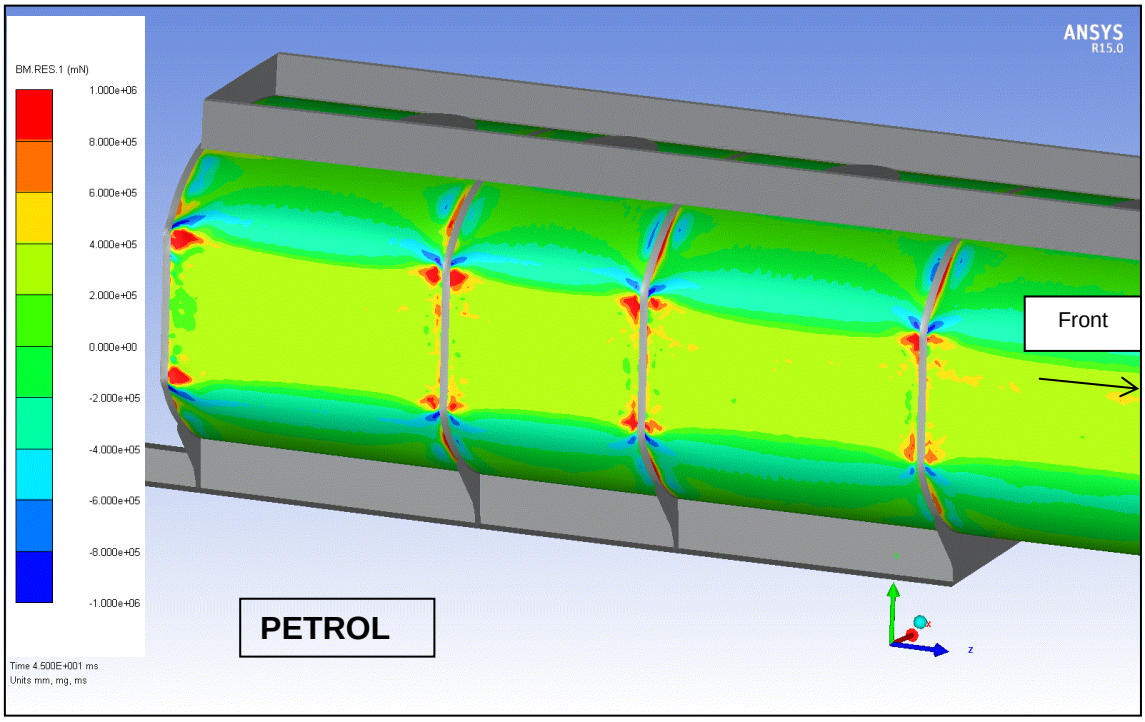

Figure 48 Bending moments per unit length at the rear of the tanker shell under petrol (2.0 rad/s) loading conditions

(for clarity, moments in other components not shown)

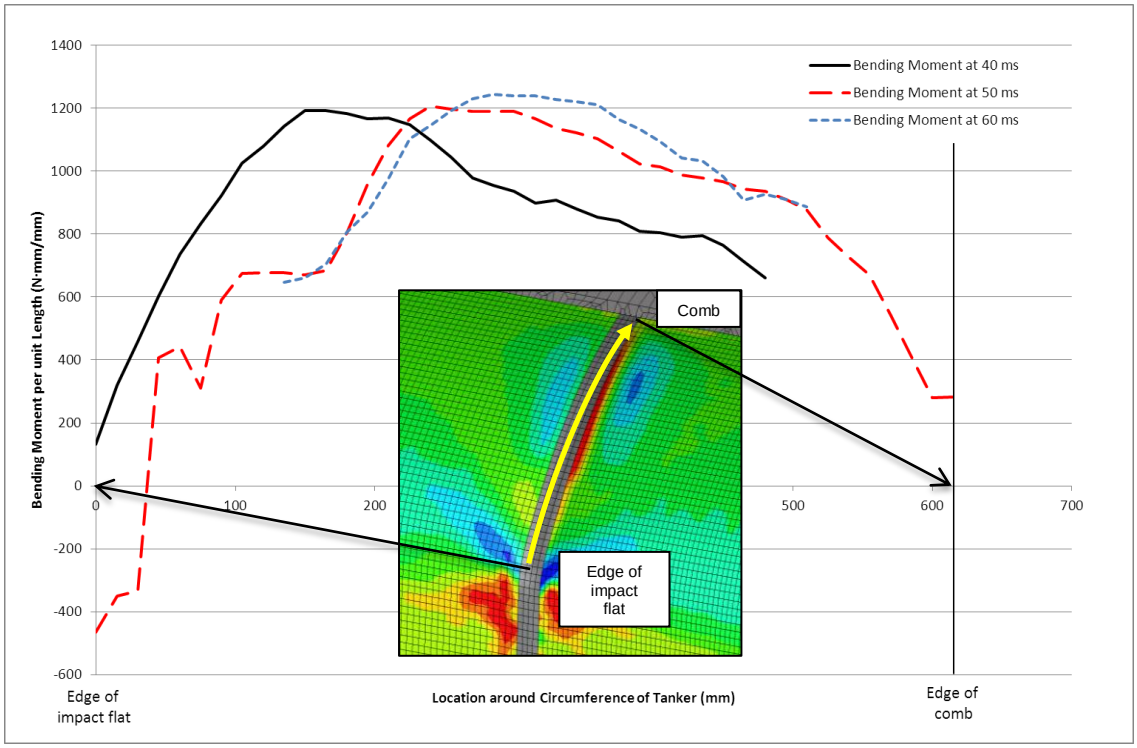

Figure 49 Bending moments next to Band F+ showing variation around the tanker circumference and with time for fuel oil (2.6 rad/s)

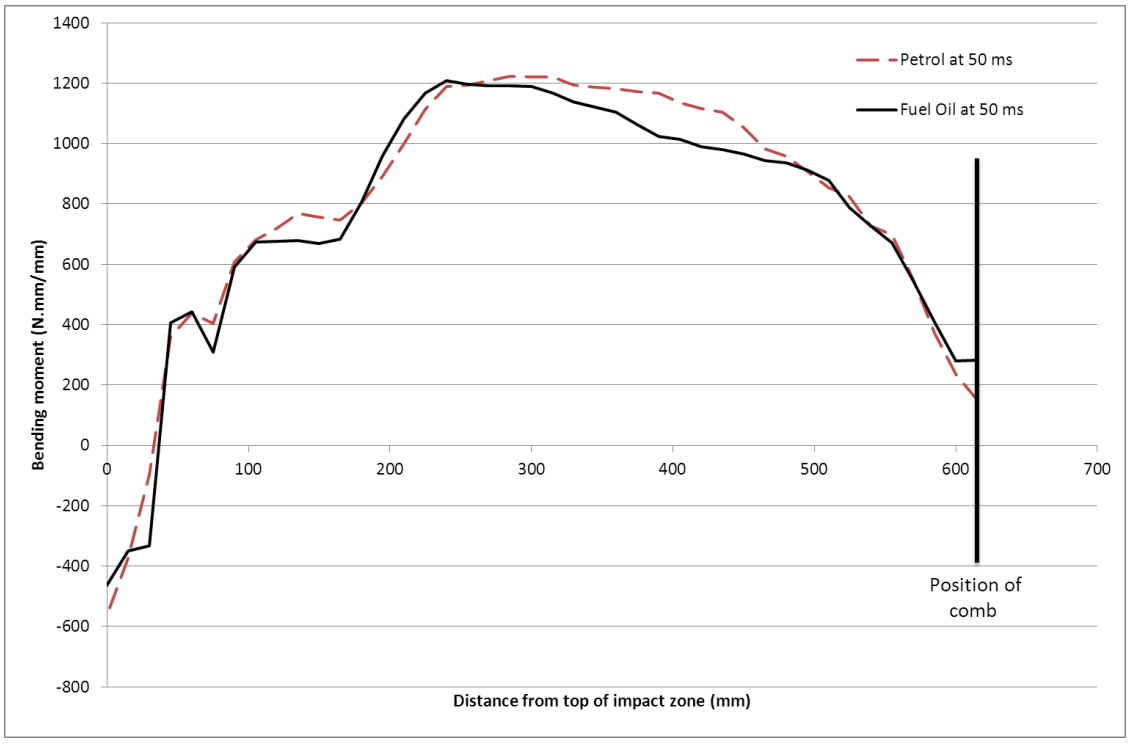

Figure 50 Bending moments next to Band F+ showing variation due to fuel (petrol 2.0 rad/s, fuel oil 2.6 rad/s)

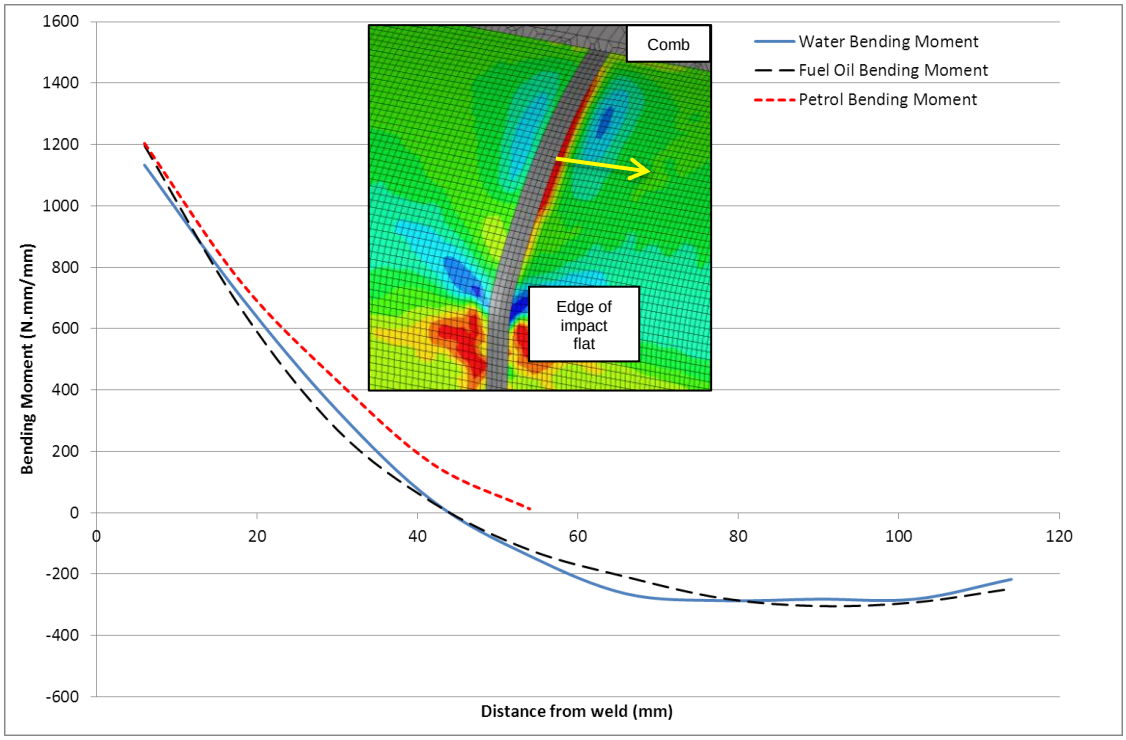

Figure 51 Variation in bending moments with distance from the weld (Band F+) for water(2.0 rad/s), fuel oil (2.6 rad/s) and petrol (2.0 rad/s)

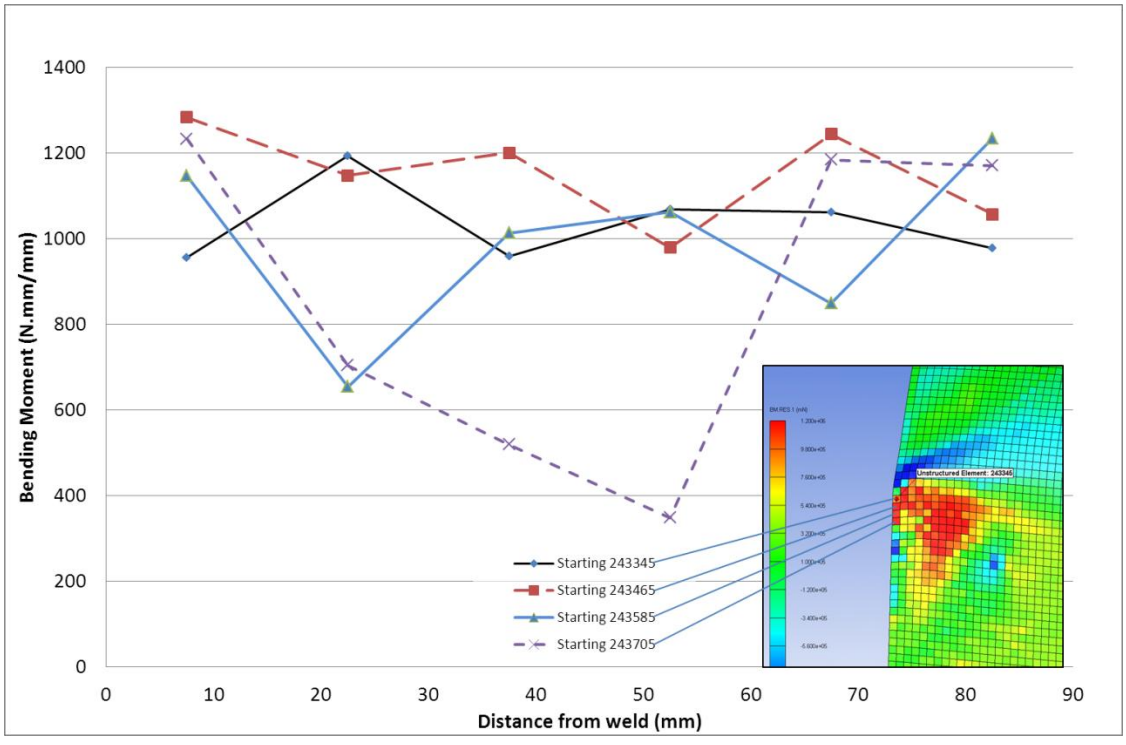

Figure 52 Variation in bending moments with distance from the rear weld (Band H+) for water at 1.89 rad/s

8 CONCLUSIONS

Model refinement

Finite element models of GRW tankers J2580 and J3910 were created, and the effect of differences between the tankers on model outputs considered. The key difference were the extrusion profile and the position of fillet welds between the extrusion band and the shell. There were only small differences between the J2580 and J3910 finite element model results. This was a similar outcome to the topple test results, which were very consistent between the tests of GRW tankers J2580 and J3910.

Impact velocity did not have a major influence on the results from the finite element analysis for the conditions modelled, which were water with impact velocities of 1.89 rad/s and 2.0 rad/s, and fuel oil with impact velocities of 2.0 rad/s and 2.6 rad/s.

The orientation of the bulkheads was shown to have a large effect on the bending moments in the tanker shell near to the extrusion bands. The bending moments were higher in the positive direction (putting the inner surface of the tanker shell in tension) on the convex side of the bulkheads. This was probably due to the buckling of the bulkheads during impact resulting in a slight twisting of the extrusion band.

Results from the models suggest that internal fillet welds between the extrusion band and the shell reduce the bending moment in the shell next to the extrusion bands. It would appear that the bending moments at the shell/extrusion band interface are reduced, and not just moved to the fillet weld location. More detailed examination, with more detailed modelling of the fillet weld, would be needed to confirm the extent of the benefits of the fillet weld and the effect of intermittent, rather than continuous, fillet welds.

Model validation

As there was little difference between the J2580 and J3910 finite element models, for validation the outputs from the J3910 model were compared to topple test data for GRW tanker J3910. Good agreement was obtained between the modified finite element model results for deformation and the topple test results based on laser scan data. All the flat lengths measured were within 15%, with the majority of locations showing less than a 5% difference.

The bending moments near to the extrusion bands showed generally good agreement between the test values and the finite element values. The largest difference between test and model results was 22%, with most other results within a few percent. The membrane stress results showed a larger variation between test and model results. Membrane stresses were generally much lower than the bending stresses at these locations, and therefore greater differences are not as important.

The finite element models did not predict the bending stresses in the central regions of the compartments well. In particular, bending moments in the longitudinal direction were significantly overestimated by the finite element models, although at this location, the bending moments were very small.

Good agreement was found between the pressures recorded during the test and those generated in the finite element analyses for the overall trends during the impact event. The magnitude of the initial pressure spikes was found, in the finite element model, to reduce rapidly as the measurement distance from the tanker wall increased. Differences in the magnitude of the initial pressure spikes between the finite element model and test values can be attributed to

difficulties in correlating the location of the finite element gauge points to the physical locations of the pressure transducers during tests.

The highest levels of plastic strain were observed in the bulkheads, at the top and bottom of the flat generated by the impact, and where of a magnitude where failure may occur. It was at the top of this flat where obvious leaks occurred during the topple tests on GRW tankers J2580 and J3910.

Overall, HSL's finite element model for J3910 correlates strongly with the topple test data for GRW tanker J3910, thus providing good validation for the model.

Modelling a real-world fuel load

Modelling a tanker with representative loads of fuel oil and petrol, as opposed to water, led to significantly higher deformations in the tanker. In fuel oil scenario, the tanker was filled to the stated capacity for each compartment except the third compartment of six from the front (the first compartment after the tanker's expanding conical section) which was left empty, in line with industry practice. The empty compartment was to prevent the tanker being overloaded due to the higher density of fuel oil than petrol.

This empty compartment resulted in differences in the stresses in the tanker shell close to the bulkheads separating the filled and empty compartments. The lower half of the bulkhead on the front side of the empty compartment, with pressure only applied by fuel oil to the convex side of the bulkhead, was partially inverted, with the direction of deformation into the empty compartment. This deformation was significantly different to that for water or petrol on both sides of the bulkhead. In contrast, deformation of the bulkhead on the rear side of the empty compartment, where pressure was only applied by fuel oil to the concave side of the bulkhead, rather than to both sides of the bulkhead by water, was not significantly different in this model to that for water.

By comparing the results for fuel models with the model for an equivalent mass of water, the water model showed lower levels of deformation and plastic strain. Therefore, the topple tests with water may not be as severe on the tanker as topple tests using fuel oil or petrol.

Outputs for WP2 Engineering Critical Assessment (ECA)

Using the 2.6 rad/s fuel oil model, single values for bending moment (1460 N·mm/mm) and membrane stress (21.5 MPa) at the front side of the rear extrusion band in compartment 4 were extrapolated from model elements close to the circumferential weld and supplied to WP2 for the detailed ECA. The limiting effect of the plastic strains in the shell means that other loading scenarios would be unlikely to give significantly different results. In addition, to support WP2 assessment of the through-wall crack along the rearmost circumferential weld at the top of the impact zone for GRW tanker J2580, values for a 1.89 rad/s water model were supplied to WP2. At the location corresponding to the crack, bending moments up to 1500 N·mm/mm were extrapolated in the same way.

9 REFERENCES

[1] I.N. Bysh and M.R. Dorn 'The generation of internal pressure in tanker rollover', HSE Contract Research Report No 109/1996.

[2] B.J. Robinson, T. Robinson, M Tress and M. Seidl, 'Technical Assessment of Petroleum Road Fuel Tankers - Accident Data and Regulatory Implications' TRL Project Report RPN2925, 2014

APPENDIX A FULL J2580/J3910 COMPARISON RESULTS WITH IMPACT VELOCITY OF 2.0 RAD/S

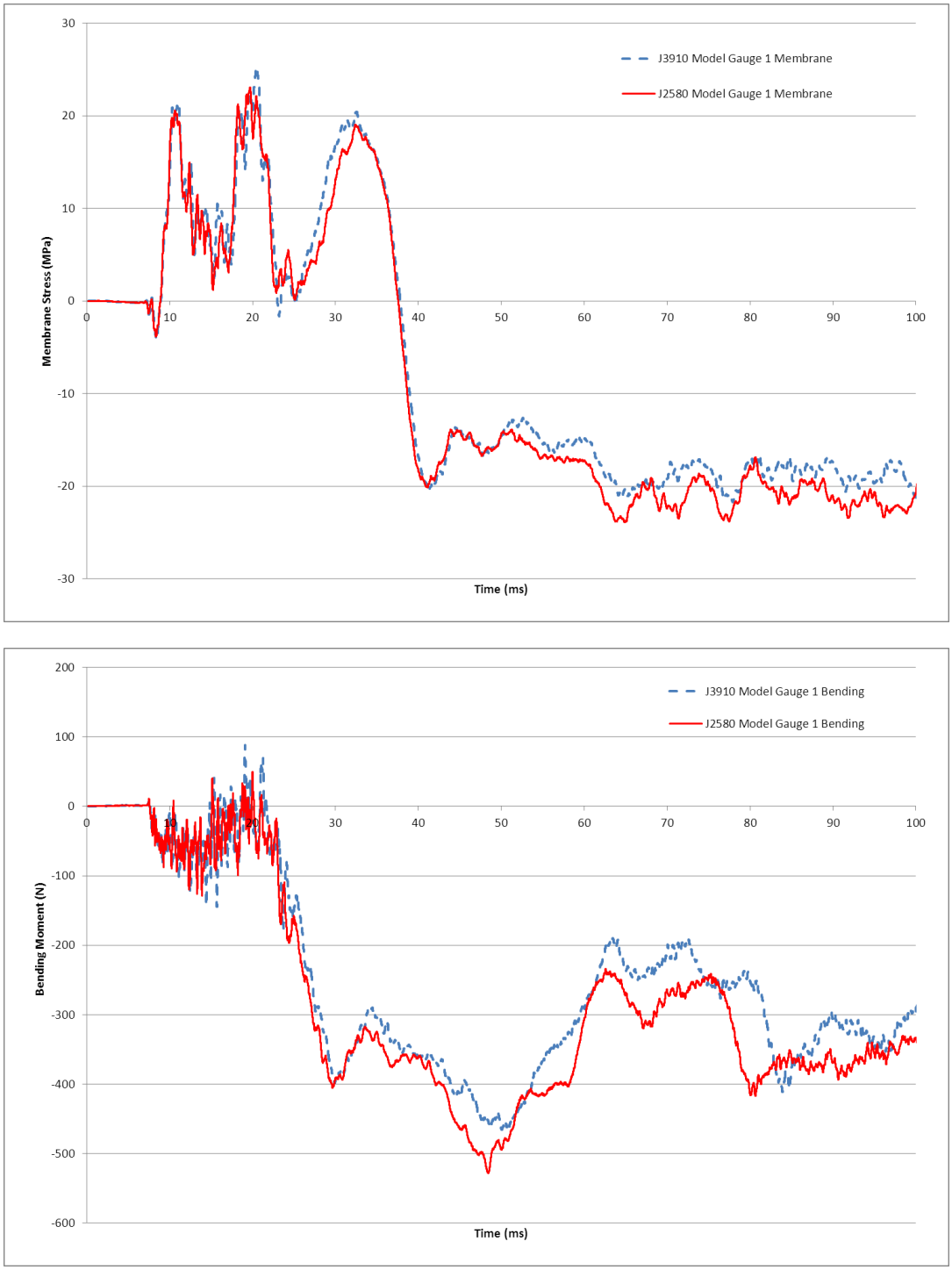

Figure A- 1 Comparison of membrane stresses (top) and bending moments (bottom) for gauge 1 location (band B) for J2580 and J3910 finite element models

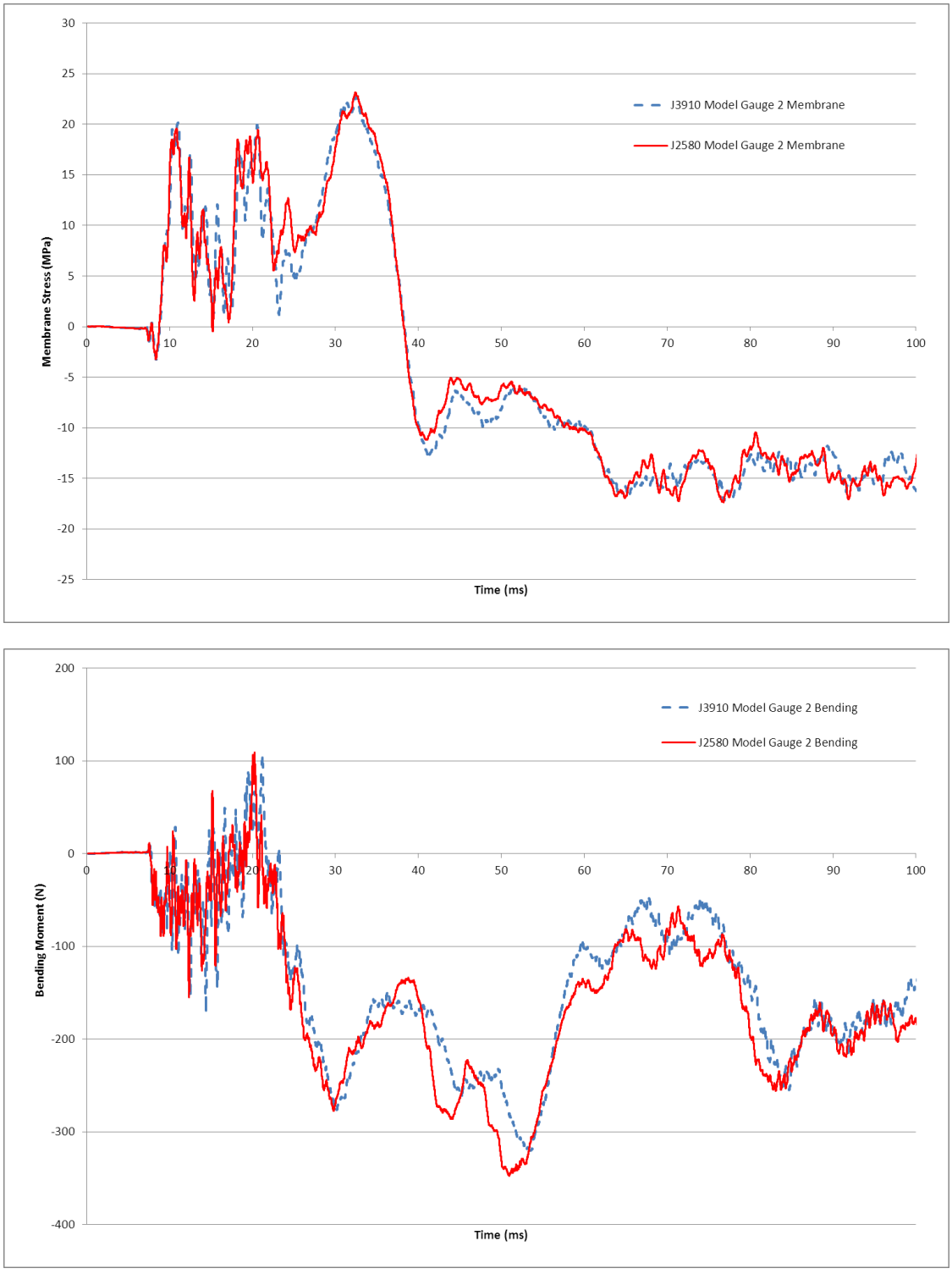

Figure A- 2 Comparison of membrane stresses (top) and bending moments (bottom) for gauge 2 location (band B) for J2580 and J3910 finite element models

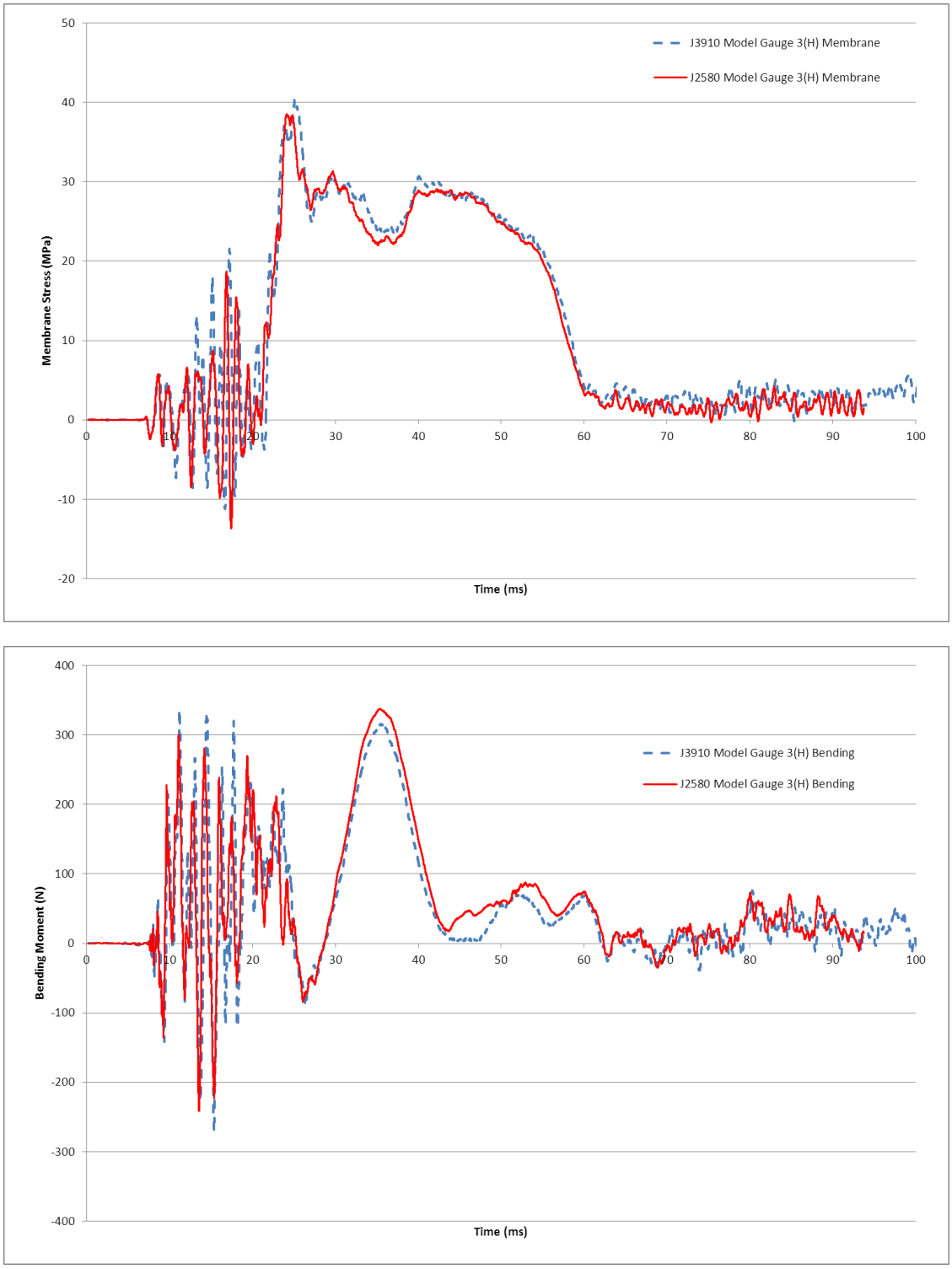

Figure A- 3 Comparison of membrane stresses (top) and bending moments (bottom) for gauge 3 location (compartment 1b, hoop) for J2580 and J3910 finite element models

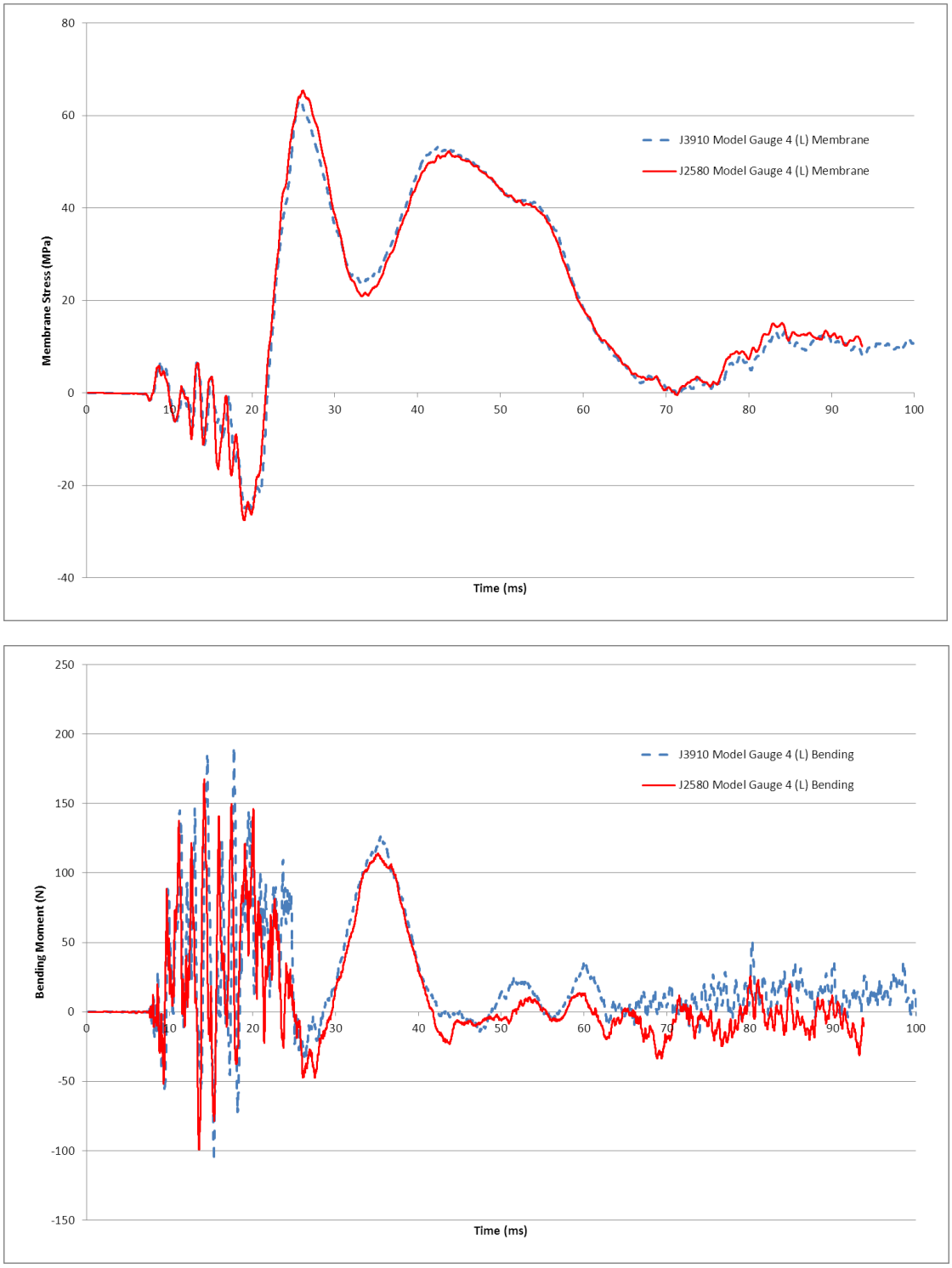

Figure A- 4 Comparison of membrane stresses (top) and bending moments (bottom) for gauge 4 location (compartment 1b, longitudinal) for J2580 and J3910 finite element models

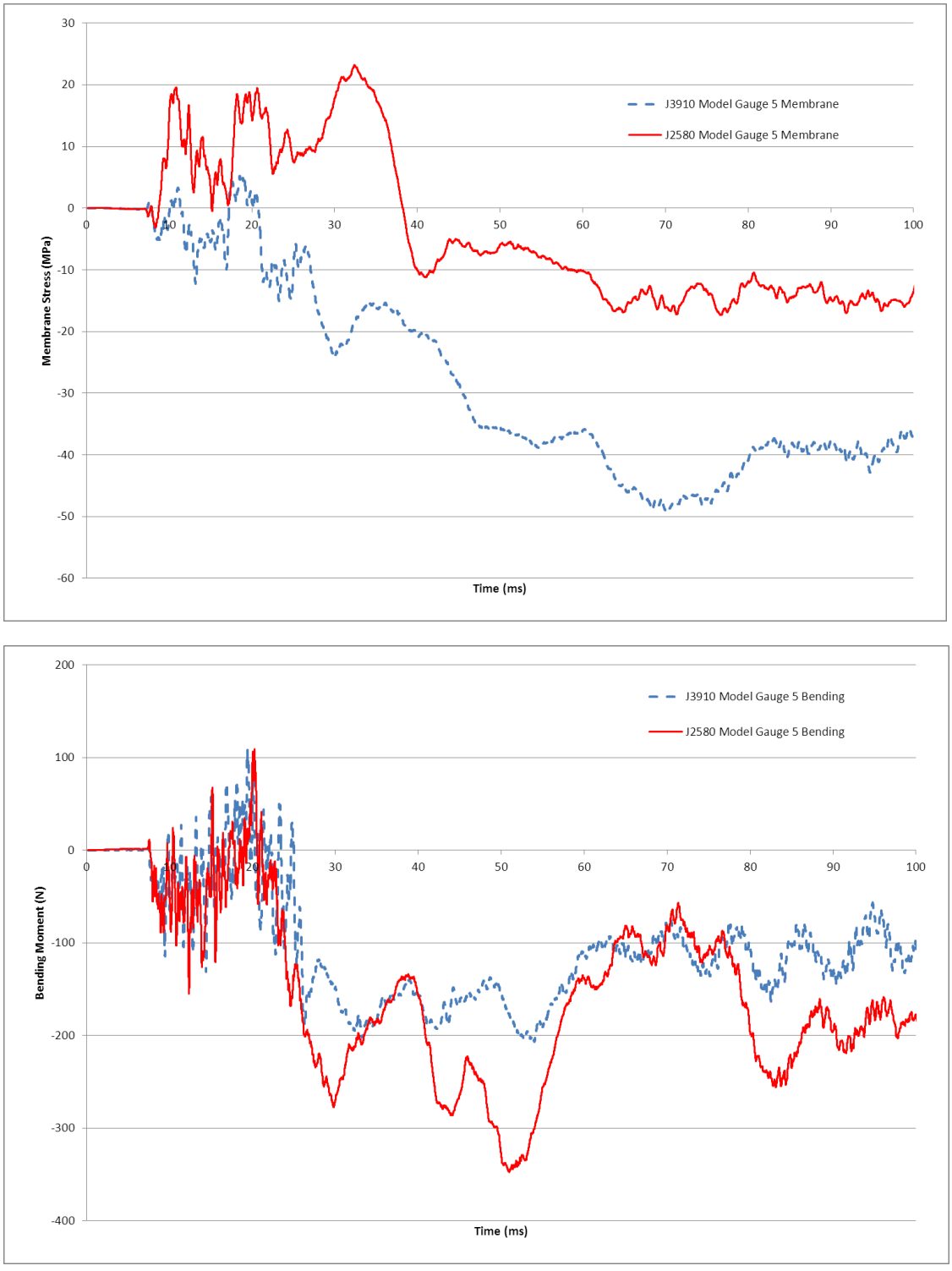

Figure A- 5 Comparison of membrane stresses (top) and bending moments (bottom) for gauge 5 location (band C) for J2580 and J3910 finite element models

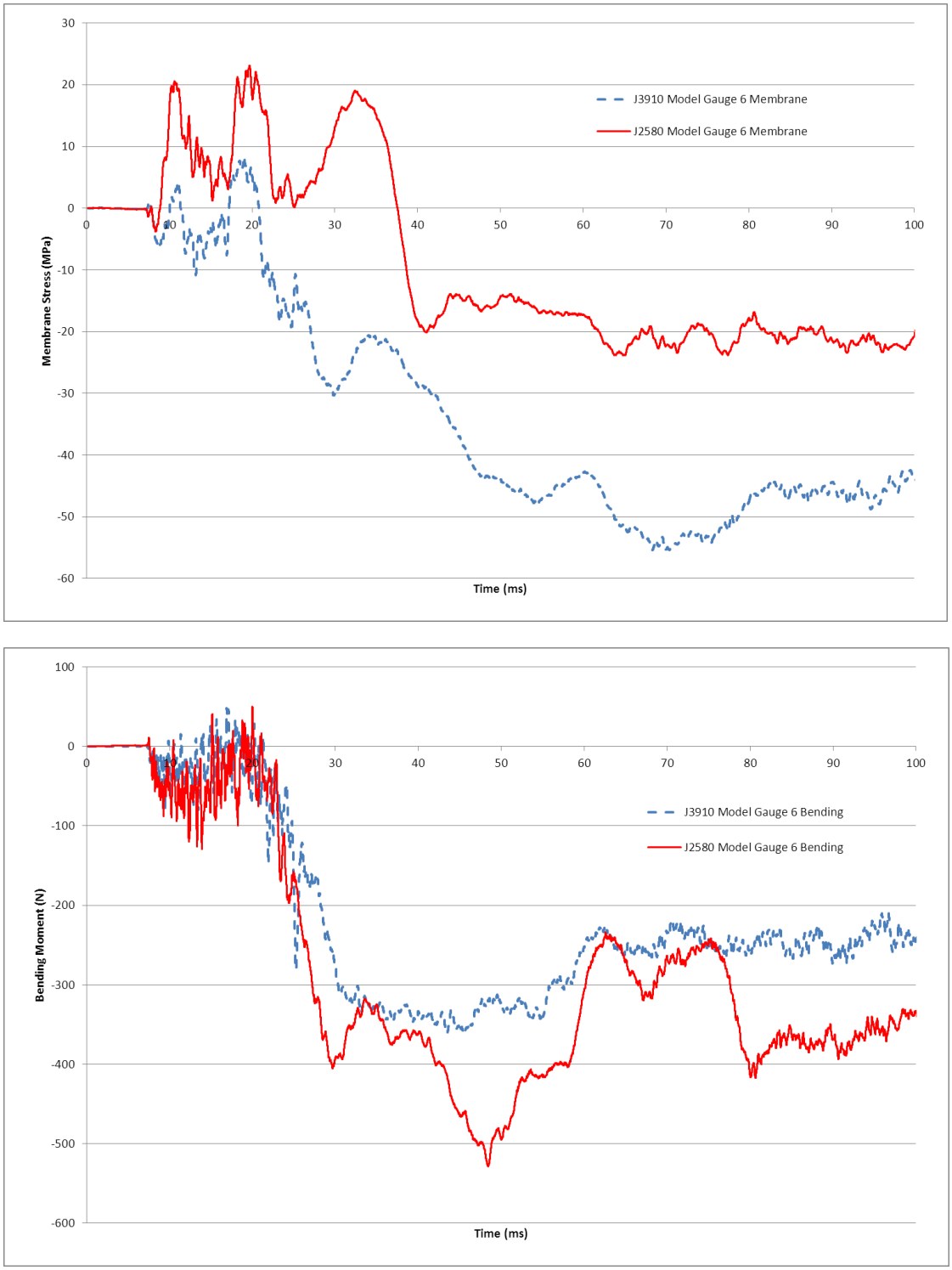

Figure A- 6 Comparison of membrane stresses (top) and bending moments (bottom) for gauge 6 location (band C) for J2580 and J3910 finite element models

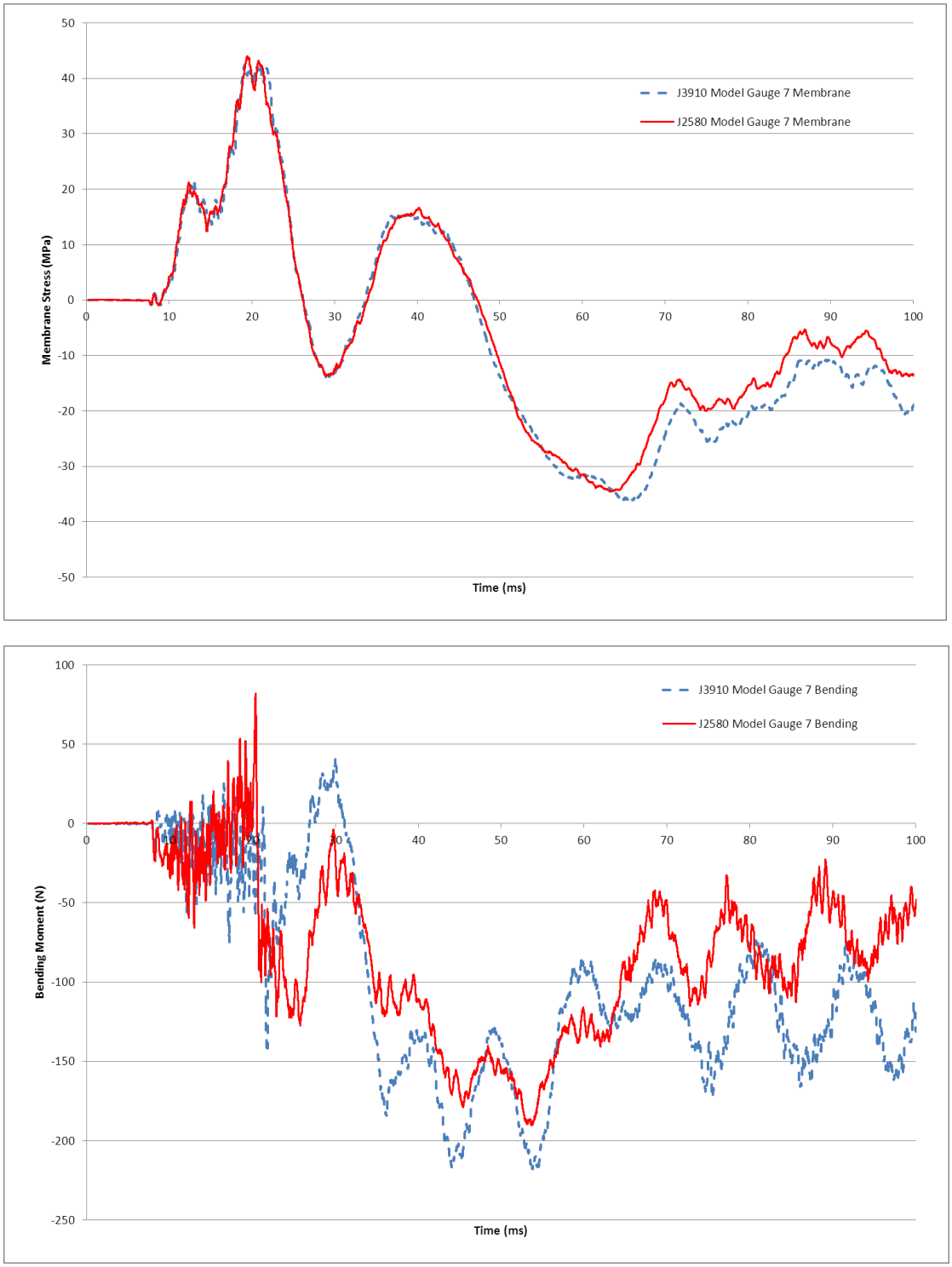

Figure A- 7 Comparison of membrane stresses (top) and bending moments (bottom) for gauge 7 location (band E) for J2580 and J3910 finite element models

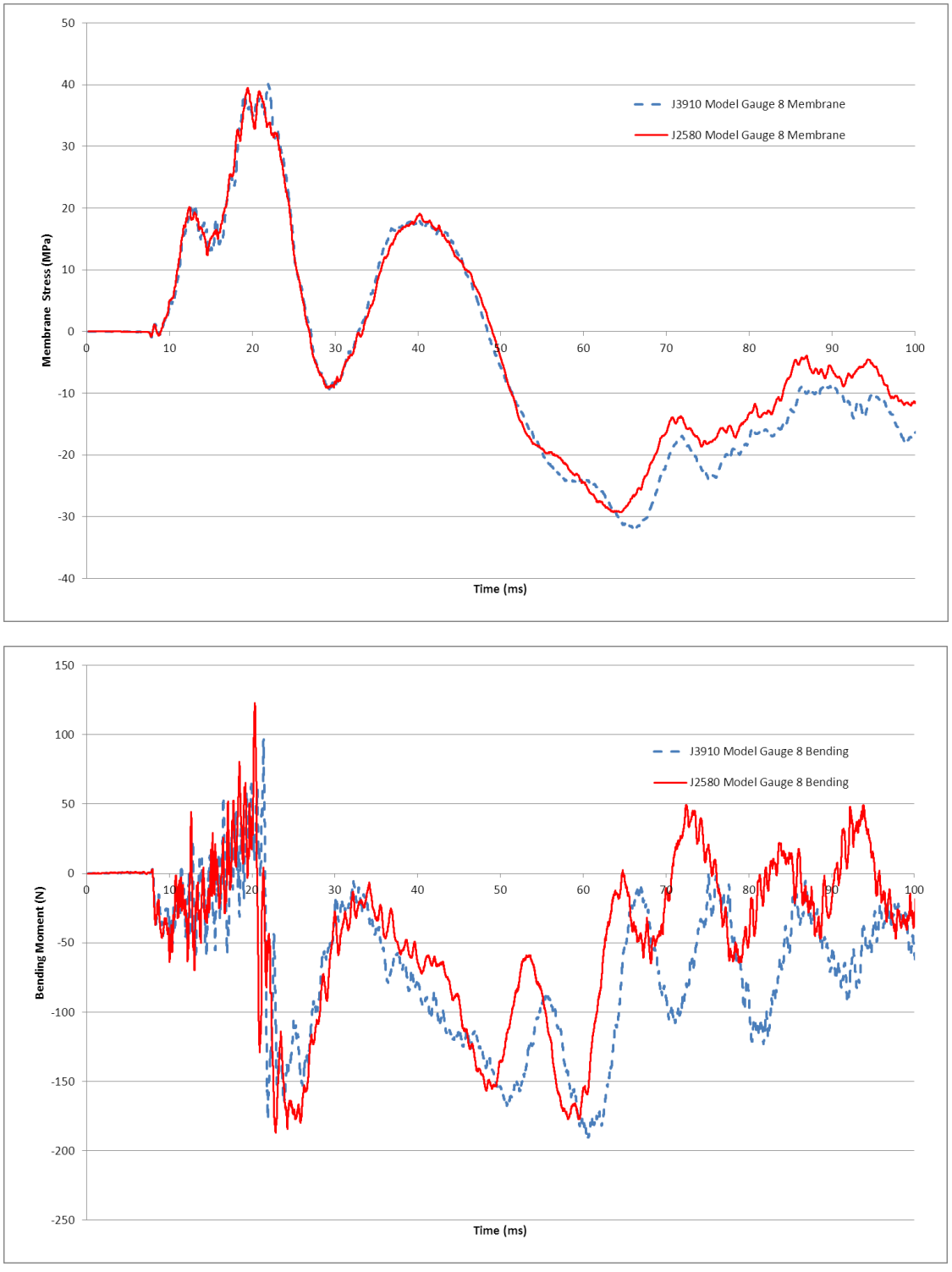

Figure A- 8 Comparison of membrane stresses (top) and bending moments (bottom) for gauge 8 location (band E) for J2580 and J3910 finite element models

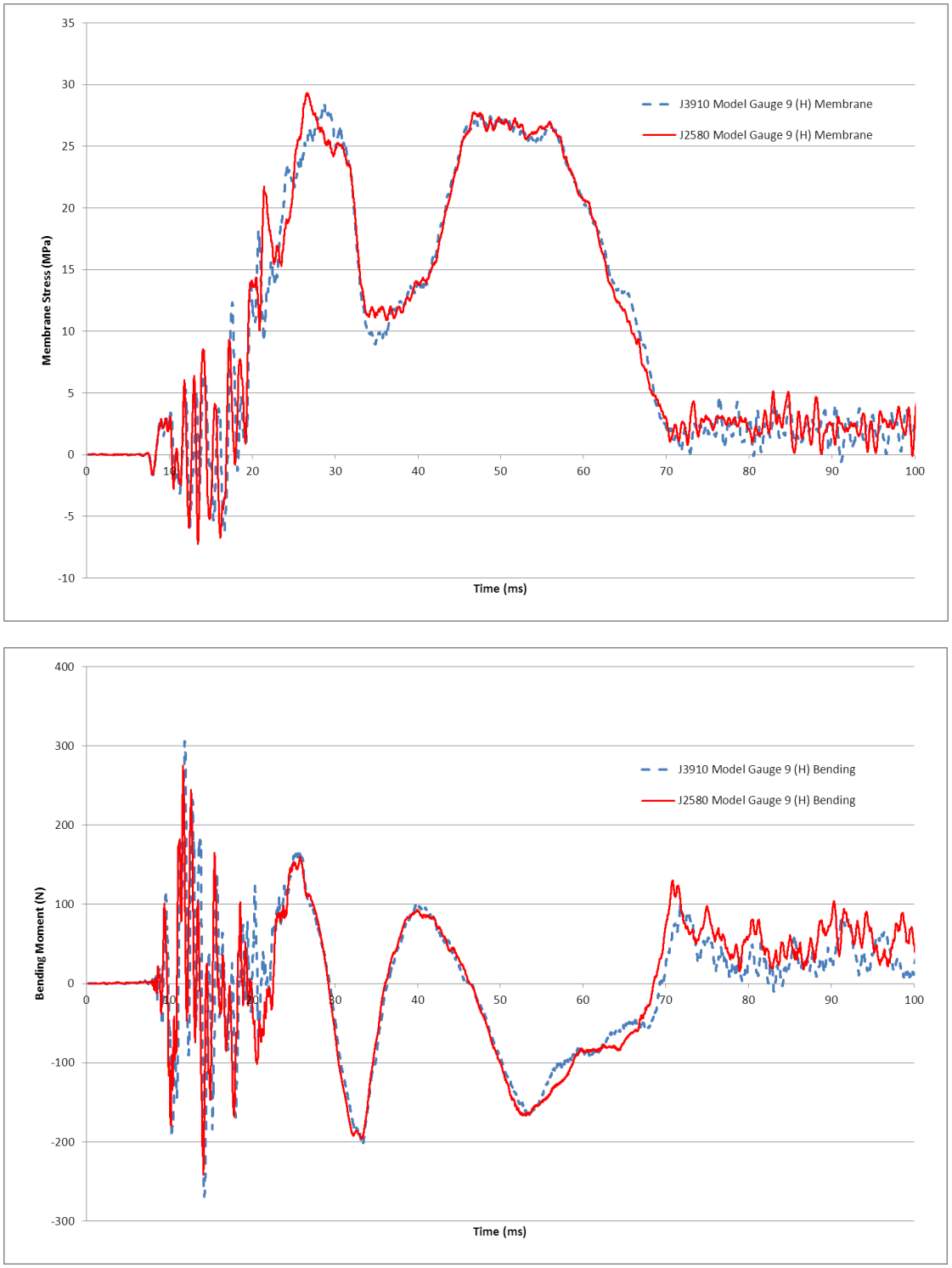

Figure A- 9 Comparison of membrane stresses (top) and bending moments (bottom) for gauge 9 location (compartment 4, hoop) for J2580 and J3910 finite element models

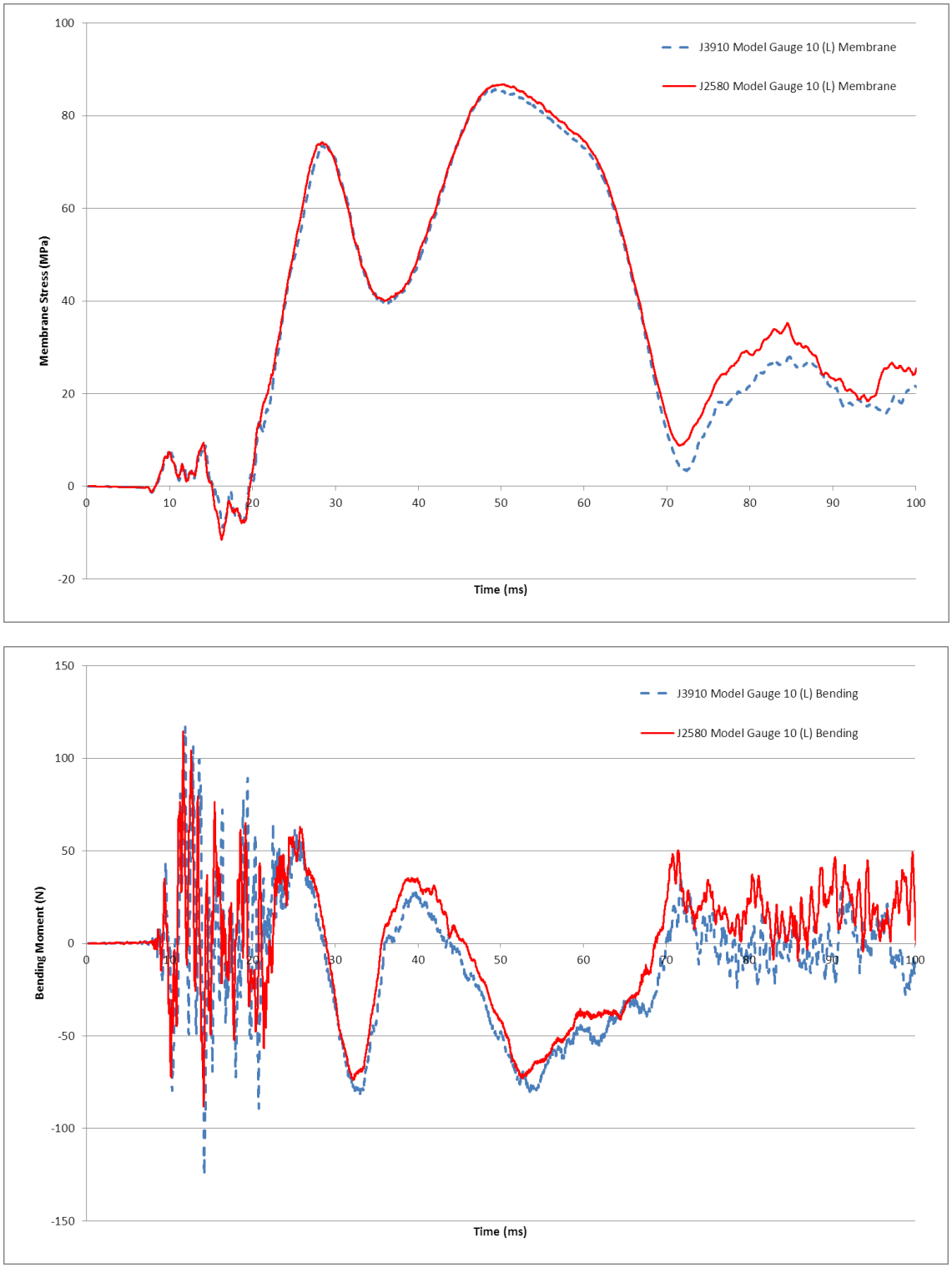

Figure A- 10 Comparison of membrane stresses (top) and bending moments (bottom) for gauge 10 location (compartment 4, longitudinal) for J2580 and J3910 finite element models

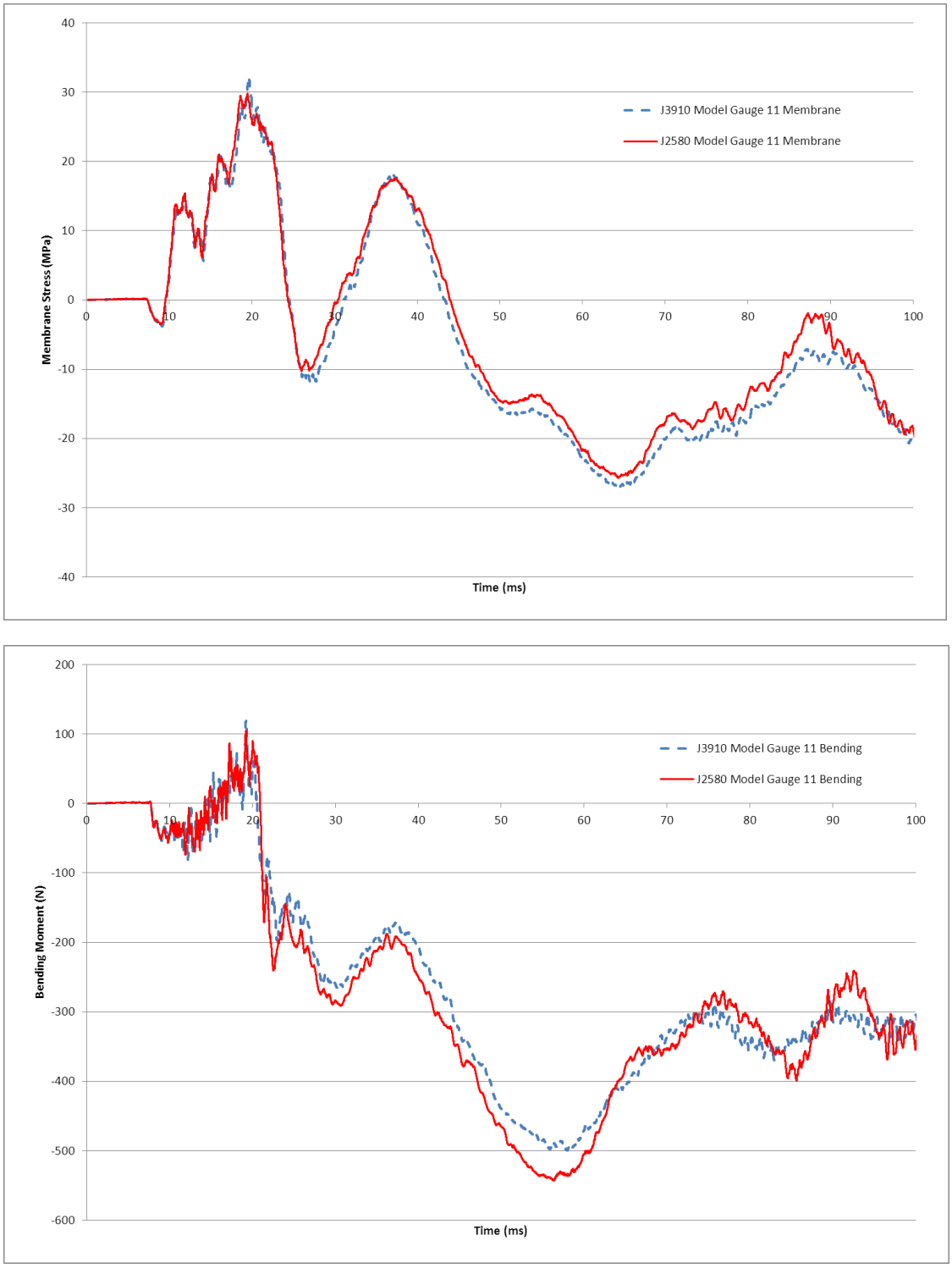

Figure A- 11 Comparison of membrane stresses (top) and bending moments (bottom) for gauge 11 location (band F) for J2580 and J3910 finite element models

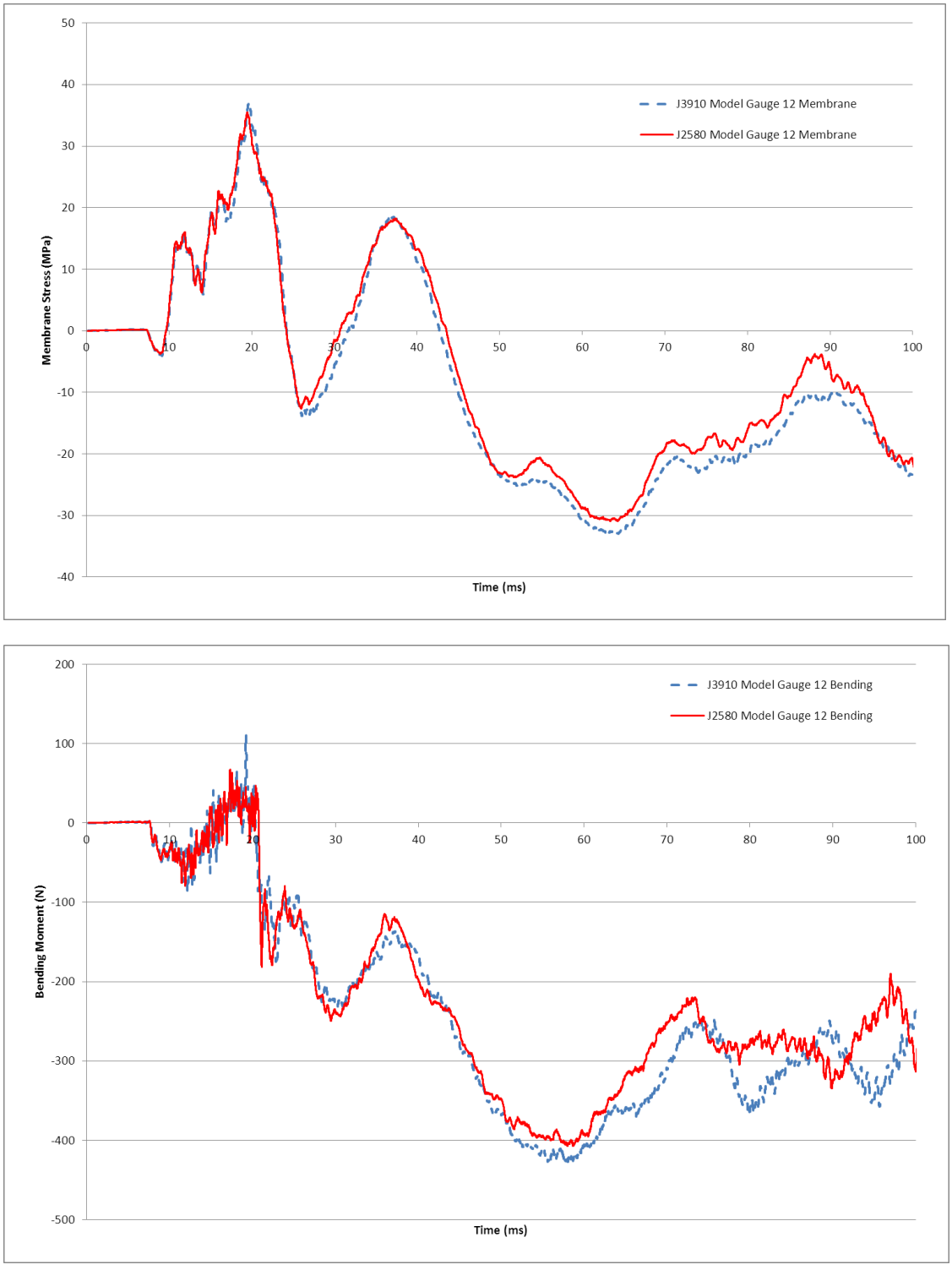

Figure A- 12 Comparison of membrane stresses (top) and bending moments (bottom) for gauge 12 location (band F) for J2580 and J3910 finite element models

APPENDIX B FULL IMPACT VELOCITY COMPARISON RESULTS

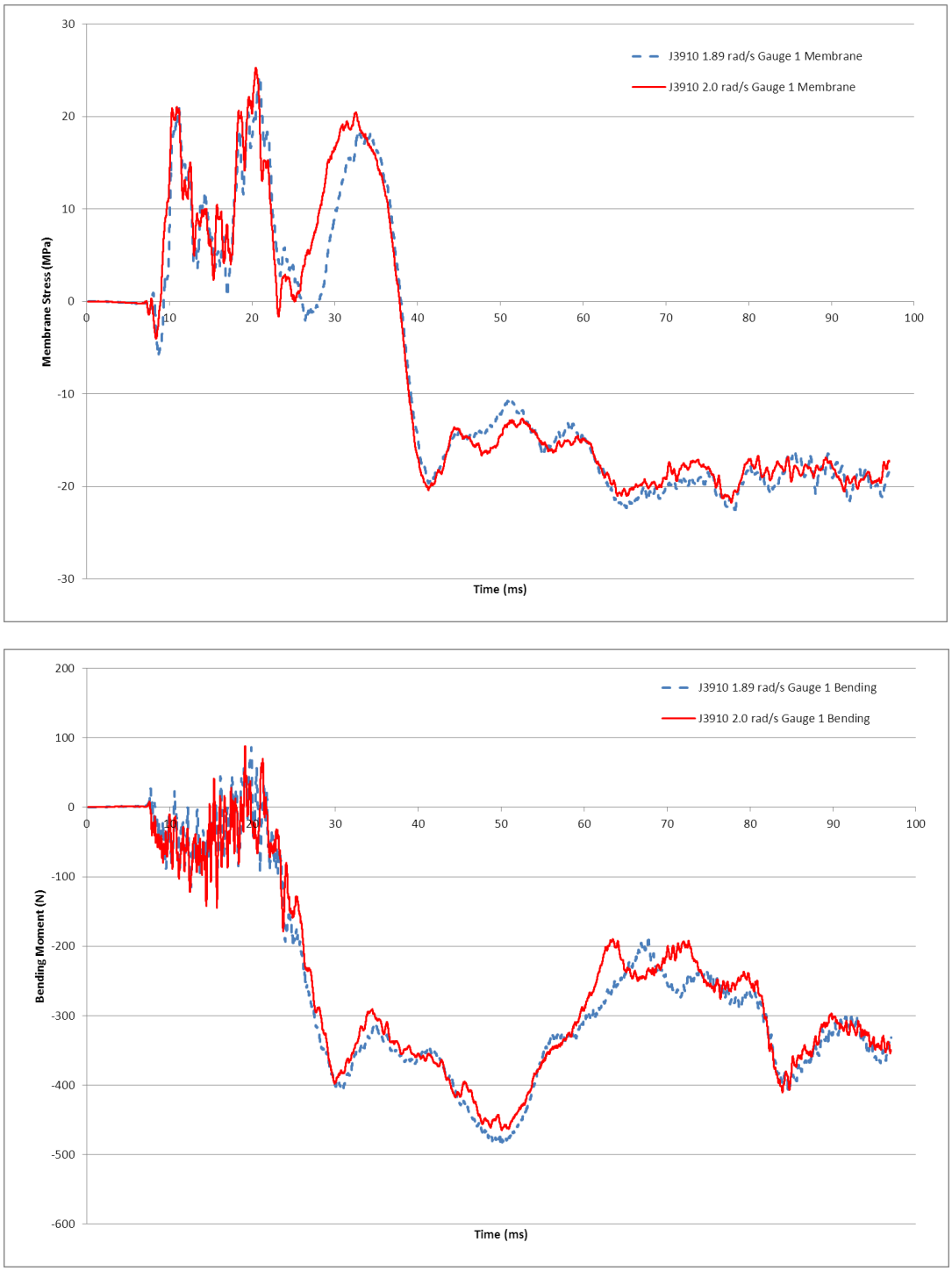

Figure B- 1 Comparison of membrane stresses (top) and bending moments (bottom) for gauge 1 location (band B) for J3910 finite element models with different impact velocities

Figure B- 2 Comparison of membrane stresses (top) and bending moments (bottom) for gauge 2 location (band B) for J3910 finite element models with different impact velocities

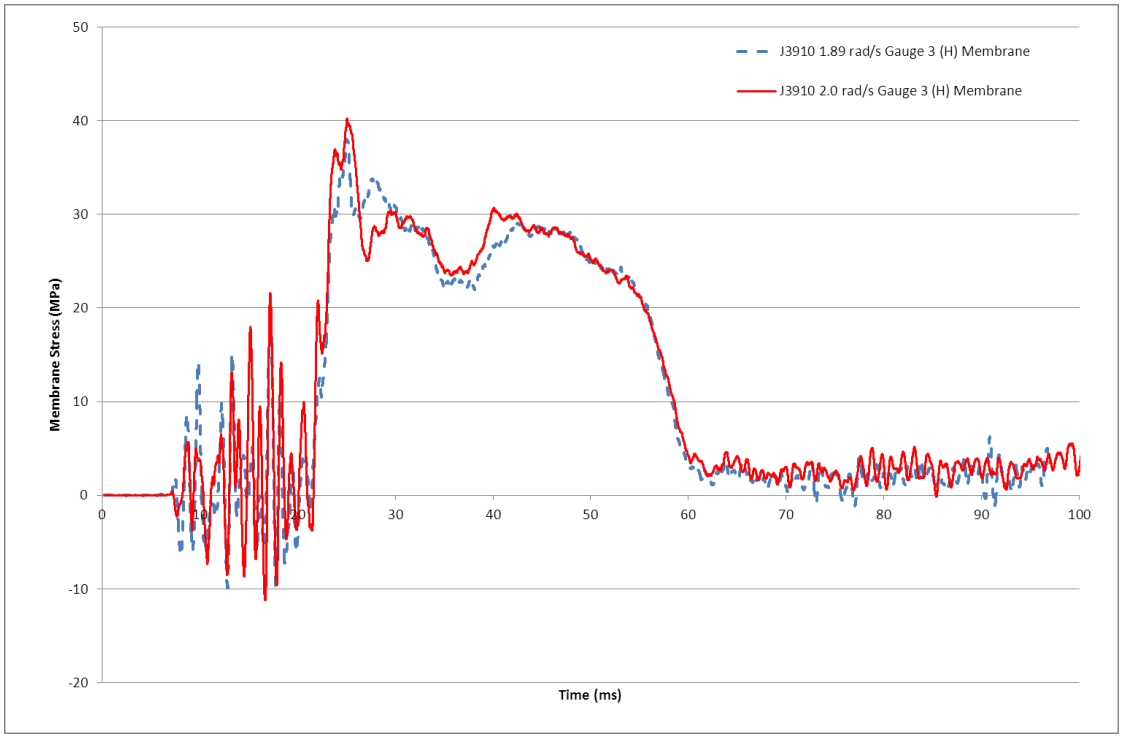

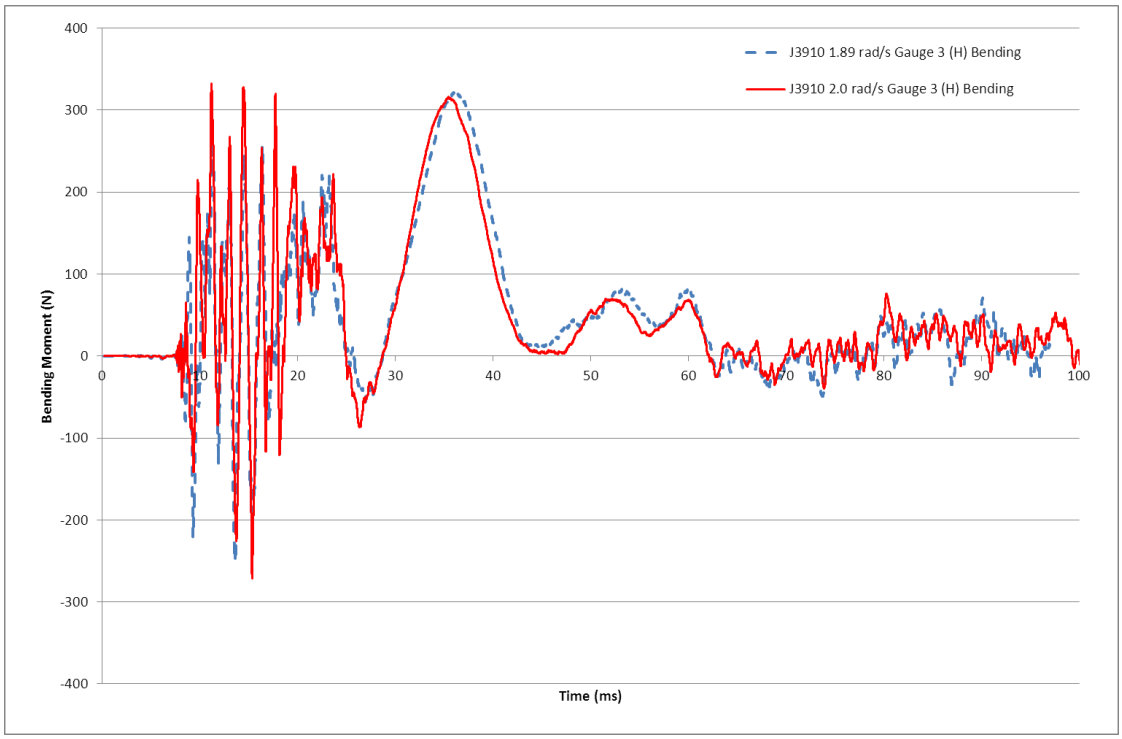

Figure B- 3 Comparison of membrane stresses (top) and bending moments (bottom) for gauge 3 location (compartment 1b, hoop) for J3910 finite element models with different impact velocities

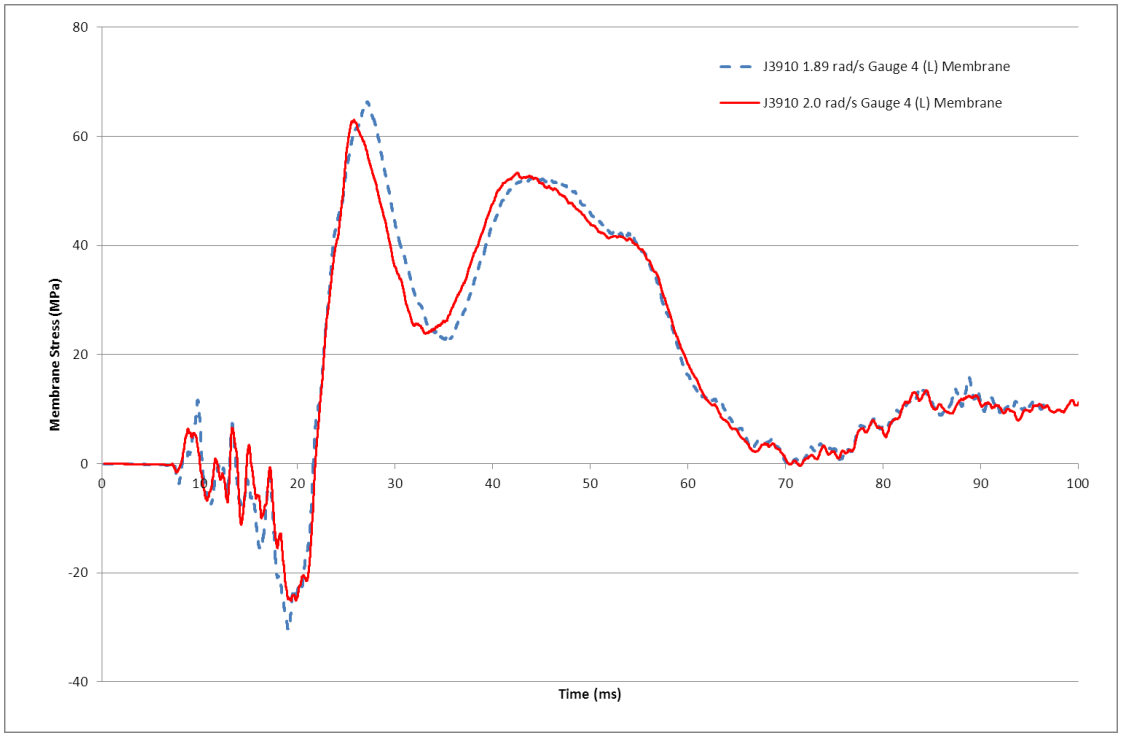

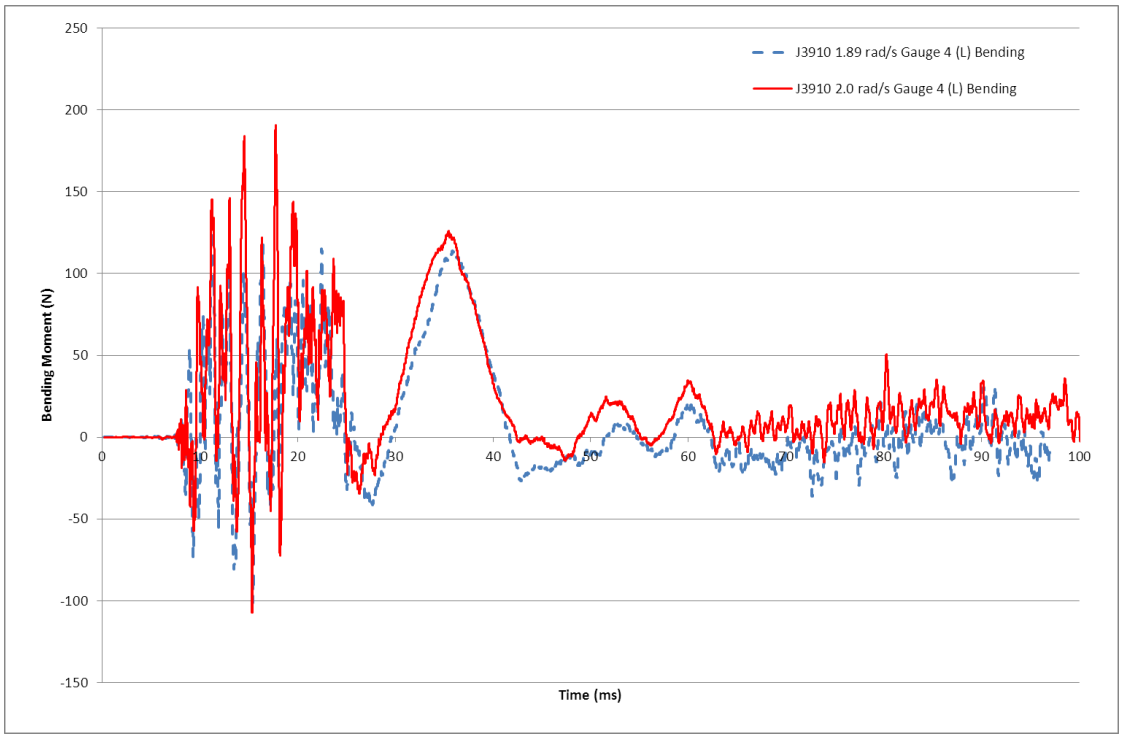

Figure B- 4 Comparison of membrane stresses (top) and bending moments (bottom) for gauge 4 location (compartment 1b, longitudinal) for J3910 finite element models with different impact velocities

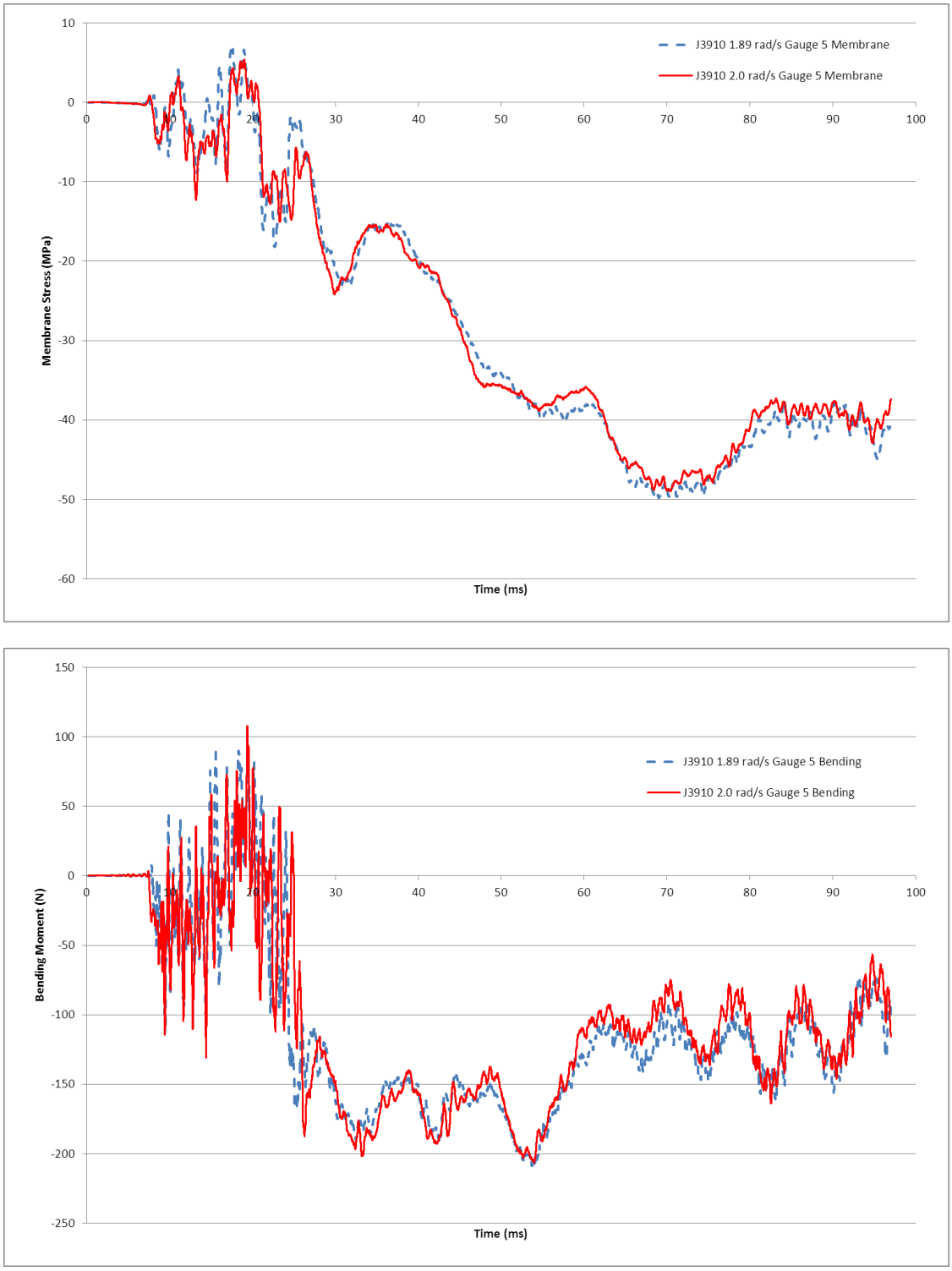

Figure B- 5 Comparison of membrane stresses (top) and bending moments (bottom) for gauge 5 location (band C) for J3910 finite element models with different impact velocities

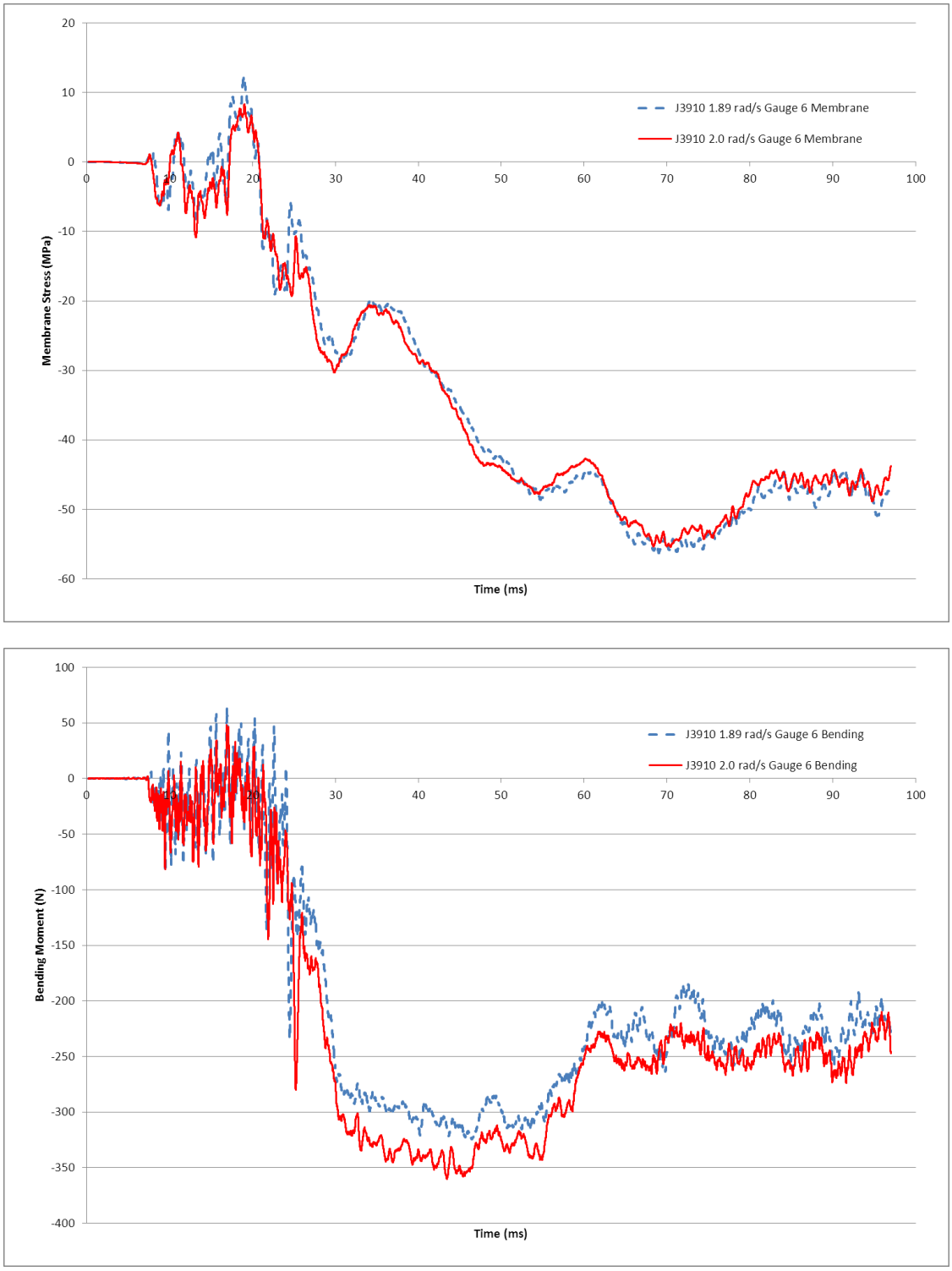

Figure B- 6 Comparison of membrane stresses (top) and bending moments (bottom) for gauge 6 location (band C) for J3910 finite element models with different impact velocities

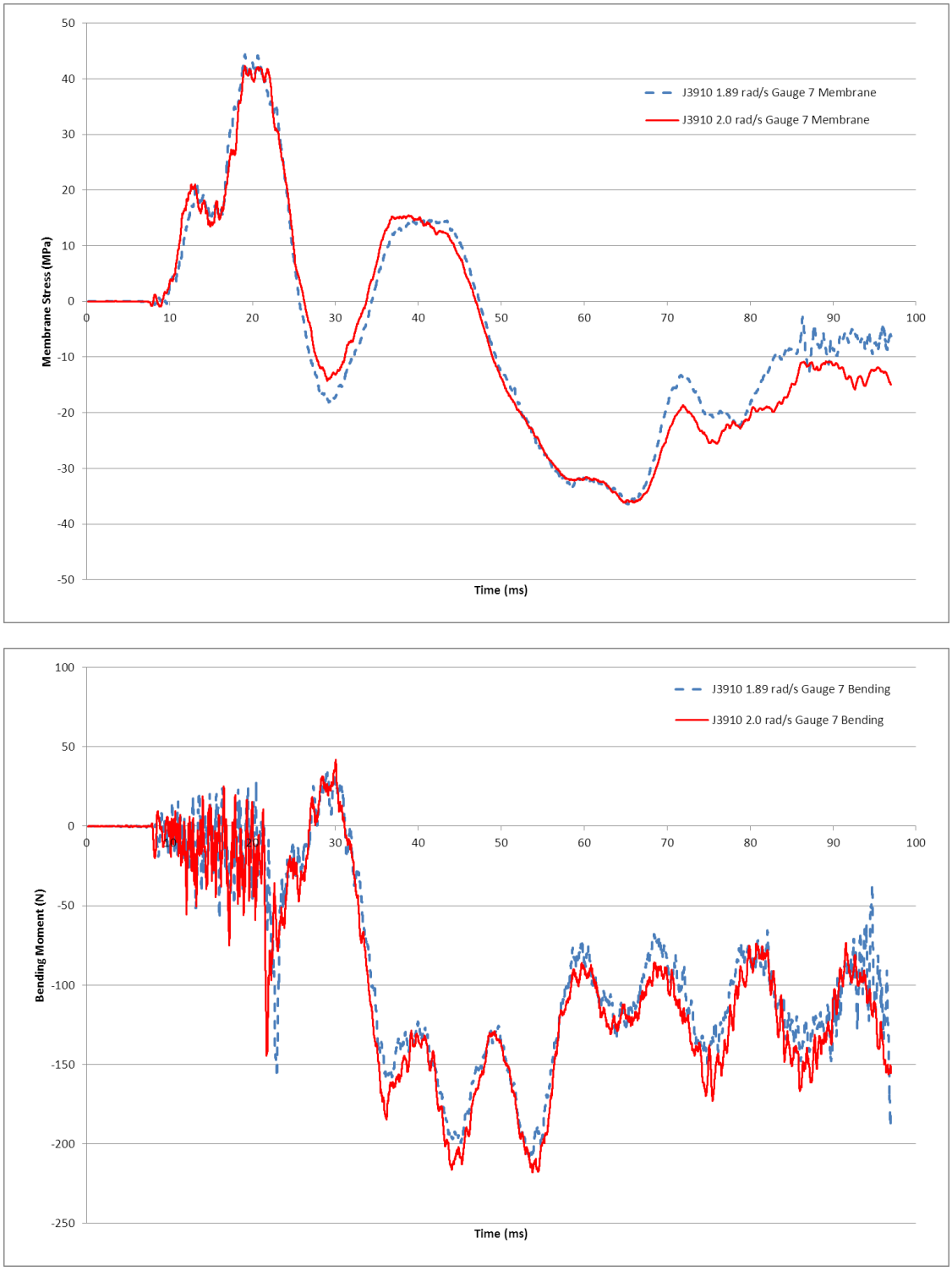

Figure B- 7 Comparison of membrane stresses (top) and bending moments (bottom) for gauge 7 location (band E) for J3910 finite element models with different impact velocities

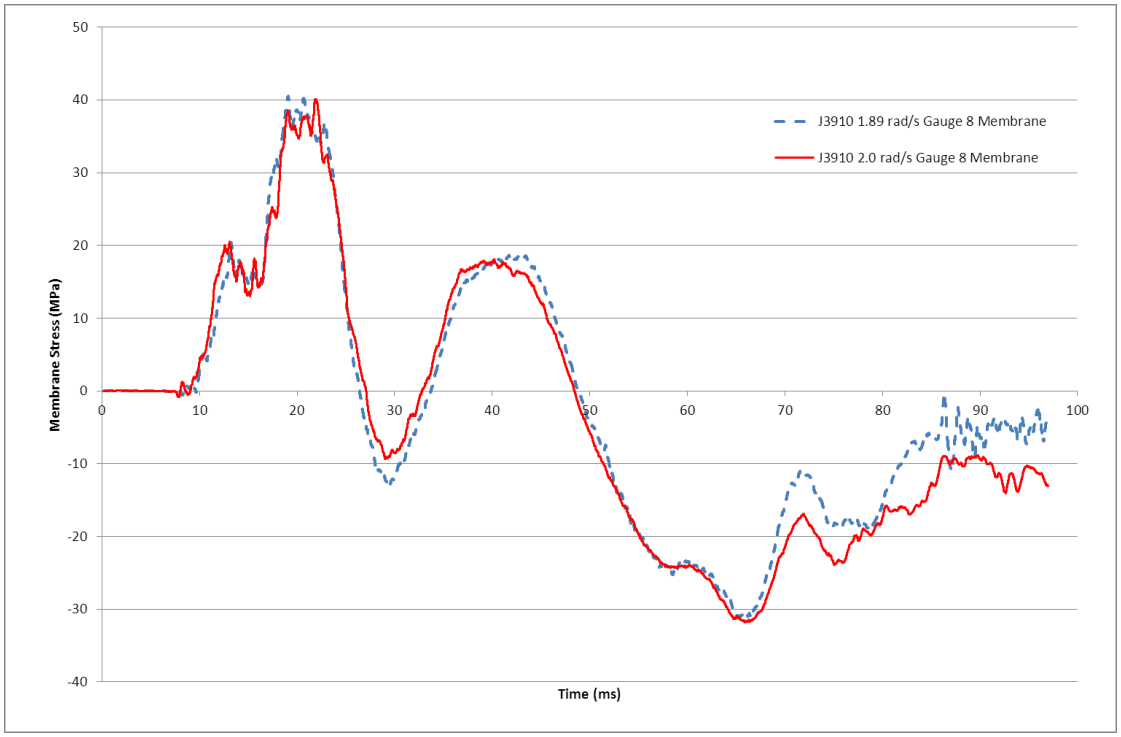

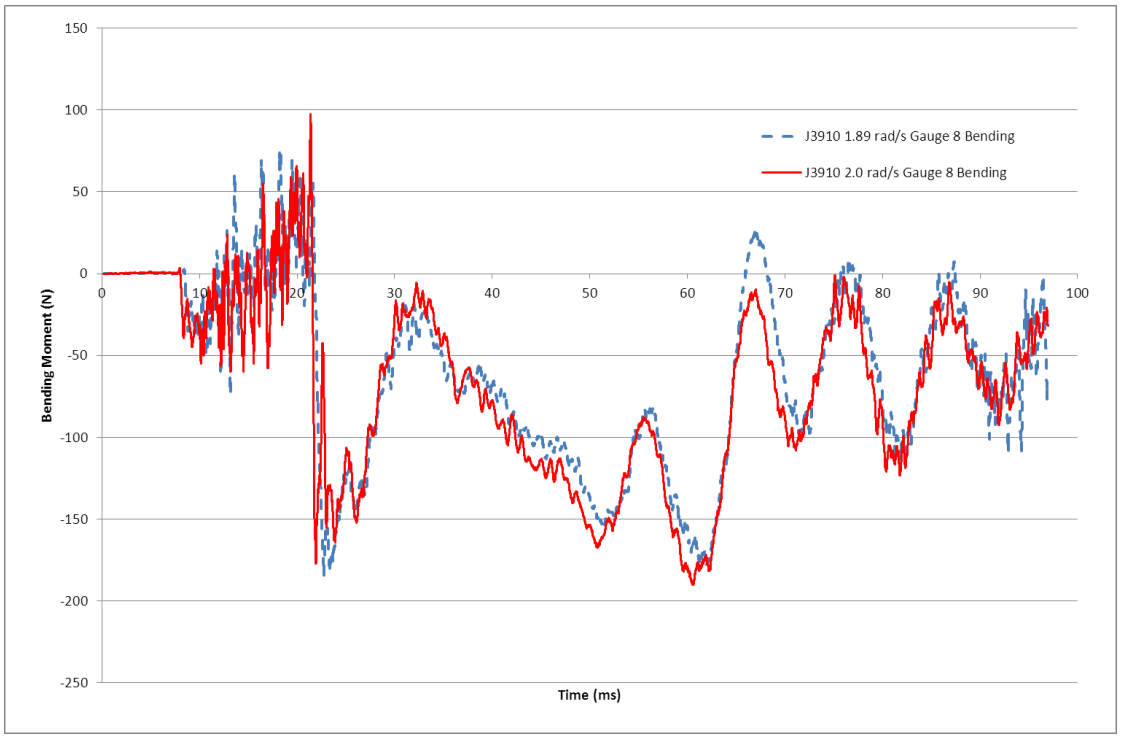

Figure B- 8 Comparison of membrane stresses (top) and bending moments (bottom) for gauge 8 location (band E) for J3910 finite element models with different impact velocities

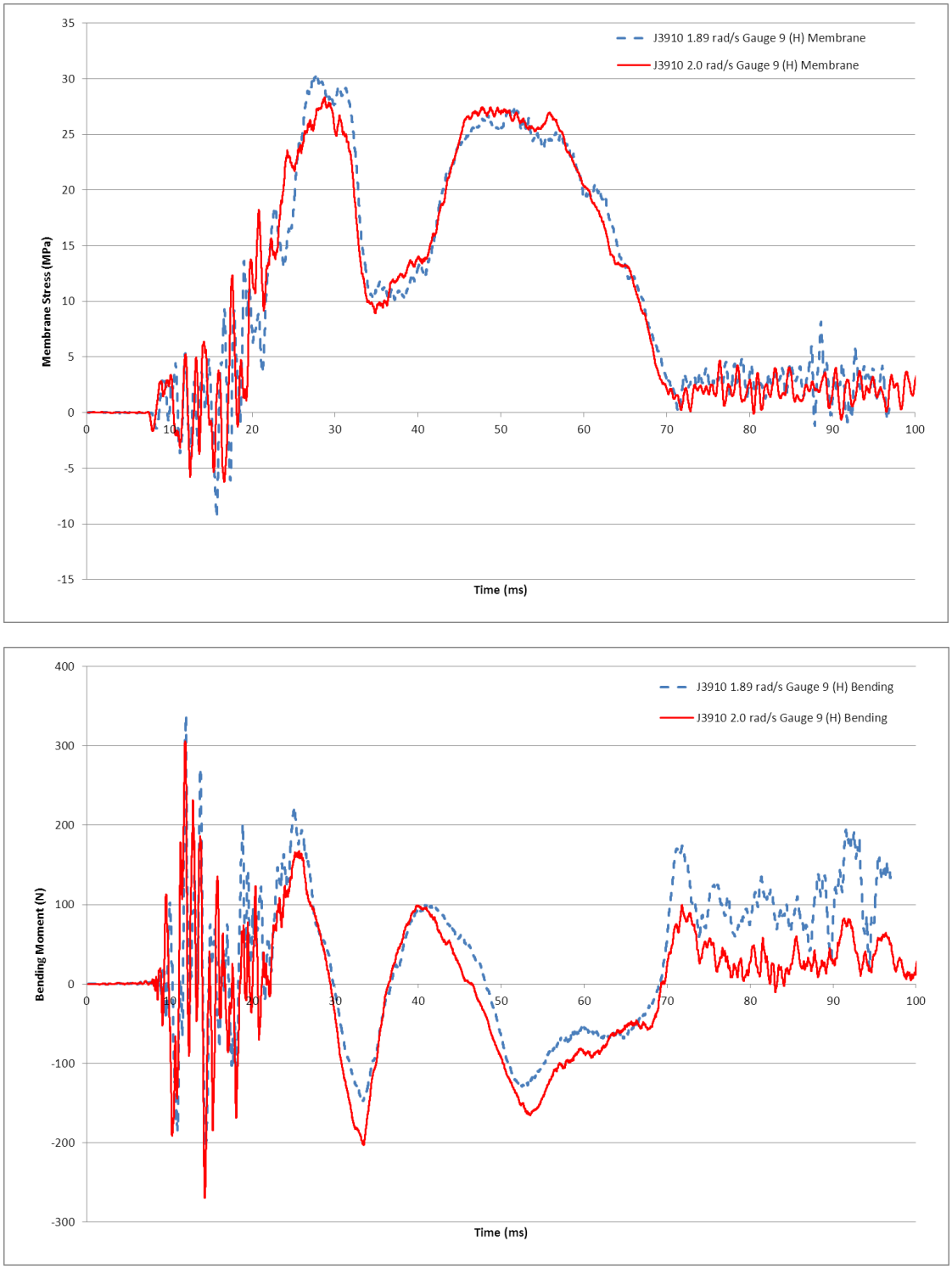

Figure B- 9 Comparison of membrane stresses (top) and bending moments (bottom) for gauge 9 location (compartment 4, hoop) for J3910 finite element models with different impact velocities

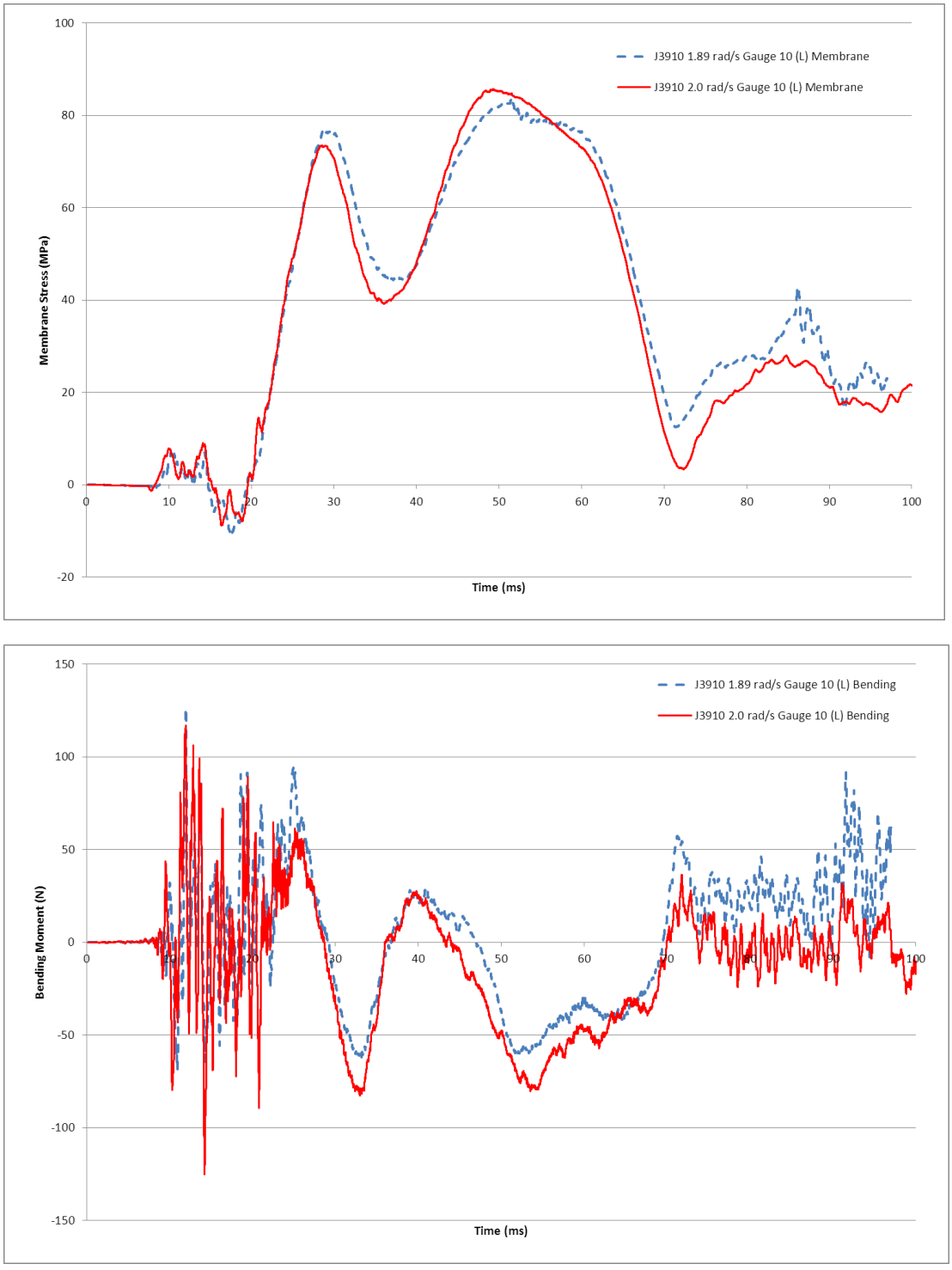

Figure B- 10 Comparison of membrane stresses (top) and bending moments (bottom) for gauge 10 location (compartment 4, longitudinal) for J3910 finite element models with different impact velocities

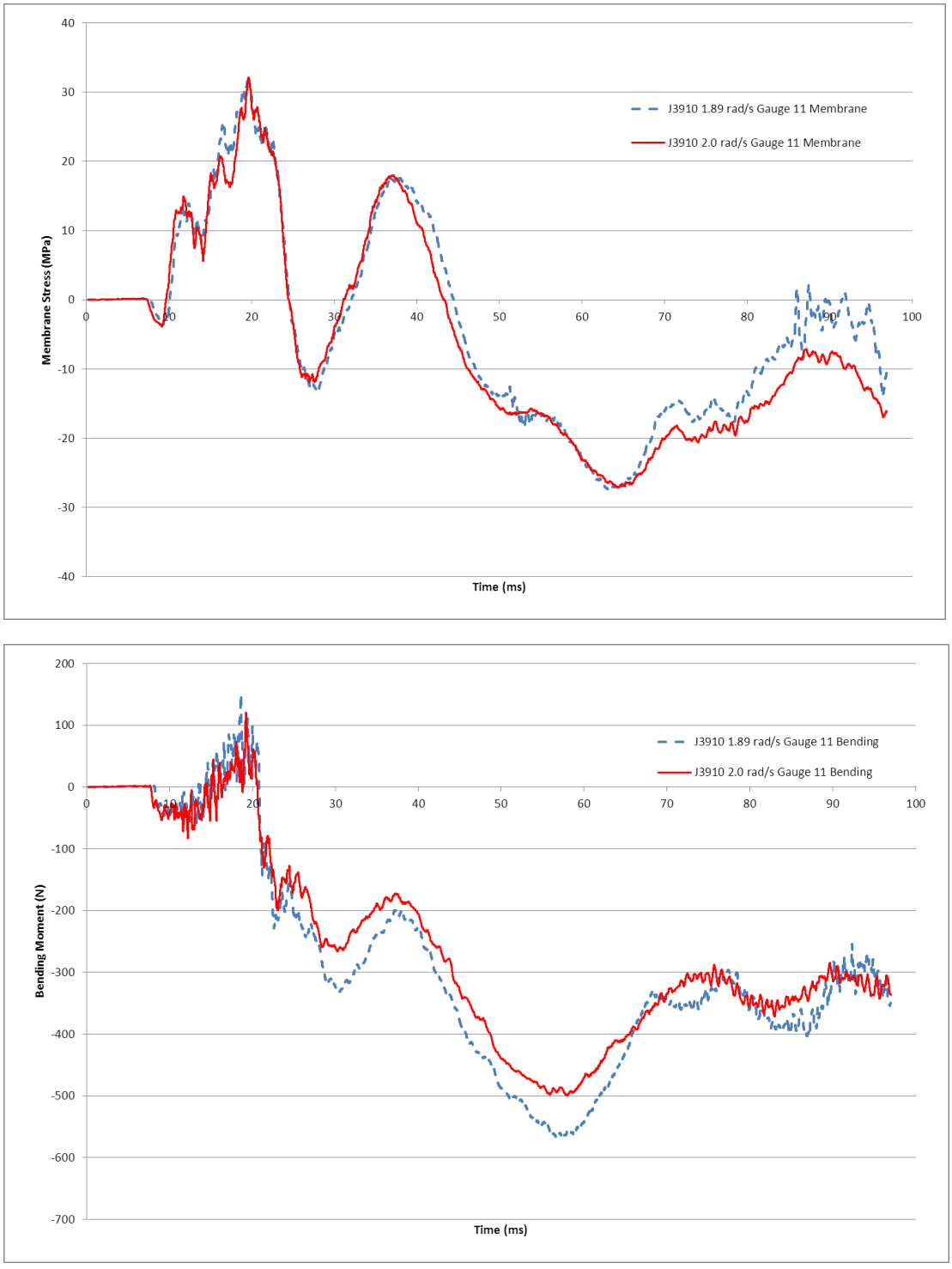

Figure B- 11 Comparison of membrane stresses (top) and bending moments (bottom) for gauge 11 location (band F) for J3910 finite element models with different impact velocities

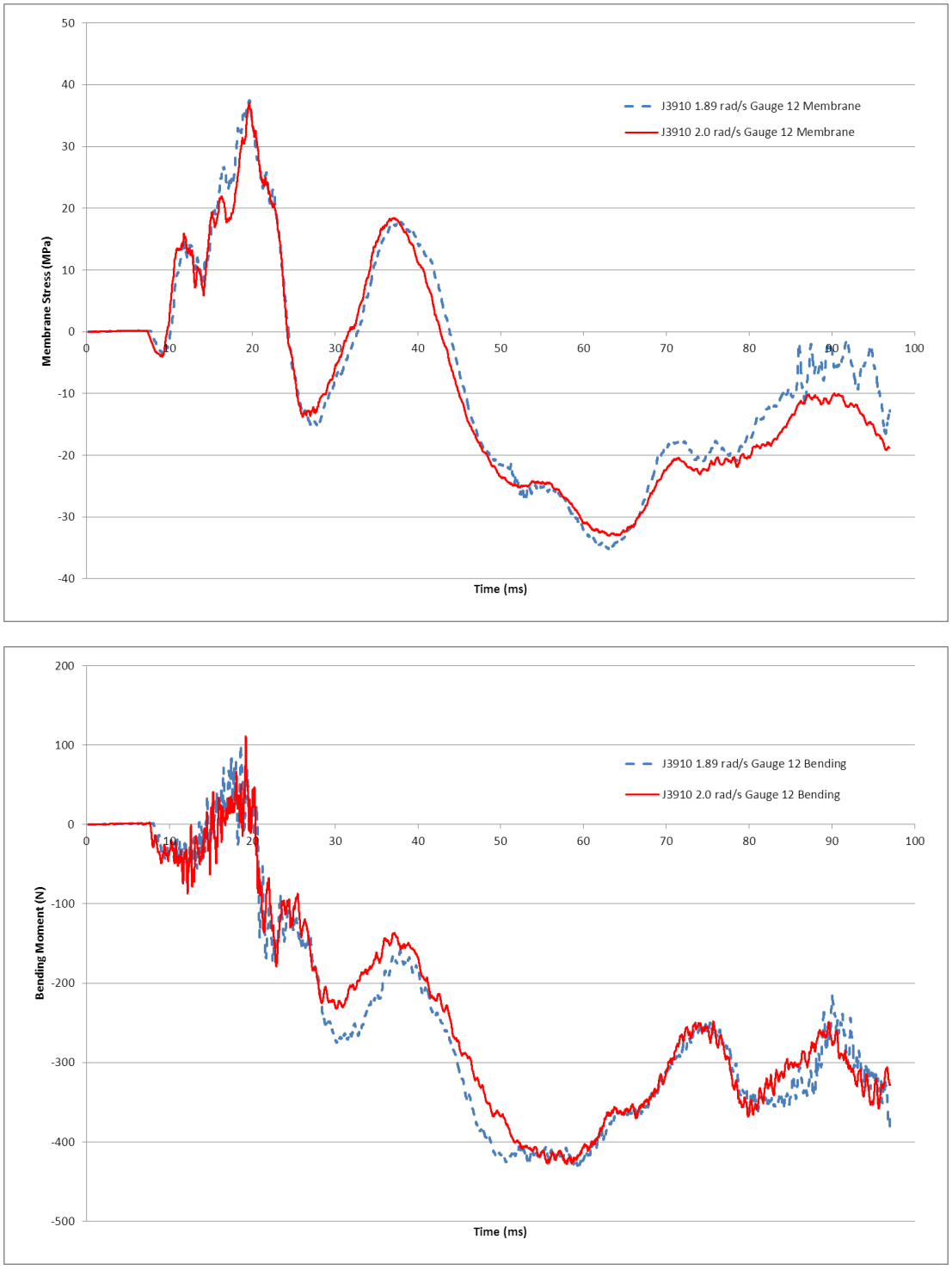

Figure B- 12 Comparison of membrane stresses (top) and bending moments (bottom) for gauge 12 location (band F) for J3910 finite element models with different impact velocities

APPENDIX C FULL VALIDATION RESULTS WITH IMPACT VELOCITY OF 1.89 RAD/S

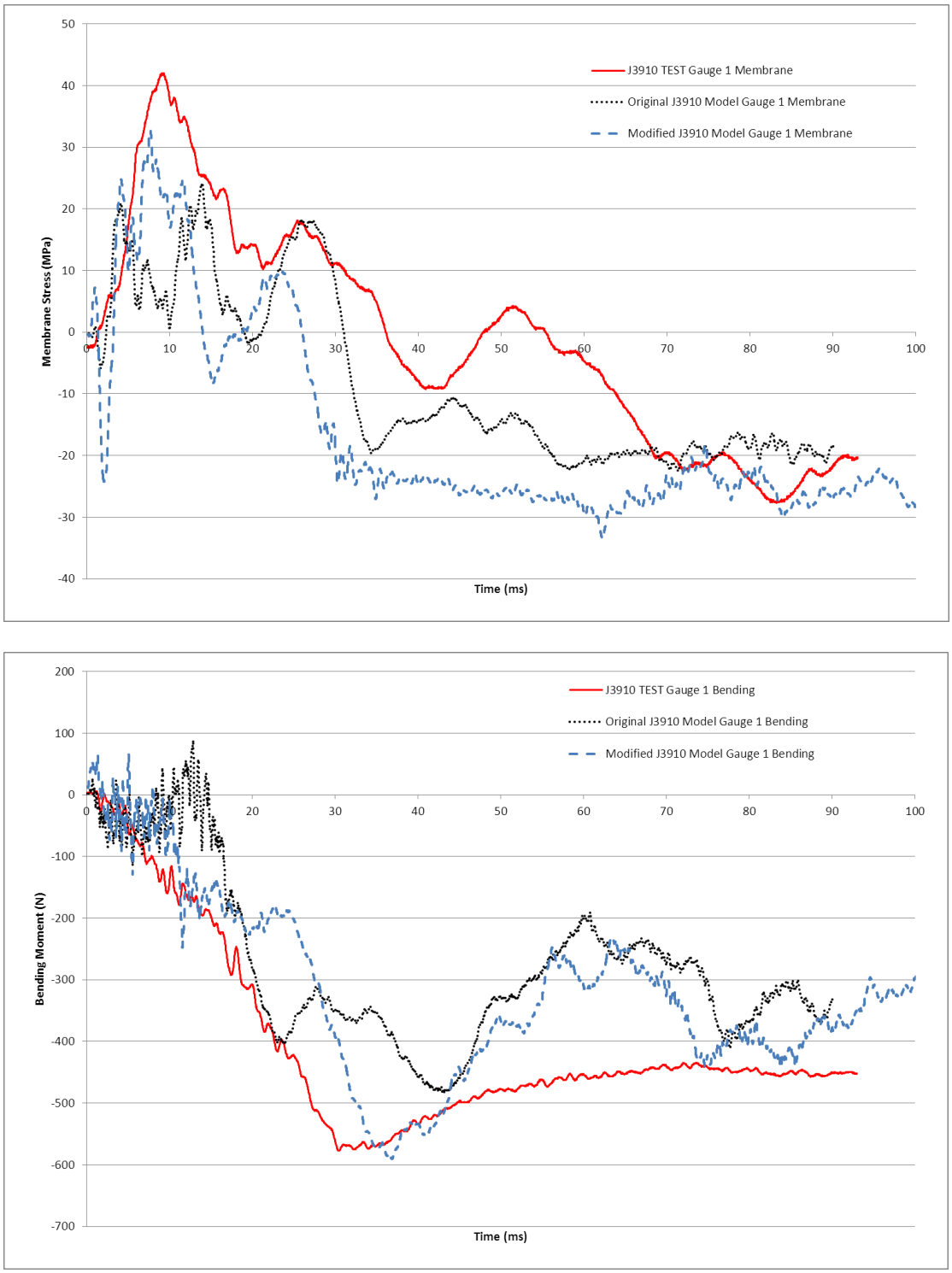

Figure C- 1 Comparison of membrane stresses (top) and bending moments (bottom) for gauge 1 location (band B) for GRW tanker J3910 topple test and finite element models

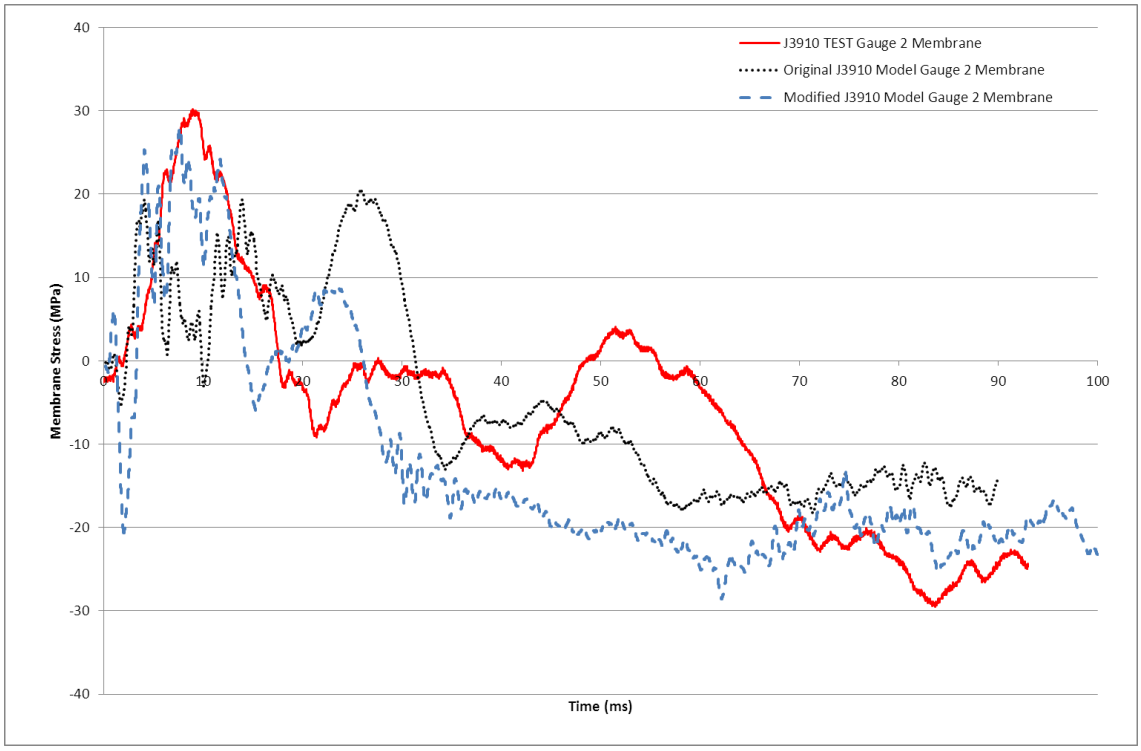

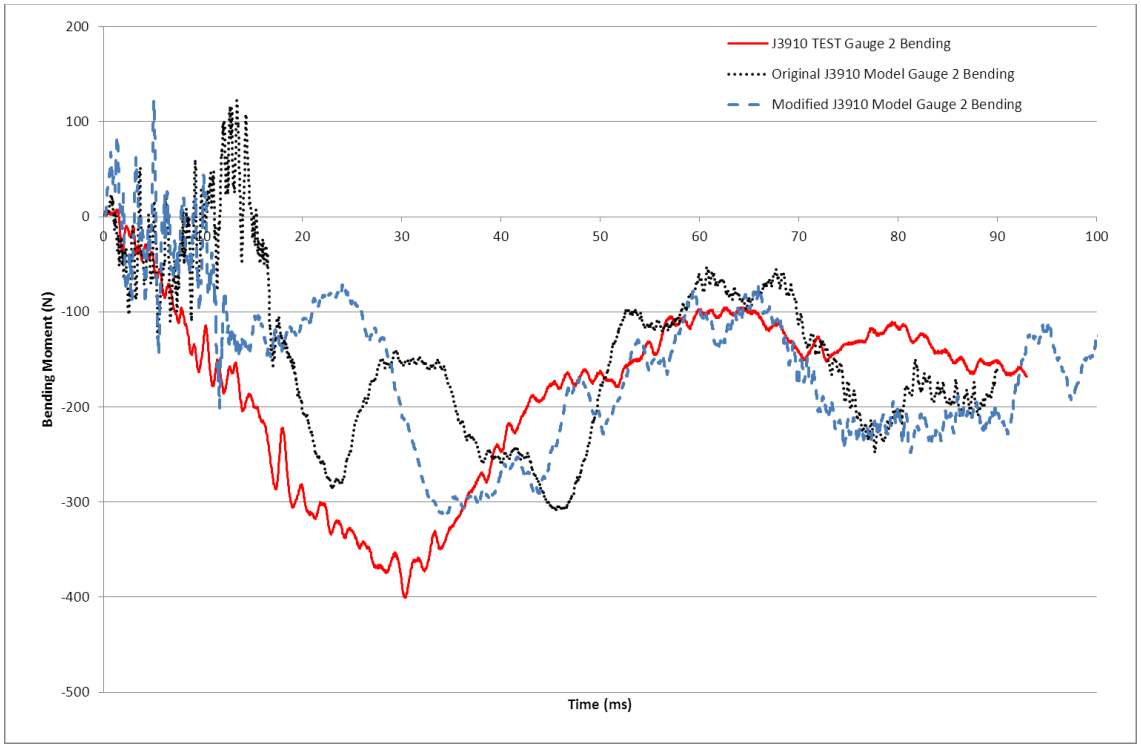

Figure C- 2 Comparison of membrane stresses (top) and bending moments (bottom) for gauge 2 location (band B) for GRW tanker J3910 topple test and finite element models

Figure C- 3 Comparison of membrane stresses (top) and bending moments (bottom) for gauge 3 location (compartment 1b, hoop) for GRW tanker J3910 topple test and finite element models

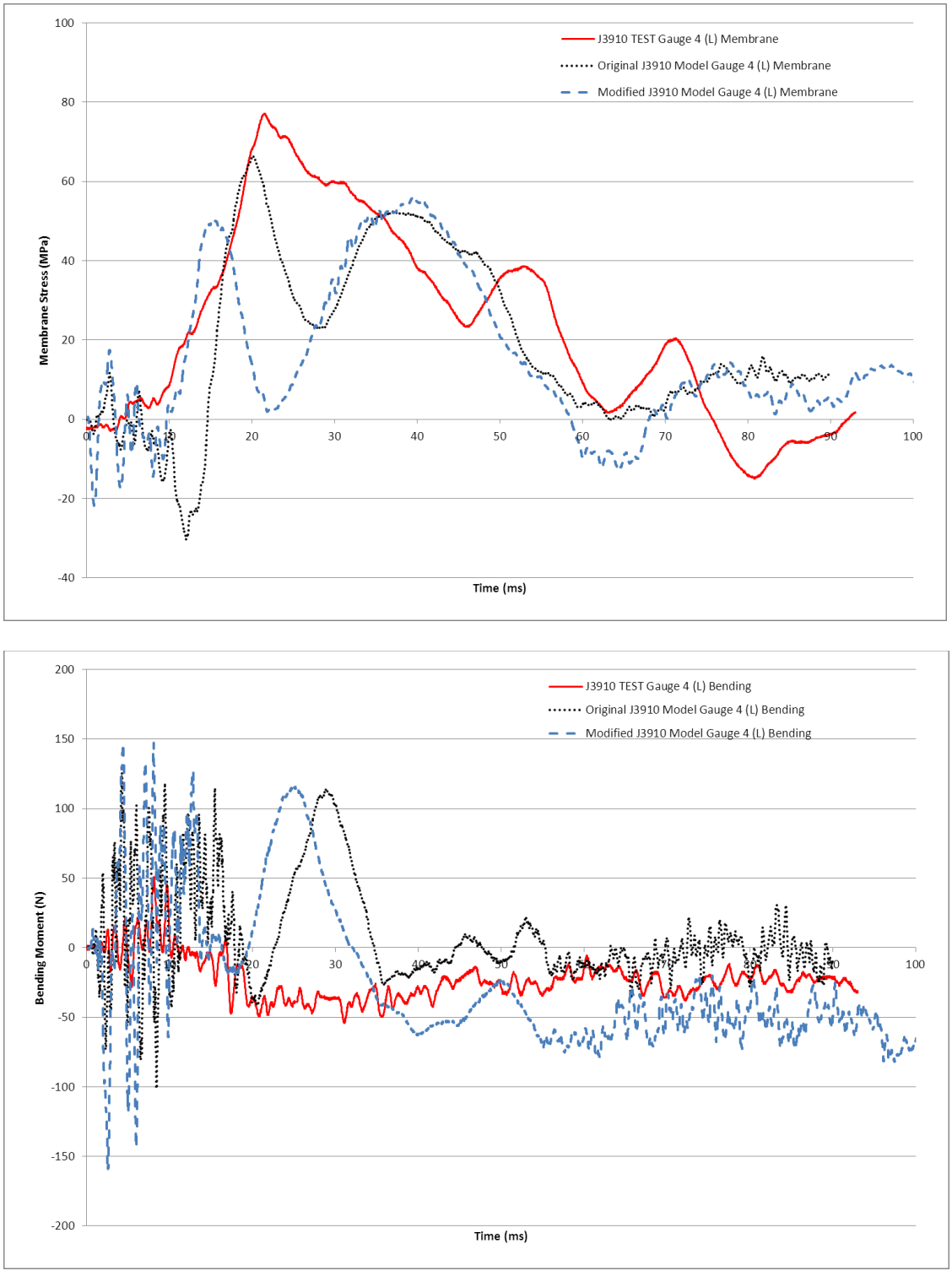

Figure C- 4 Comparison of membrane stresses (top) and bending moments (bottom) for gauge 4 location (compartment 1b, longitudinal) for GRW tanker J3910 topple test and finite element models

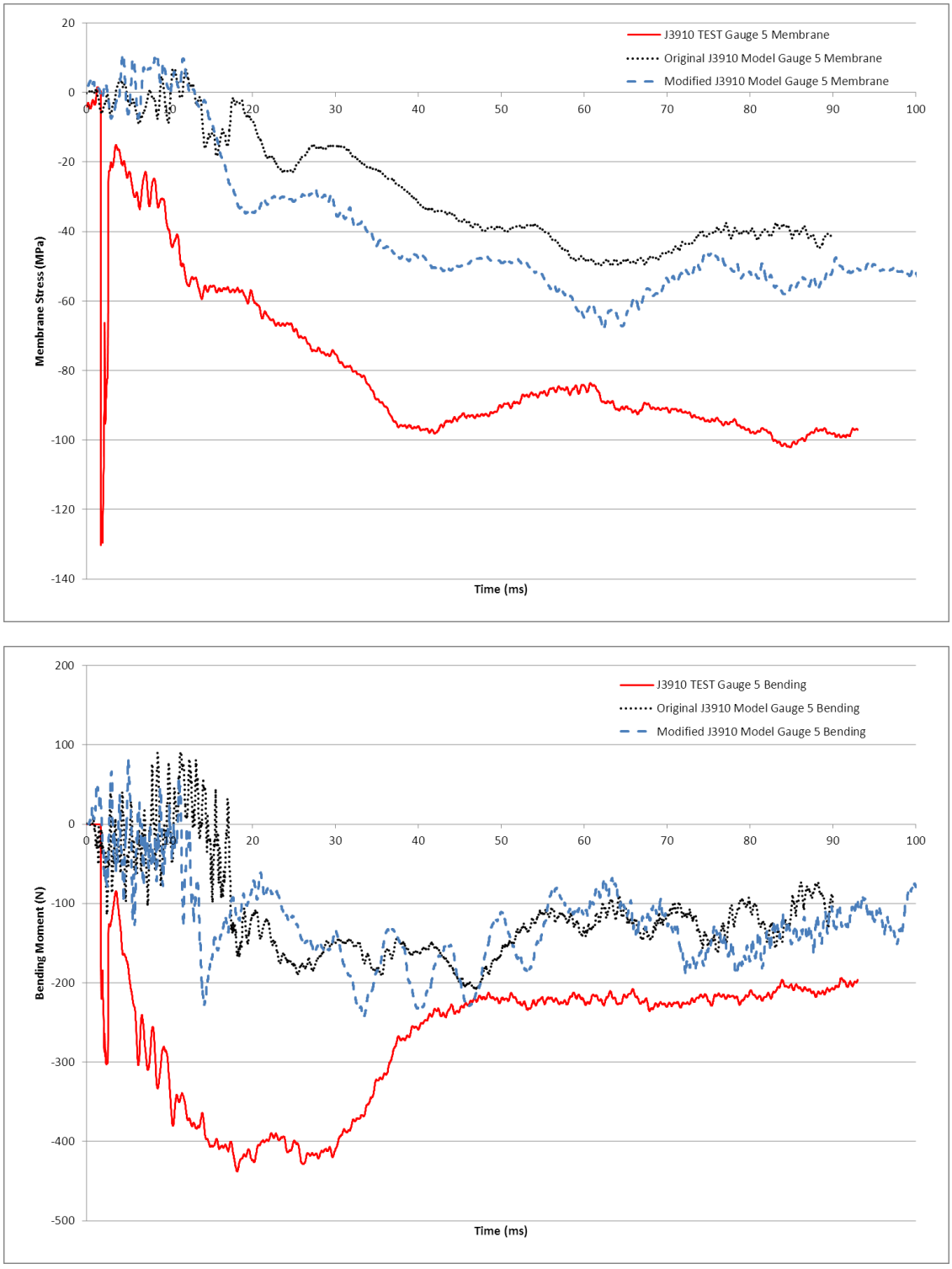

Figure C- 5 Comparison of membrane stresses (top) and bending moments (bottom) for gauge 5 location (band C) for GRW tanker J3910 topple test and finite element models. NB – FAULT ON STRAIN GAUGE

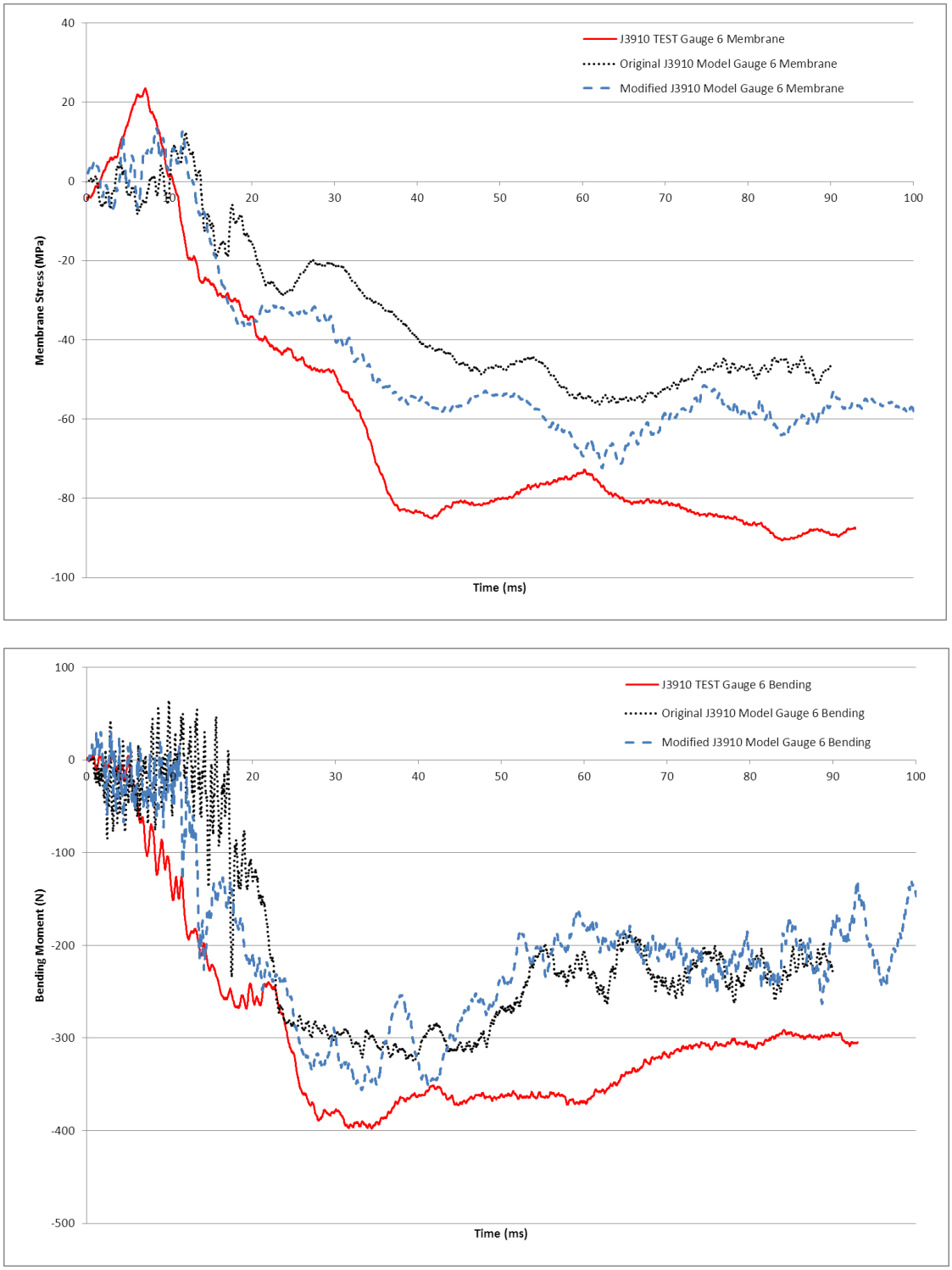

Figure C- 6 Comparison of membrane stresses (top) and bending moments (bottom) for gauge 6 location (band C) for GRW tanker J3910 topple test and finite element models

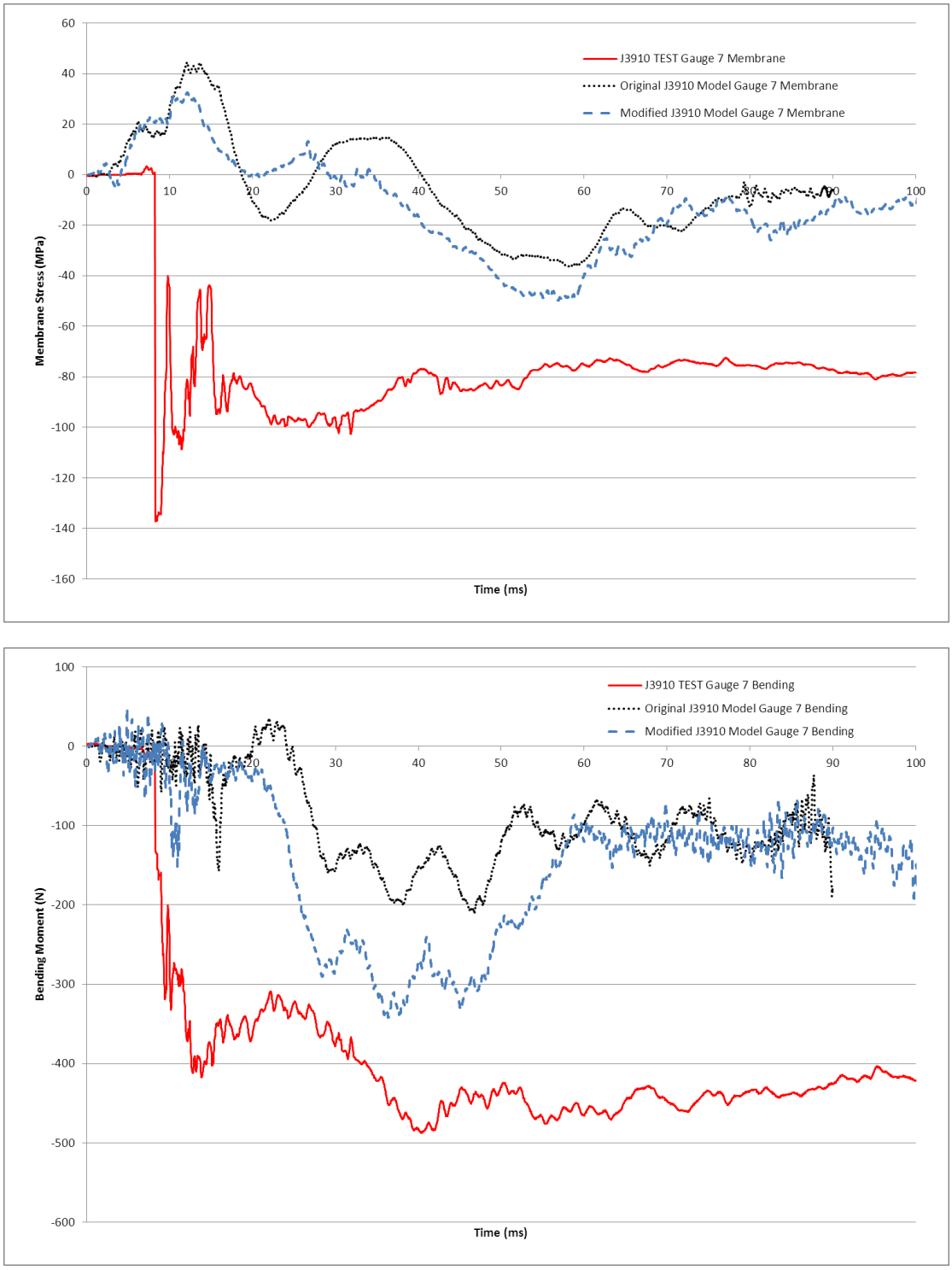

Figure C- 7 Comparison of membrane stresses (top) and bending moments (bottom) for gauge 7 location (band E) for GRW tanker J3910 topple test and finite element models NB – FAULT ON STRAIN GAUGE

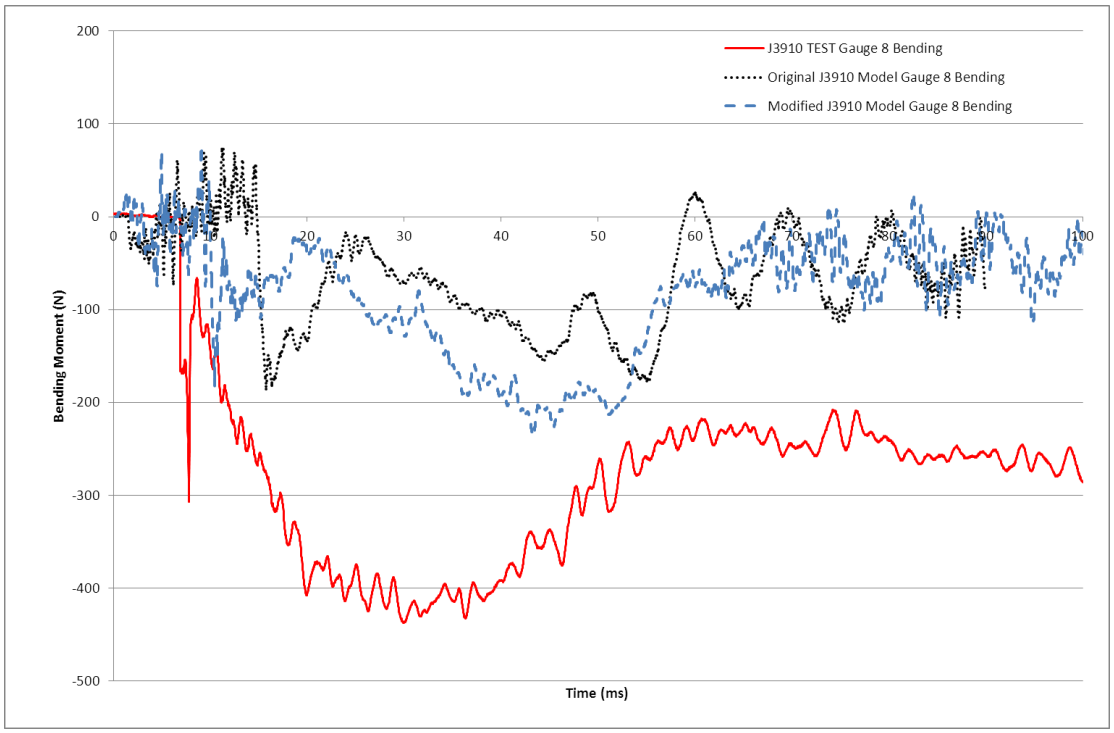

Figure C- 8 Comparison of membrane stresses (top) and bending moments (bottom) for gauge 8 location (band E) for GRW tanker J3910 topple test and finite element models NB – FAULT ON STRAIN GAUGE

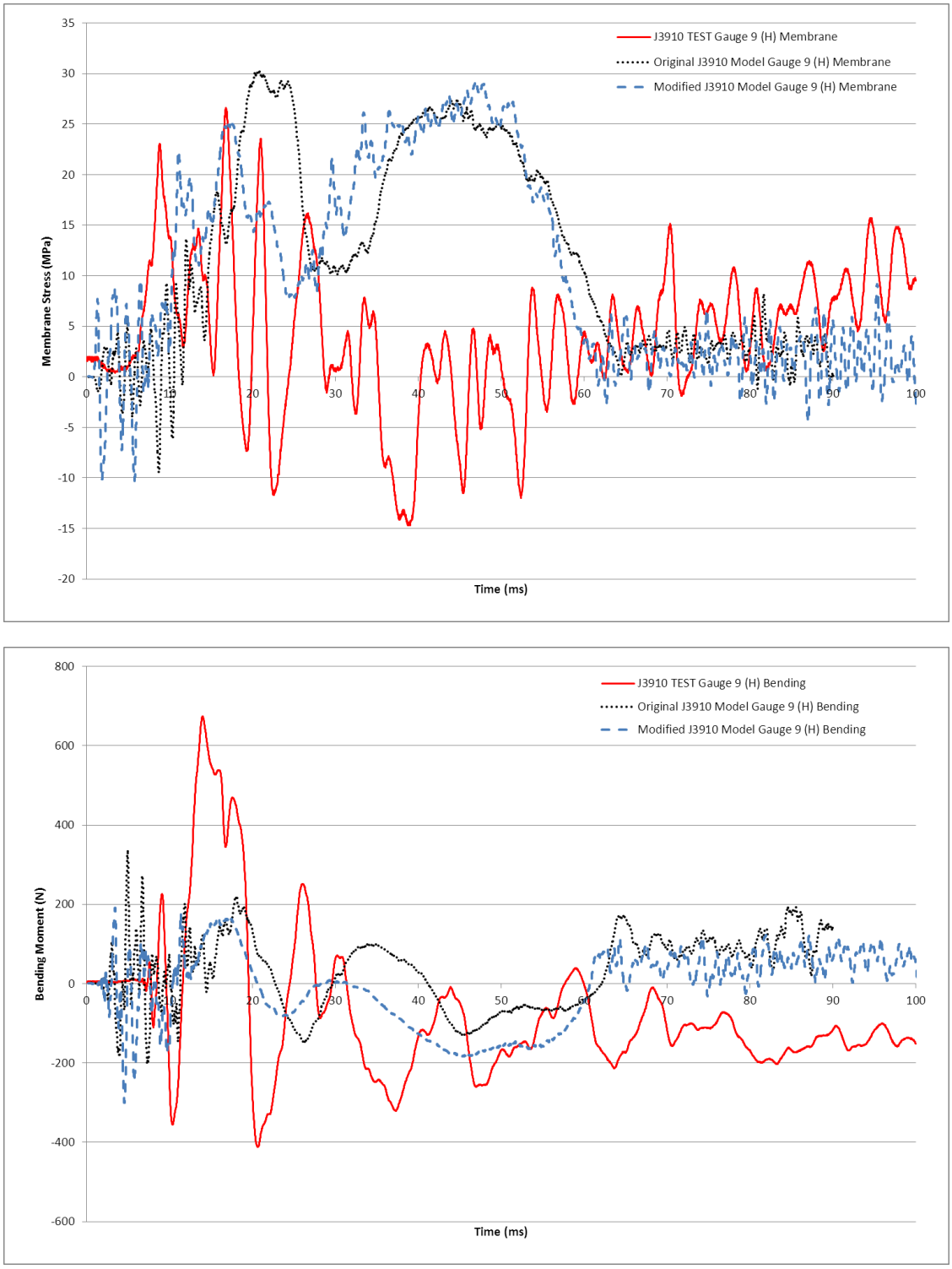

Figure C- 9 Comparison of membrane stresses (top) and bending moments (bottom) for gauge 9 location (compartment 4, hoop) for GRW tanker J3910 topple test and finite element models

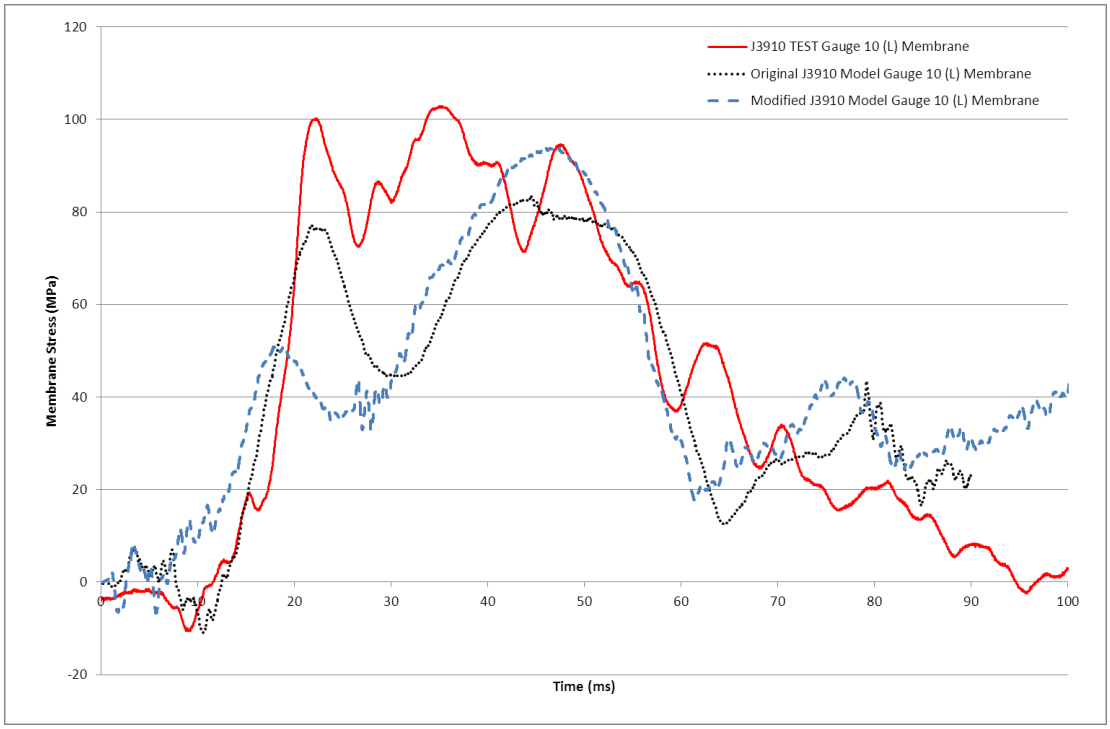

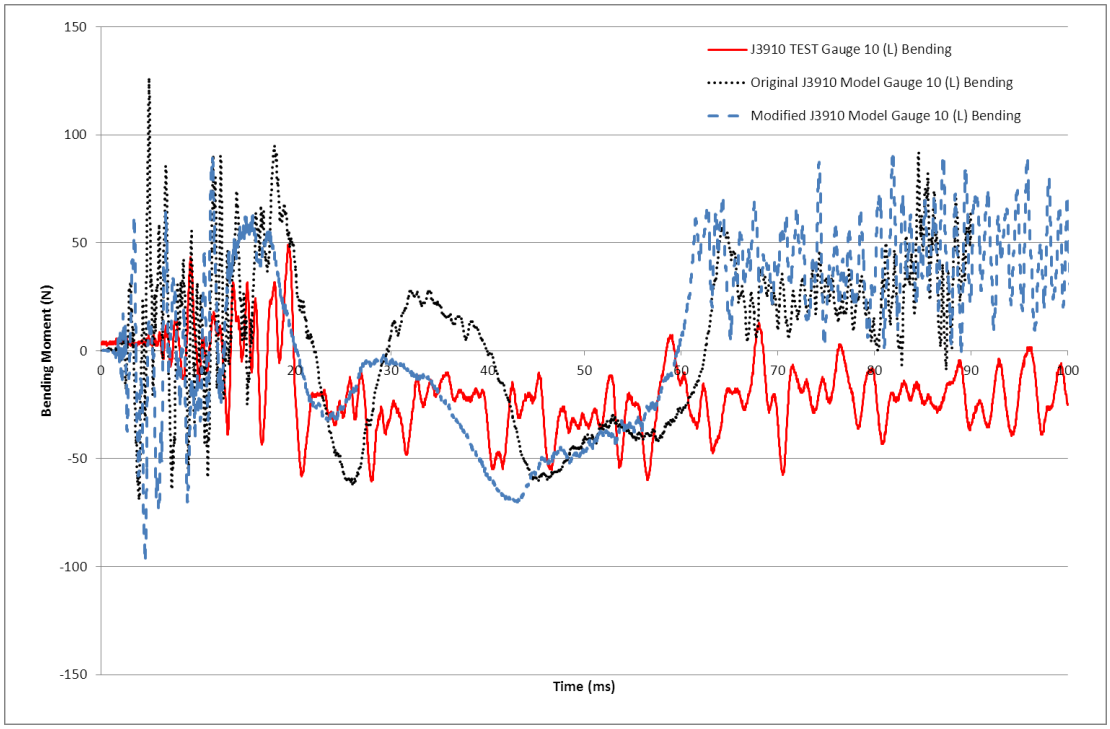

Figure C- 10 Comparison of membrane stresses (top) and bending moments (bottom) for gauge 10 location (compartment 4, longitudinal) for GRW tanker J3910 topple test and finite element models

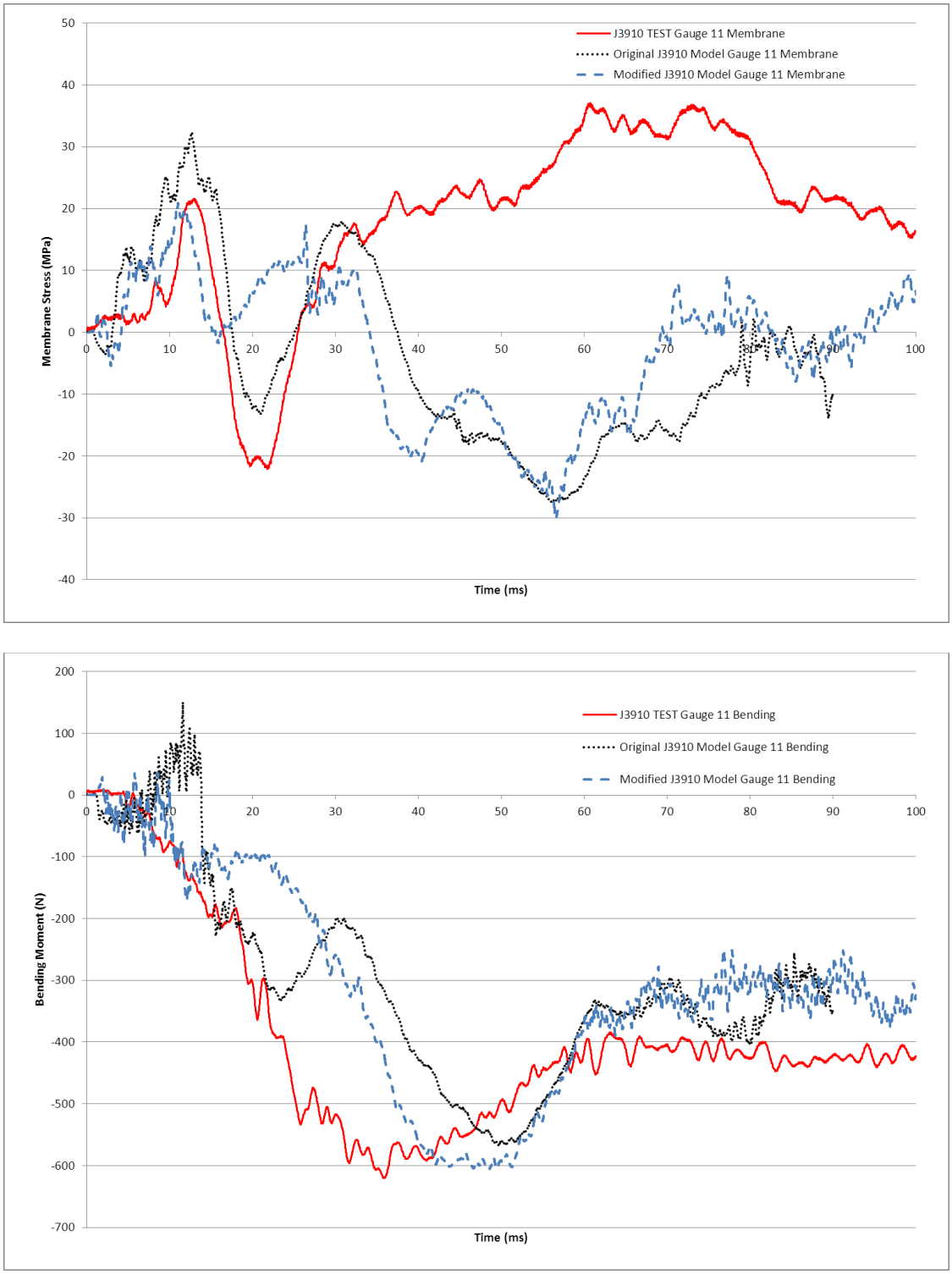

Figure C- 11 Comparison of membrane stresses (top) and bending moments (bottom) for gauge 11 location (band F) for GRW tanker J3910 topple test and finite element models

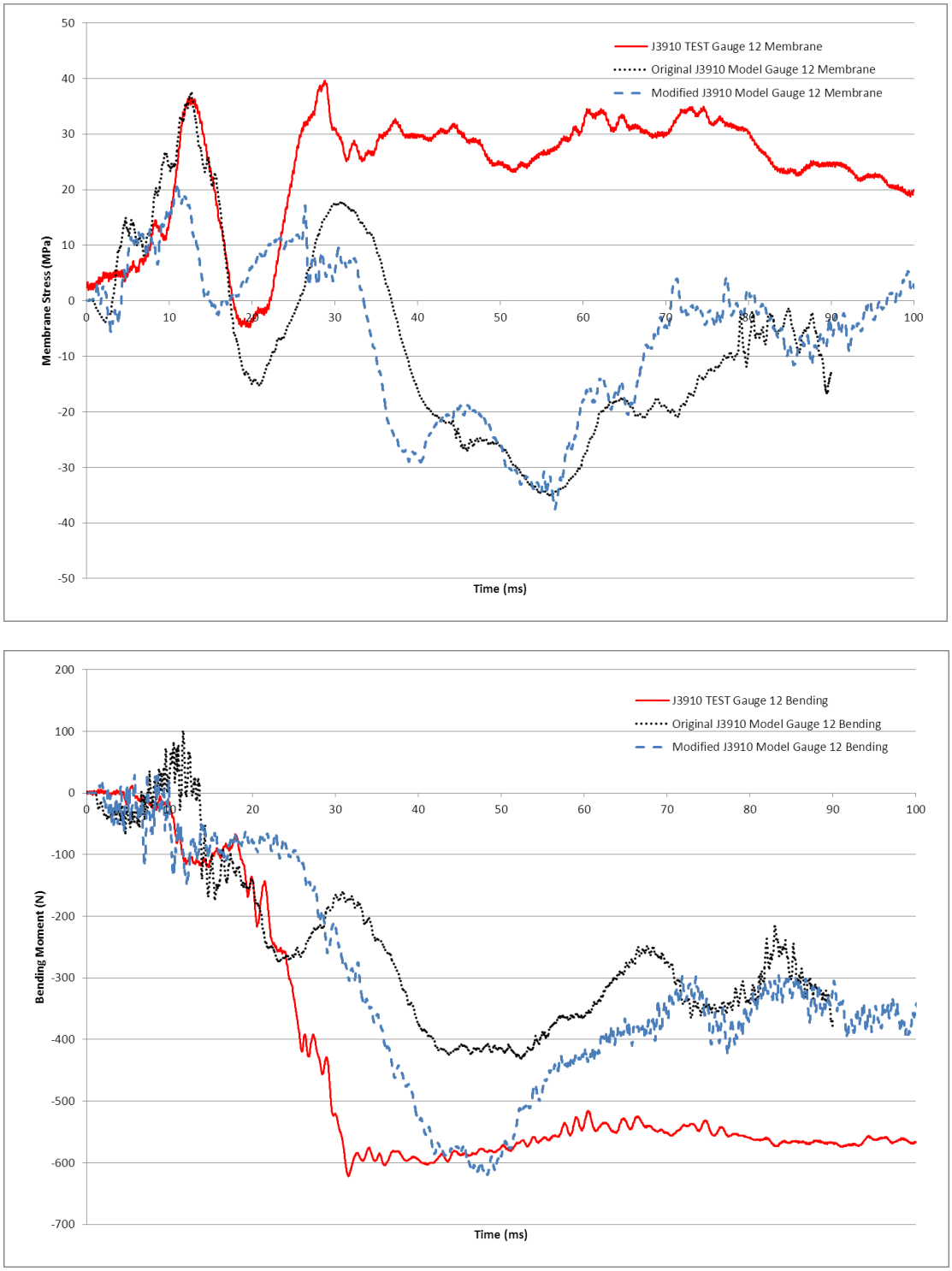

Figure C- 12 Comparison of membrane stresses (top) and bending moments (bottom) for gauge 12 location (band F) for GRW tanker J3910 topple test and finite element models

APPENDIX D FULL FUEL OIL RESULTS

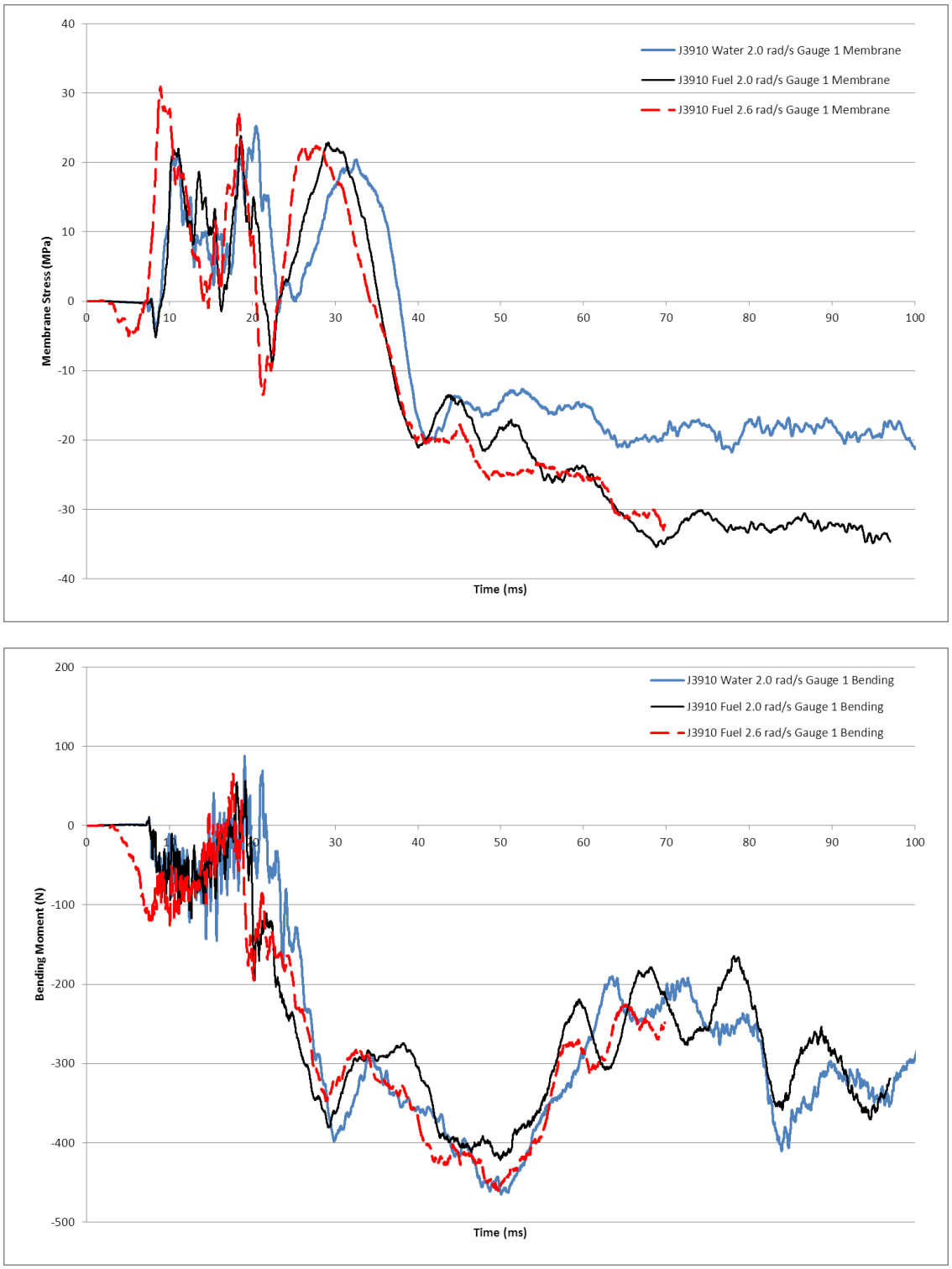

Figure D- 1 Comparison of membrane stresses (top) and bending moments (bottom) for gauge 1 location (band B) for J3910 models with water and fuel oil

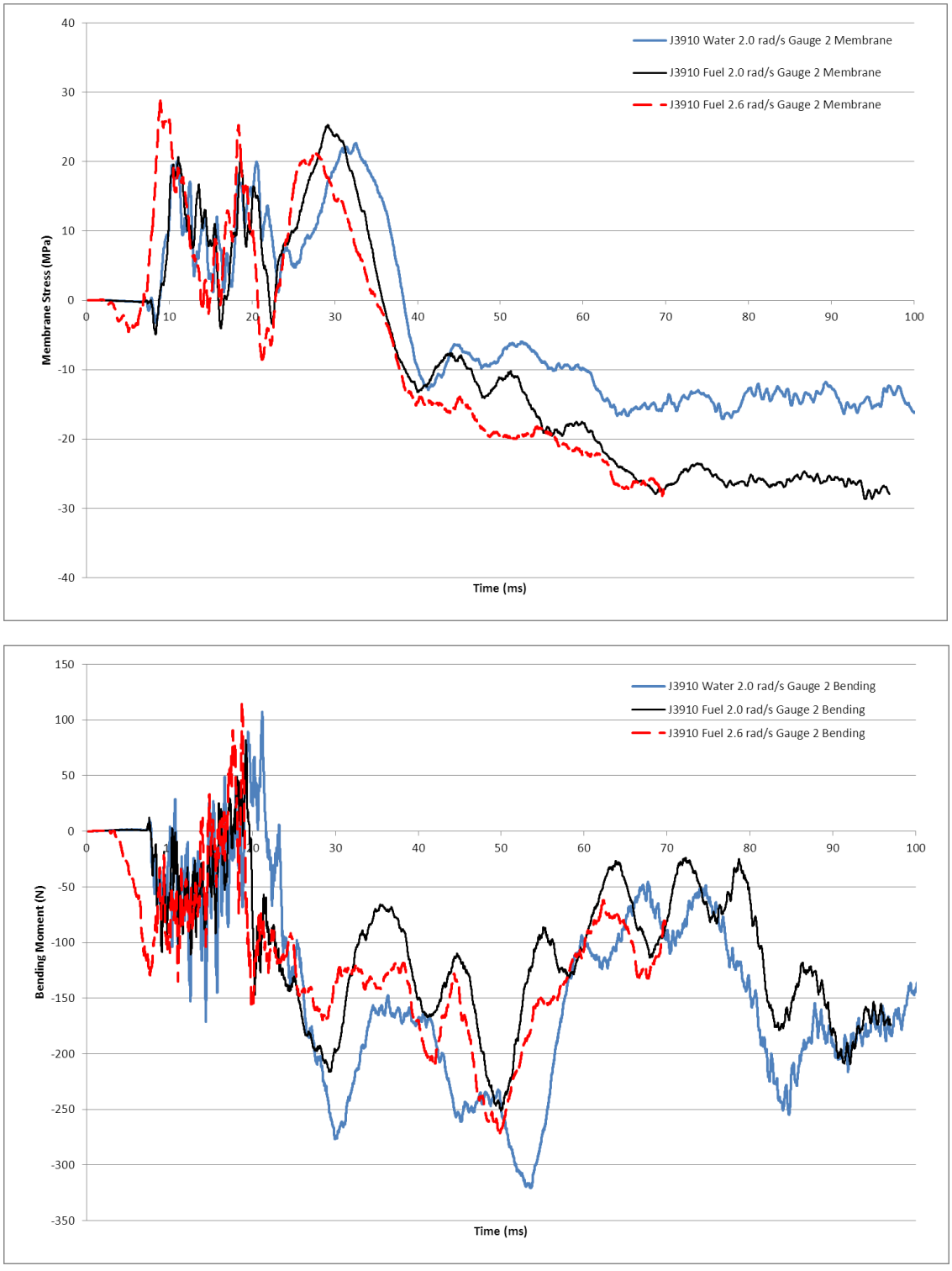

Figure D- 2 Comparison of membrane stresses (top) and bending moments (bottom) for gauge 2 location (band B) for J3910 models with water and fuel oil

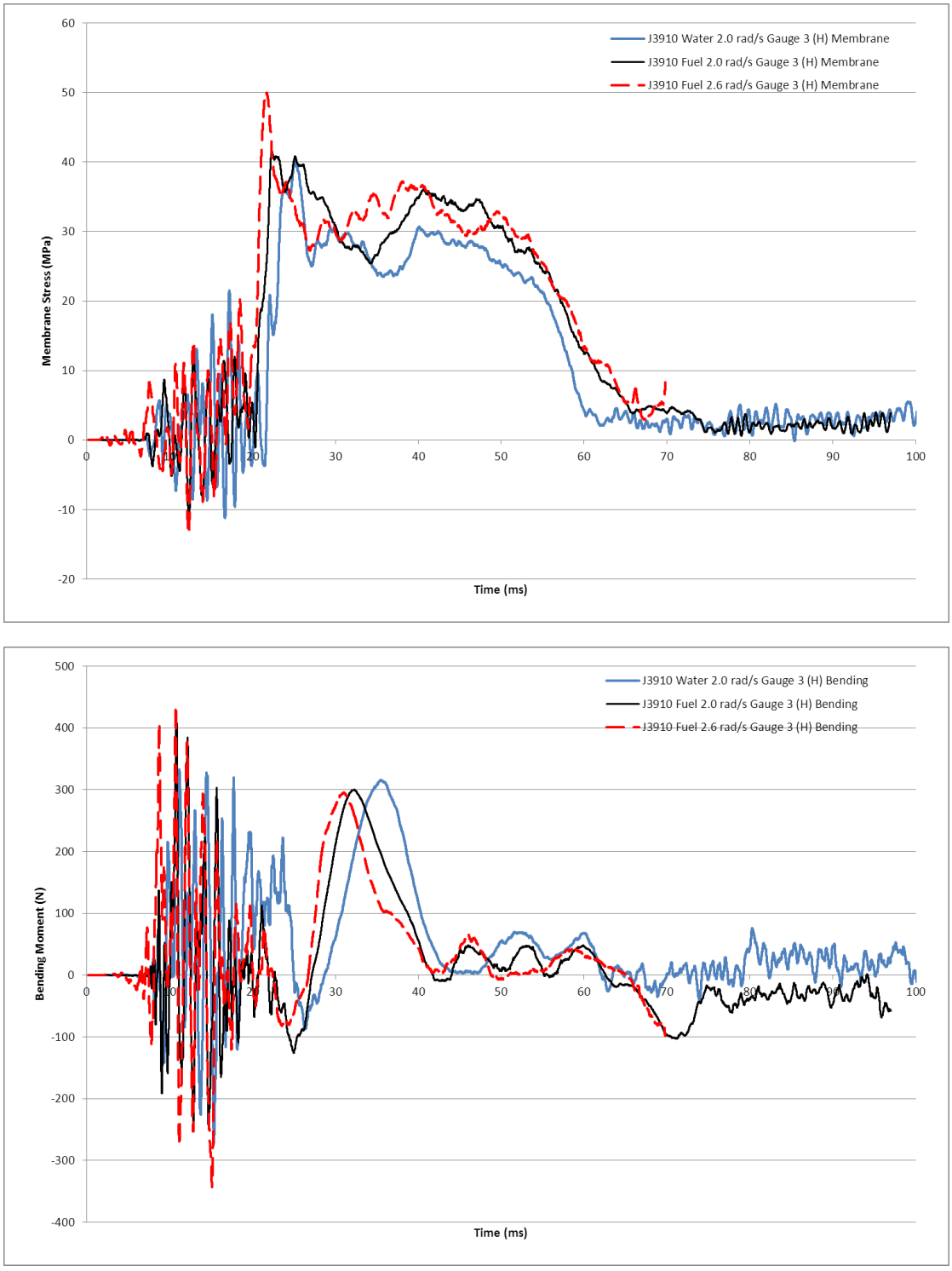

Figure D- 3 Comparison of membrane stresses (top) and bending moments (bottom) for gauge 3 location (compartment 1b, hoop) for J3910 models with water and fuel oil

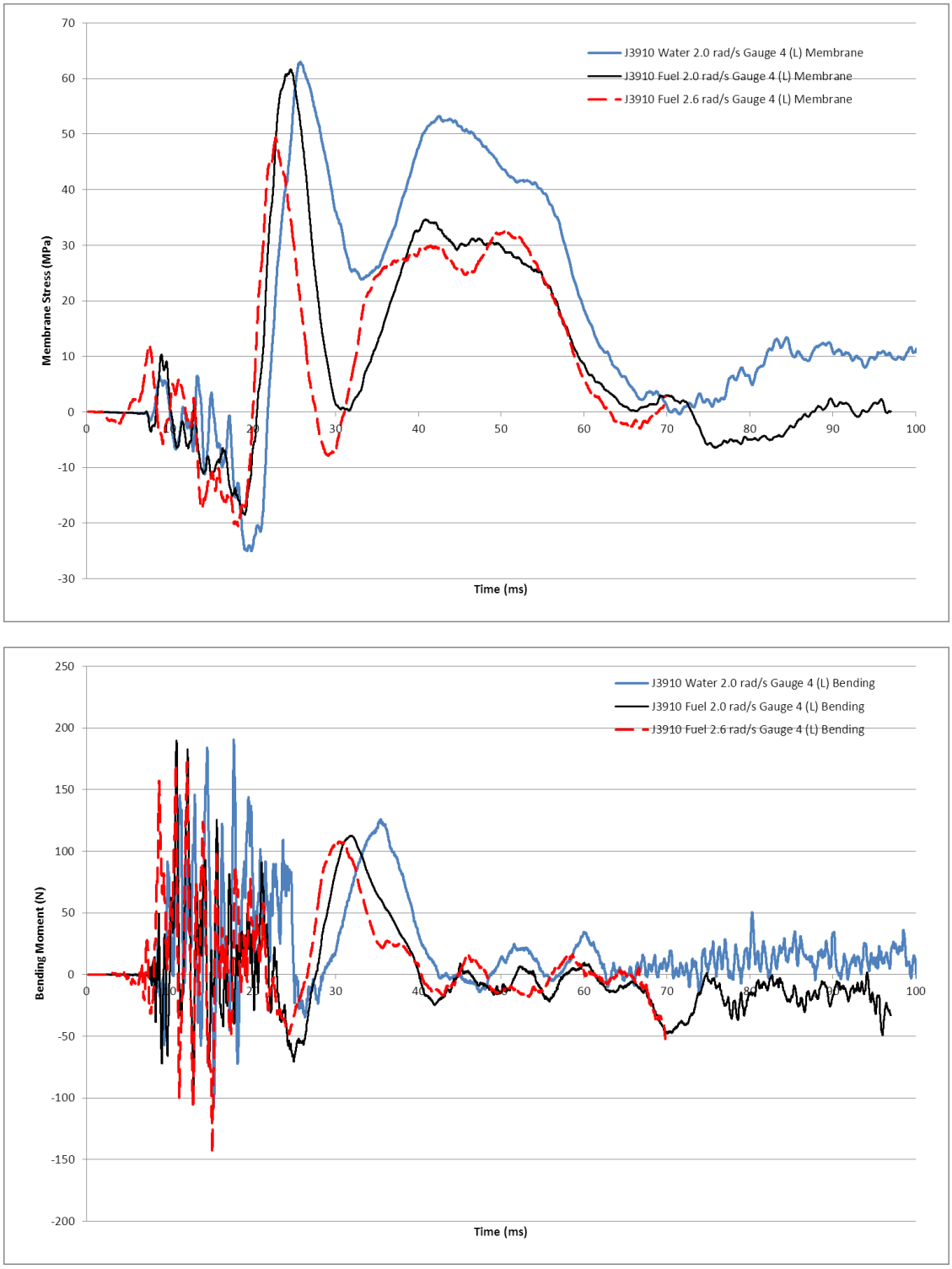

Figure D- 4 Comparison of membrane stresses (top) and bending moments (bottom) for gauge 4 location (compartment 1b, longitudinal) for J3910 models with water and fuel oil

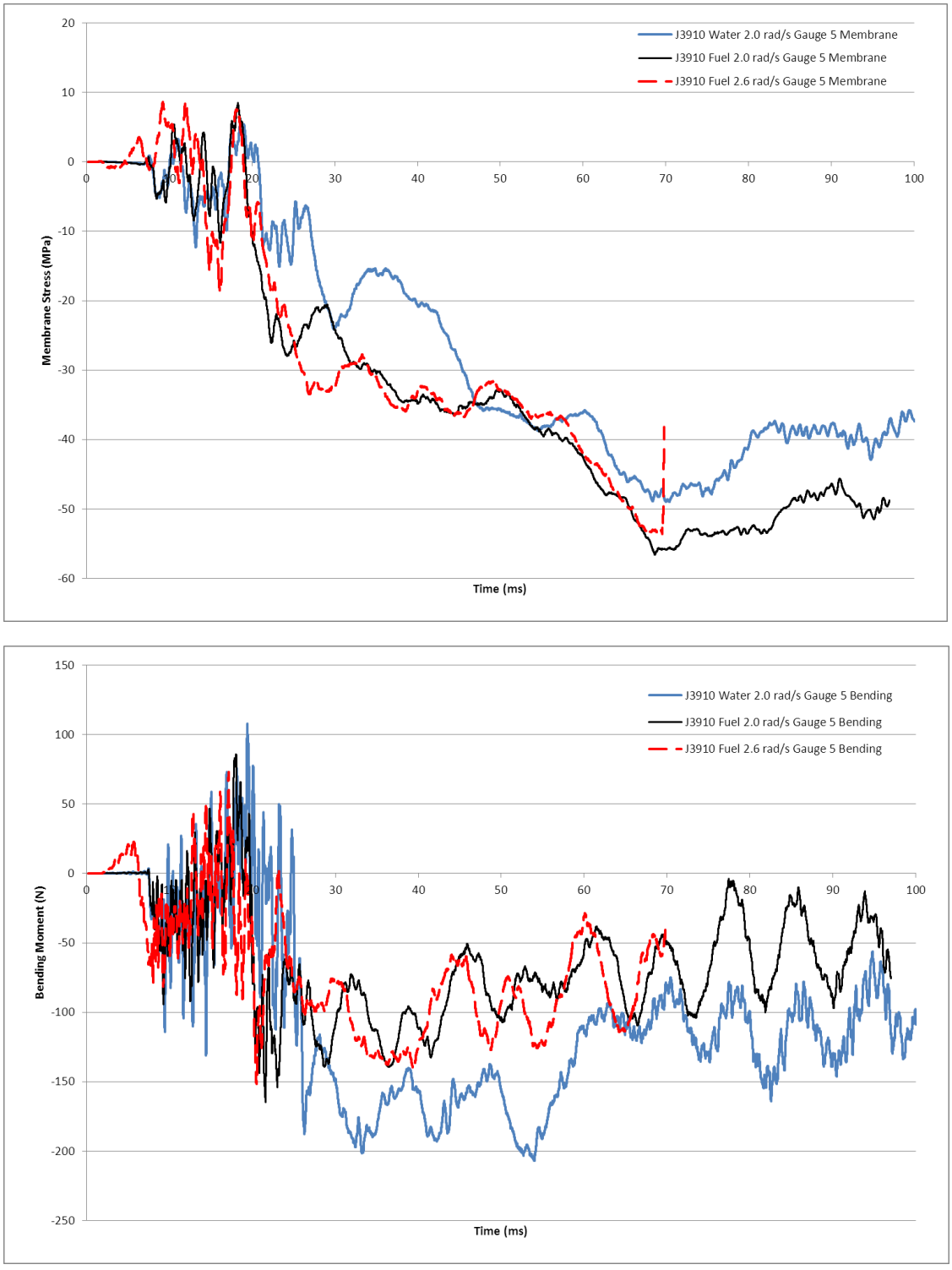

Figure D- 5 Comparison of membrane stresses (top) and bending moments (bottom) for gauge 5 location (band C) for J3910 models with water and fuel oil

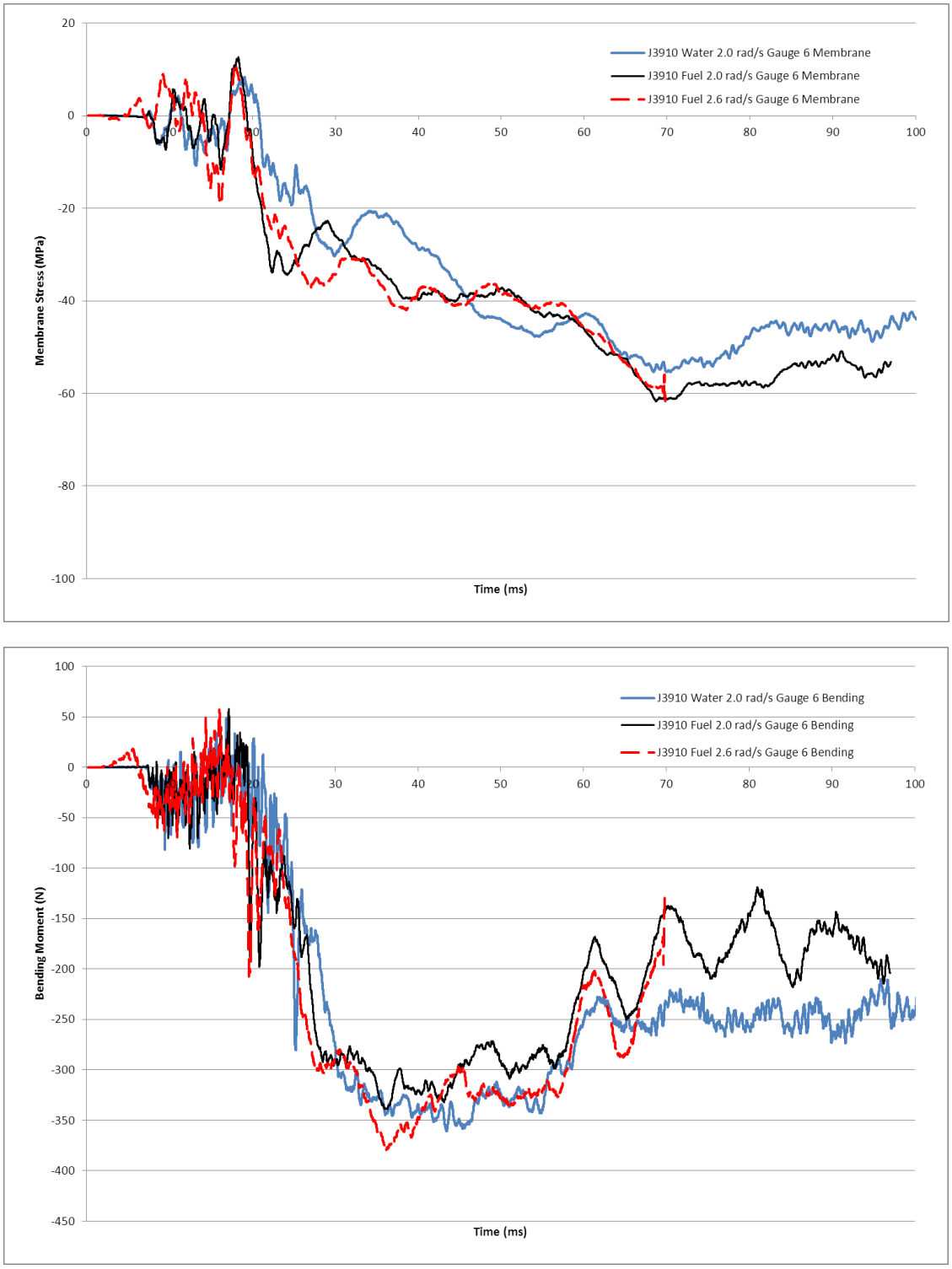

Figure D- 6 Comparison of membrane stresses (top) and bending moments (bottom) for gauge 6 location (band C) for J3910 models with water and fuel oil

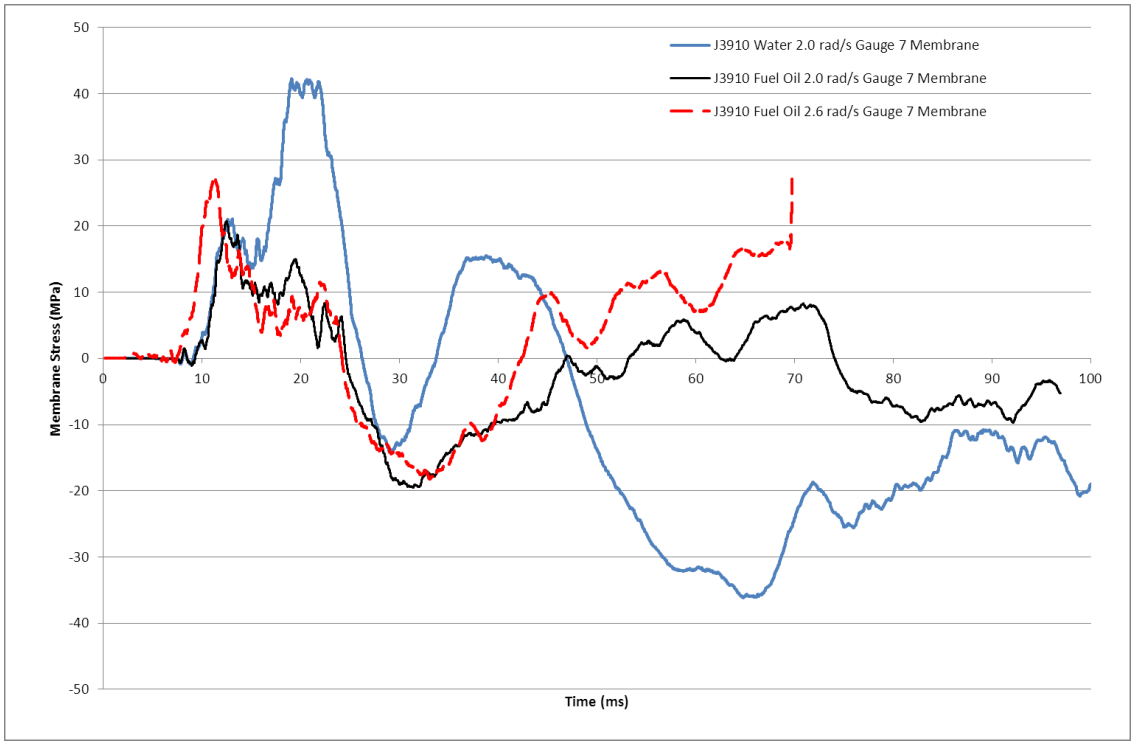

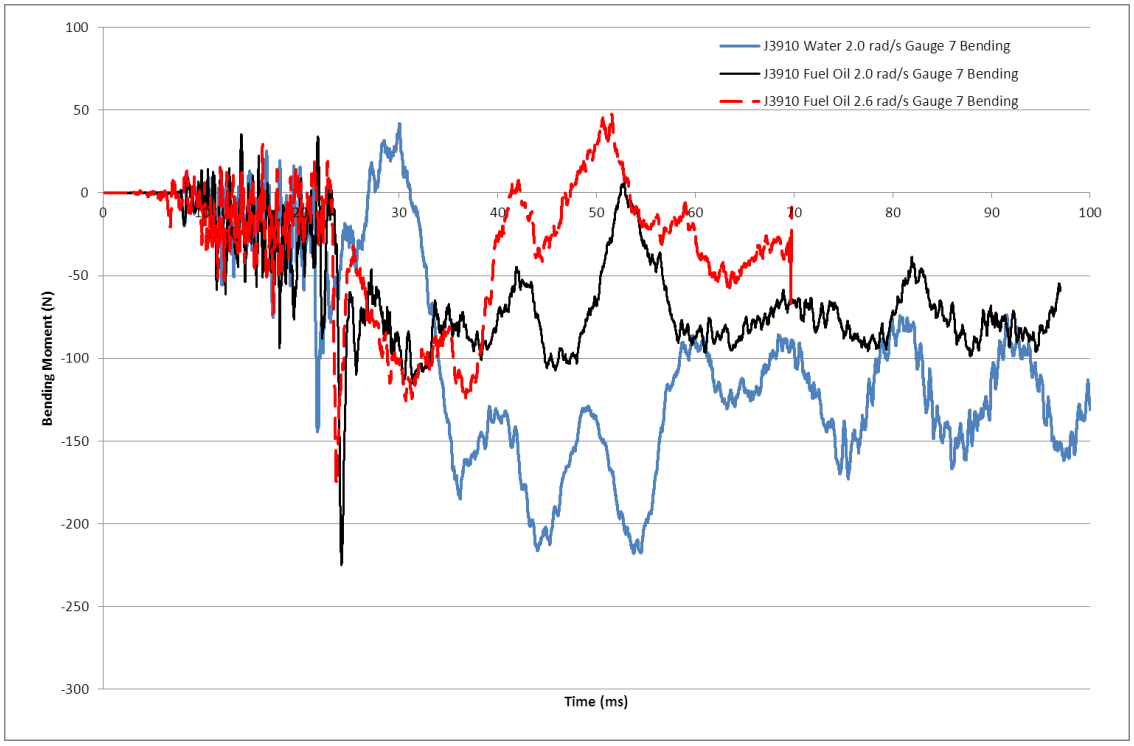

Figure D- 7 Comparison of membrane stresses (top) and bending moments (bottom) for gauge 7 location (band E) for J3910 models with water and fuel oil

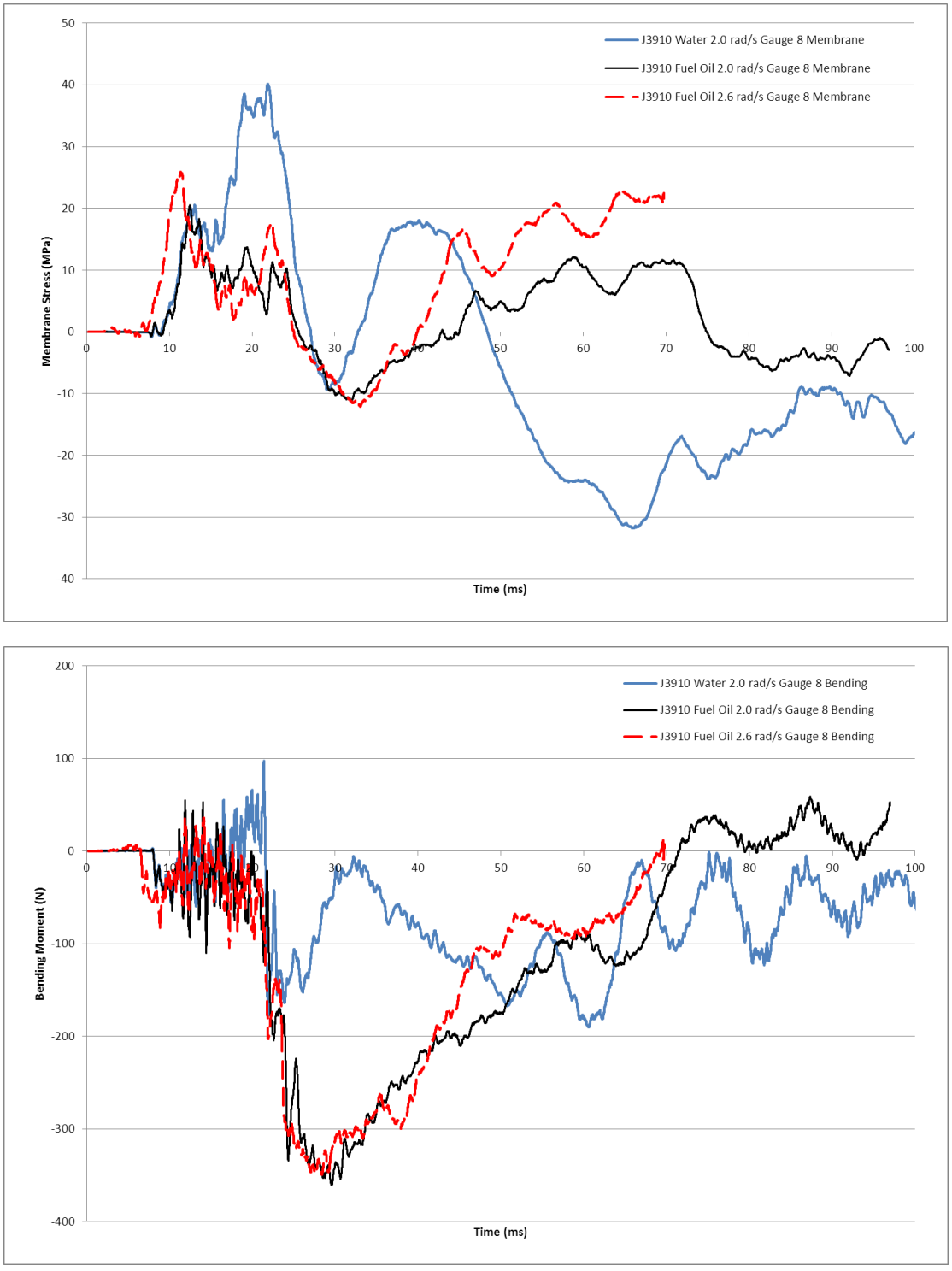

Figure D- 8 Comparison of membrane stresses (top) and bending moments (bottom) for gauge 8 location (band E) for J3910 models with water and fuel oil

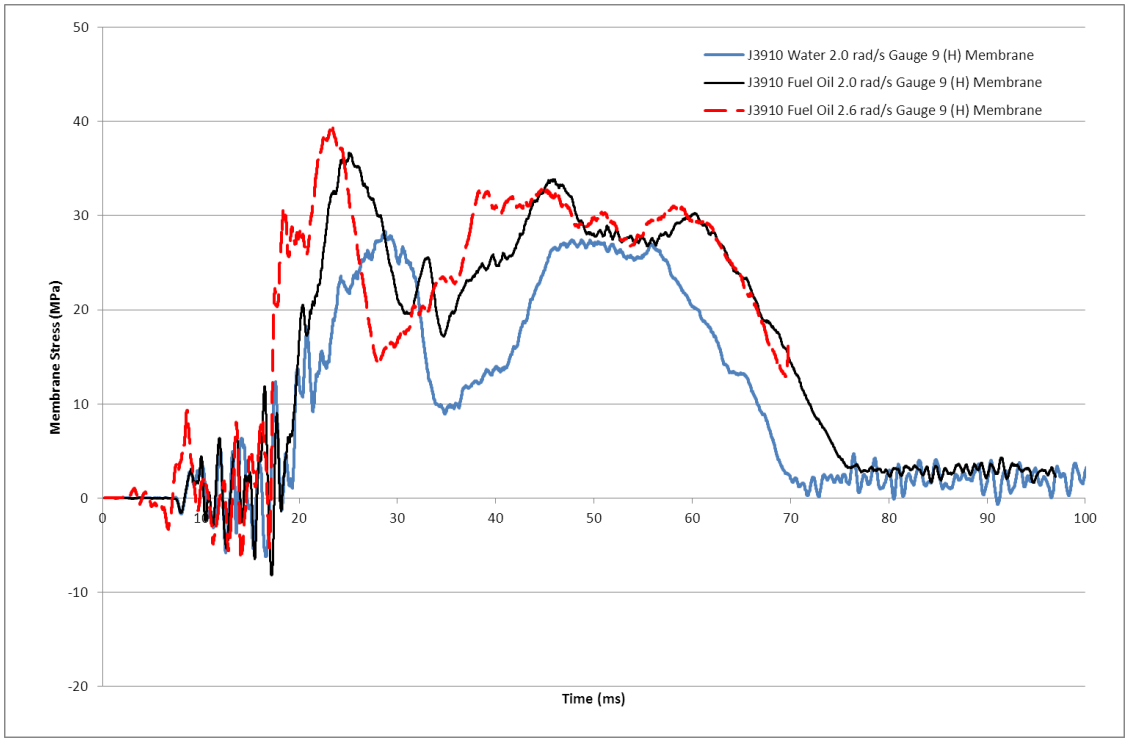

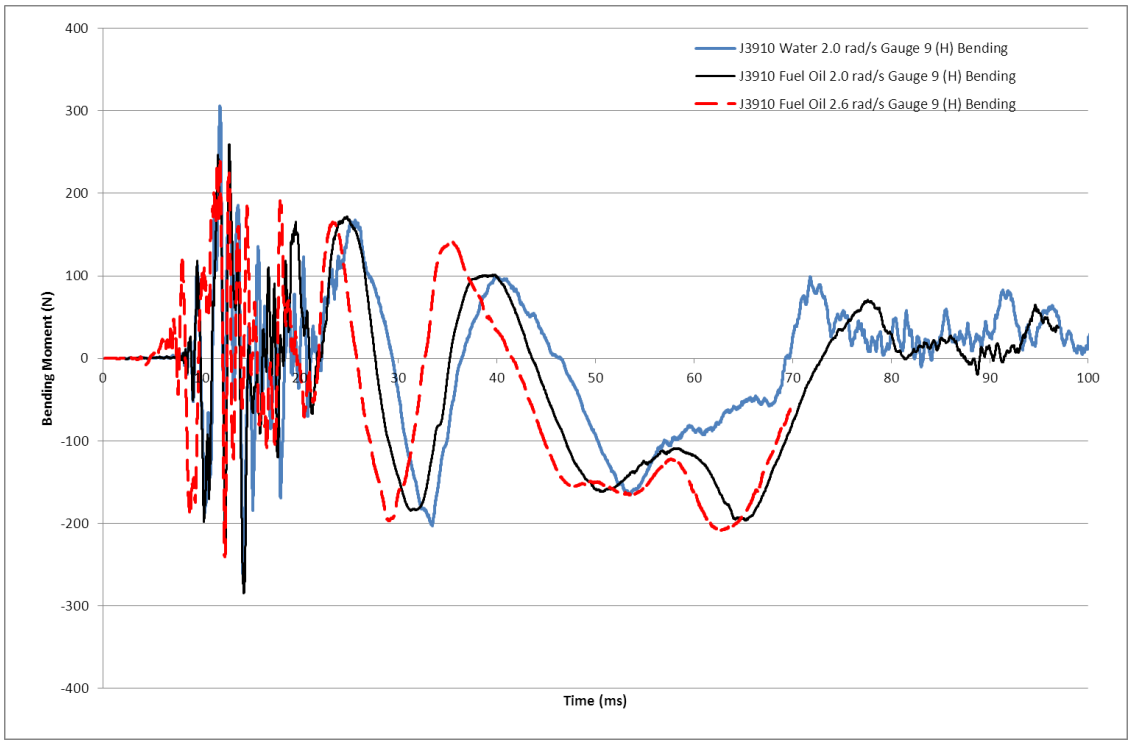

Figure D- 9 Comparison of membrane stresses (top) and bending moments (bottom) for gauge 9 location (compartment 4, hoop) for J3910 models with water and fuel oil

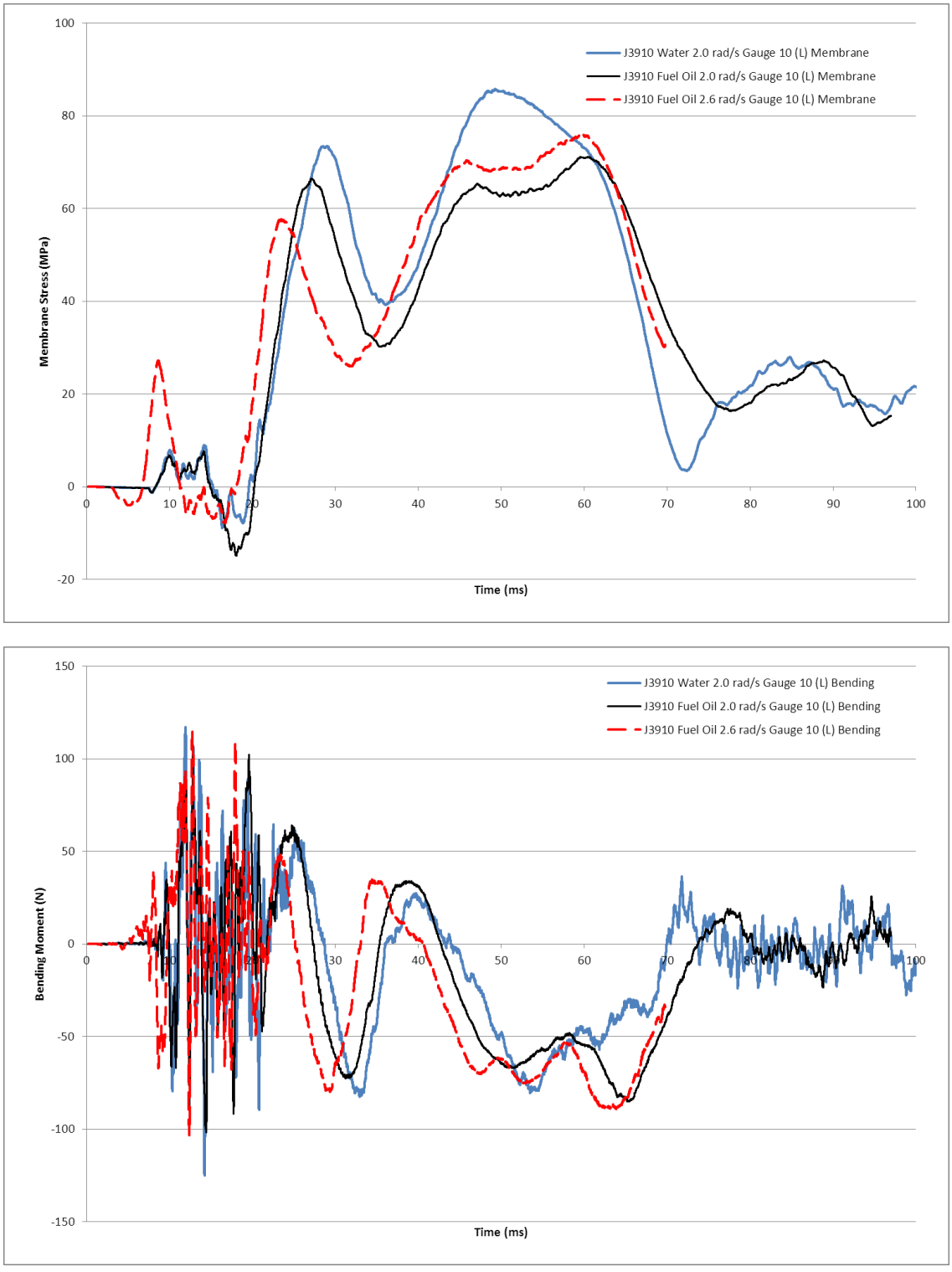

Figure D- 10 Comparison of membrane stresses (top) and bending moments (bottom) for gauge 10 location (compartment 4, longitudinal) for J3910 models with water and fuel oil

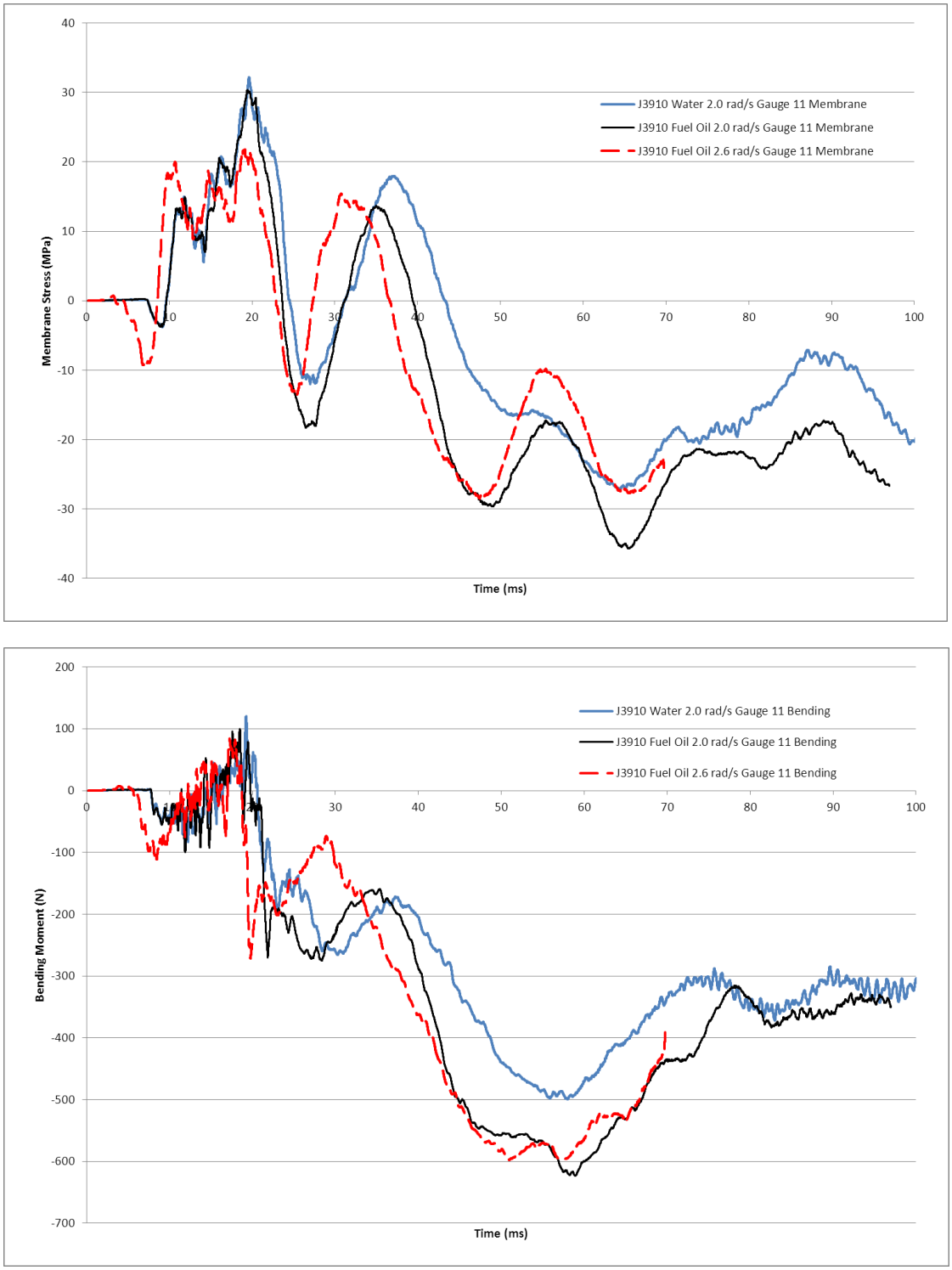

Figure D- 11 Comparison of membrane stresses (top) and bending moments (bottom) for gauge 11 location (band F) for J3910 models with water and fuel oil

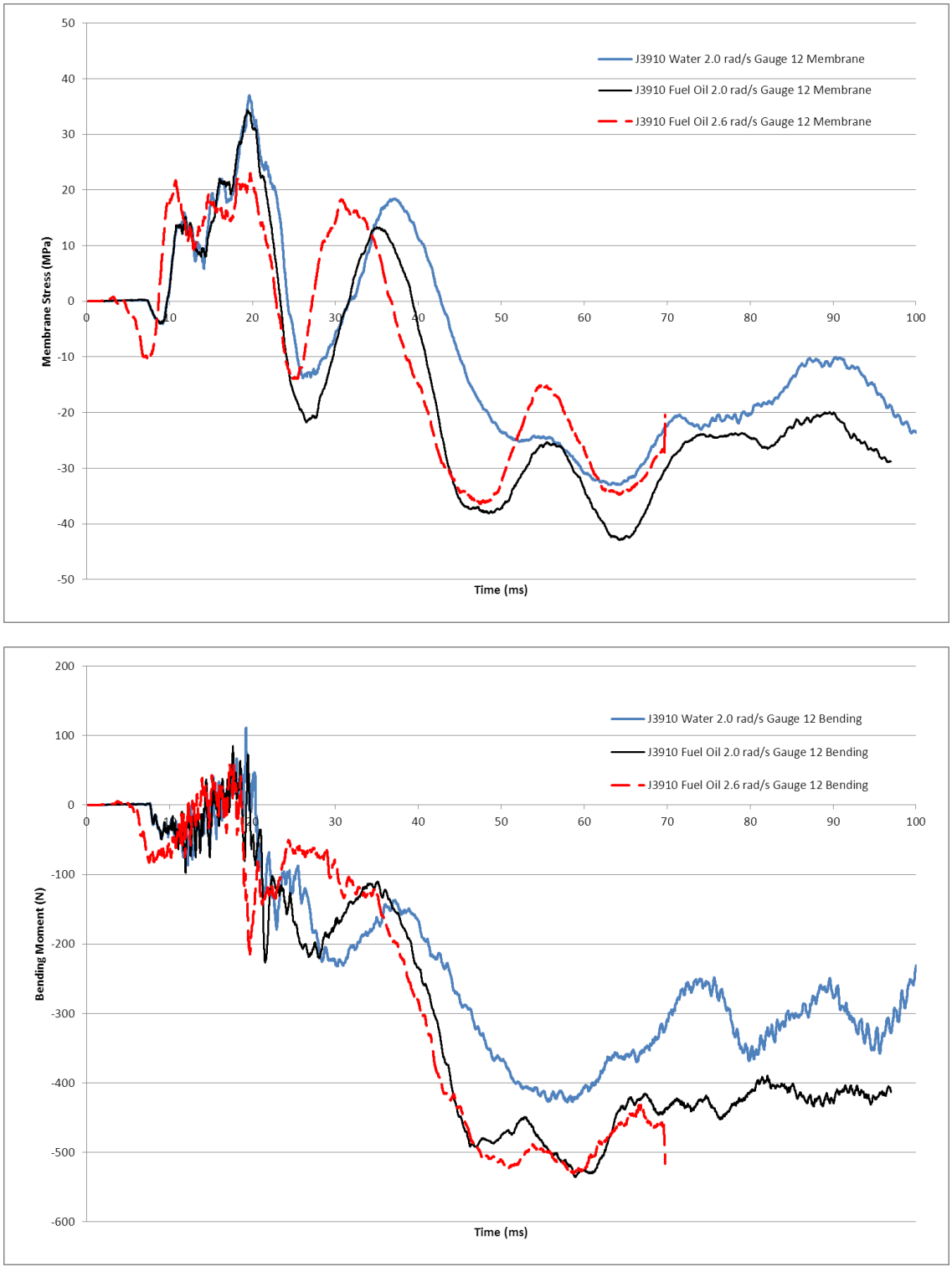

Figure D- 12 Comparison of membrane stresses (top) and bending moments (bottom) for gauge 12 location (band F) for J3910 models with water and fuel oil